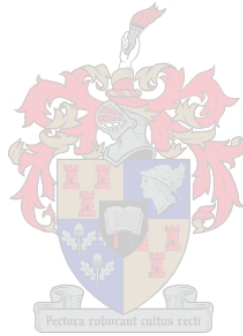


NUMERICAL MODELING AND EXPERIMENTAL INVESTIGATION OF THE FLOW AND THERMAL PROCESSES IN A MOTOR CAR VEHICLE UNDERHOOD

Josebus Maree van Zyl

**Thesis presented in partial fulfilment of the requirements for the degree of MSc. in
Mechanical Engineering at Stellenbosch University**



Thesis Supervisors:
Professor T.M. Harms
Department of Mechanical Engineering
Doctor A.B. Taylor
Stellenbosch Automotive Engineering

December 2006

DECLARATION

I, the undersigned, hereby declare that the work contained in this thesis is my own original work and that I have not previously in its entirety or in part submitted it at any university for a degree.

Signature:

Date:



ABSTRACT

The project aimed at numerically modeling the flow and thermal processes occurring in a Volkswagen Citi Golf Chico underhood using computational fluid dynamics (CFD). The motivation for this investigation was to develop and demonstrate the capability of CFD as an automotive analysis tool. This would allow local automobile analysts and designers enhanced analyses of the thermal and flow conditions occurring in this compact environment, leading to improved local vehicles.

A review of relevant literature indicated that the CFD community in South Africa is small with comparison to the international sector. The application of CFD to analyse automobiles in South Africa is limited and practised by few. This experience requires development and refinement, such that South Africa may improve vehicles manufacture in the country. The review also indicated that CFD used in the international communities provides good results, promoting simulation-based engineering.

The experimental investigation involved parking a vehicle in the subsonic wind tunnel intake at the Mechanical Engineering Department in Stellenbosch. This tunnel is 3.7 m wide, 4 m long and 2.8 m tall, capable of wind speeds up to 90 m/s. Various equipment including thermocouples, a thermal imager and a hand held hot-wire anemometer provided temperature and velocity measurements within the underhood. A pitot-static probe connected to a pressure transducer measured the wind tunnel velocities.

The numerical investigation started with the creation of a three-dimensional geometry of the underhood from measurements taken of the vehicle. This geometry, created with Solid Edge version 14, formed the domain for automatically generating discretised grids using STAR-Design version 3.2. Subsequently, boundary conditions and numerical models were applied to the grids, which included simplified fan and radiator models. The analysis concluded with results obtained from the numerical CFD simulations, performed with STAR-CD version 3.24.

The validity and accuracy of the numerical solutions was verified and quantified with the numerical results. The evaluation consisted of two test cases (wind tunnel speeds of 0 m/s and 5 m/s), each simulated at three different grid resolutions. Each simulation continued until they fully converged to a single solution. The comparison of the three simulations from each case indicated that the results were grid independent. The final in-

spection of the results in terms of y^+ values and boundary conditions indicated that the models implemented were valid.

The comparison of the numerical results for temperatures and fan inlet velocities with the experimentally measured data served as a measure to quantify the applicability of CFD for underhood investigations. The comparison between the two sets of results proved acceptable, with a maximum difference of 10%, indicating that CFD is capable of predicting temperatures and flow fields with reasonable accuracy.

The numerical results indicated that while the vehicle travels at higher velocities, the underhood remains well ventilated. The underhood tends to trap the hot air from the radiator and other heat sources when the vehicle remains stationary, causing the air to heat further. This can be addressed by the installation of vents in the side panels near the top of the underhood environment. This should allow the hot air to escape, possibly resulting in a significant reduction of the underhood temperatures.

Momentum and energy source terms modelled the effects from the fan and radiator. These models worked well for both cases, but improvement is necessary. Special attention should be given to the condition where the radiator fan obstructs the flow through the radiator.

A further result of the project was the establishment of a flexible foundation for conducting numerical simulations on automobiles. It allows for the inclusion of additional components and the implementation of more advanced models for representing effects from various engine components.

OPSOMMING

Die doel van die projek was om die vloeï en termiese prosesse wat binne 'n Volkswagen Citi Golf Chico plaasvind, numeries te modelleer deur van berekeningsvloeidinamika (BVD) gebruik te maak. Die motivering vir die ondersoek was om die vermoë van BVD te ontwikkel en as 'n motorbedryf analiese gereedskap te demonstree. Dit sal toelaat dat plaaslike motoranaliste en -ontwerpers verbeterde analises van die termiese en vloeï omstandighede wat in hierdie kompakte omgewing plaasvind, te kan doen. Dit kan lei tot verbeterde plaaslike voertuie.

'n Oorsig van relevante literatuur dui aan dat die BVD-gemeenskap in Suid Afrika baie klein in vergelyking met die internasionale sektor is. Die toepassing van BVD om motors te analiseer in Suid Afrika is beperk en word deur min beoefen en verg ontwikkelings en verfyning om sodoende Suid Afrika voertuie wat in die land vervaardig word, te kan verbeter. Die oorsig het ook aangedui dat die gebruik van BVD in die internasionale gemeenskap goeie resultate lewer wat simulasië gebaseerde ingenieurswese bevorder.

Vir die eksperimentele ondersoek is 'n voertuig in die subsoniese windtonnelinlaat by die Meganiese Ingenieurs Departement in Stellenbosch parkering. Hierdie tonnel is 3.7 m wyd, 4 m lank en 2.8 m hoog, en kan windsnelhede van tot 90 m/s genereer. Met verskeie toerusting, insluitend termokoppels, 'n termiese afbeelder en 'n handhandteerdewarmfilm anemometer, is die temperatuur en snelheidmetings binne die onderkap verkry. Die windtonnelnelhede is met 'n Pitot-statiëse oeler gekonnekteer aan 'n drukmeter gemeet.

Die numeriese ondersoek het begin met die skep van 'n drie-dimensionele geometrie van die onderkap vanaf mates wat van die voertuig geneem is. Hierdie geometrie, geskep met Solid Edge veergawe 14, het die domein vir die automatiese generasie van gediskreteerde roosters met die gebruik van STAR-Design veergawe 3.2 gevorm. Hierna is genseerdes en numeriese modelle op die rooster toegepas, wat eenvoudige waaier en verkoeler modelle ingesluit het. Resultate verkry vanaf die numeriese BVD simulasië, gedoen deur STAR-CD weergawe 3.24, het die analiese afgesluit.

Die geldigheid en akkuraatheid van die numeriese oplossings is met numeriese resultate bevestig en gekwantifiseer. Die evaluasie is by twee toetsgevalle (windtonnelnelhede van 0 m/s en 5 m/s) gedoen, elk was gesimuleer met drie verskillende roosterresolu-

sies. Elke simulاسie is voortgesit totdat hulle ten volle tot 'n enkele oplossing gekonvergeer het. Die vergelyking van die simulاسie van elke geval het aangedui dat die resultate rooster-onafhanklik is. Die finale inspeksie van die resultate in terme van y^+ -en grenswaardes het aangedui dat die modelle wat gebruik was, geldig was.

Die vergelyking van die numeriese resultate vir temperature en waaierinlaatsnelhede met ekperimenteel bepaalde data het as 'n maatstaf om die toepaslikheid van BVD vir onderkapondersoeke te kwantifiseer, bedien. Die vergelyking tussen die twee stelle resultate met 'n maksimum verskil van 10% was aanvaarbaar, wat aandui dat BVD in staat is om temperature en vloeivelde met redelike akkuraatheid te voorspel.

Die numeriese resultate het aangedui dat terwyl die voertuig met hoër snelhede ry, die onderkap goed geventileer bly. Die onderkap is geneig om warm lug vanaf die verkoeler en ander hitte bronne was te keer terwyl die voertuig stilstaan, wat verdere verwarming van die lug veroorsaak. Die probleem kan voorkom word deur luggate in die sy panele naby die bokant van die onderkapomgewing te installeer. Dit behoort die warm lug toe te laat om te ontsnap en die onderkaptemperatuur sal waarskynlik beduidende afneem.

Momentum- en energiebronterme is gebruik om die effekte van die waaier en verkoeler te modelleer. Hierdie modelle het goed vir die stilstaande geval gewerk, maar verbetering is nodig. Spesiale aandag moet gegee word aan die geval waar die waaier afgeskakel is en 'n obstruksie tot die vloei veroorsaak.

'n Verdere resultaat van die projek was die vestiging van 'n buigsame fondasie om numeriese simulاسies van motors te doen. Dit laat toe dat addisionele onderdele bygevoeg kan word en vir die implementering van meer gevorderde modelle wat die effekte van verskeie enjinkomponente voorstel.

ACKNOWLEDGEMENTS

The following people receive acknowledgement and recognition for their contribution to the success of this project.

Prof. Thomas Harms, the supervisor, for all the insight and advice concerning the project and thesis

Dr. Andrew Taylor, the managing director of CAE, for the funding and contributions to this research project

Cobus Zietsman and Ferdi Zietsman for their advice and assistance concerning the experimental tests

Calvin Hamerse, technical assistant, for his assistance with the installation of the radiator for experimental tests

Dr. Martin van Staden, an engineering consultant from Aerotherm, for his services and assistance regarding the application of the CFD Software

The author's family, for their morale support and love during the course of the project

God, for His blessings and guidance from above

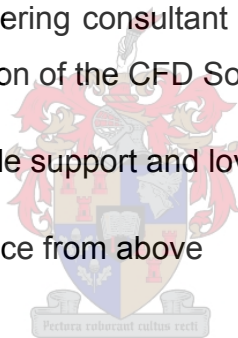
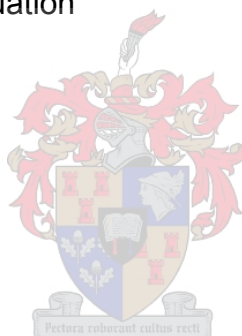


TABLE OF CONTENTS

	Page
DECLARATION	i
ABSTRACT	ii
OPSOMMING	iv
ACKNOWLEDGEMENTS	vi
LIST OF FIGURES	ix
LIST OF TABLES	xi
NOMENCLATURE	xii
1 INTRODUCTION	1
2 LITERATURE REVIEW	3
2.1 Overview	3
2.2 Objectives	3
2.3 Present South Africa Situation	3
2.4 Previous Work	4
2.5 Discussion	7
3 EXPERIMENTAL WORK	9
3.1 Overview	9
3.2 Objectives	9
3.3 Equipment	10
3.3.1 Subsonic wind tunnel	10
3.3.2 Vehicle	15
3.3.3 Radiator test facility	17
3.3.4 Measuring equipment	18
3.4 Calibration	21
3.5 Radiator Tests	22
3.5.1 Procedures	22
3.5.2 Results	23
3.6 Underhood Tests	25
3.6.1 Procedures	25
3.6.2 Results	29
3.7 Discussion	30
4 NUMERICAL WORK	31
	vii



4.1	Overview	31
4.2	Objectives	31
4.3	Equipment	31
4.4	Assumptions	32
4.5	Geometry	33
4.6	Mesh Generation	35
4.7	Simulation Parameters and Models	40
4.8	Solver	44
4.9	Results	45
4.9.1	Stationary case	45
4.9.2	Moving case	49
4.10	Discussion	52
5	NUMERICAL VERIFICATION	53
5.1	Overview	53
5.2	Objectives	53
5.3	Numerical Evaluation	53
5.3.1	Residuals	54
5.4	Discussion	63
6	EXPERIMENTAL COMPARISON	64
6.1	Overview	64
6.2	Objectives	64
6.3	Experimental comparison	64
6.4	Discussion	65
7	CONCLUSION AND RECOMMENDATIONS	66
7.1	Conclusions	66
7.2	Recommendations	67
8	REFERENCES	69



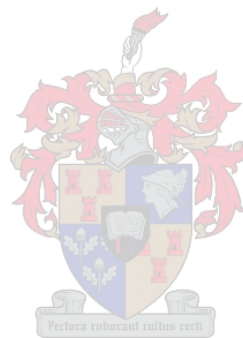
LIST OF FIGURES

	Page
Figure 1: Schematic layout of the subsonic wind tunnel (Stander, 2004).....	11
Figure 2: The suction fan of the wind tunnel	12
Figure 3: The hydraulic actuated doors in the closed position	13
Figure 4: Wind tunnel intake section as seen from within	14
Figure 5: Wind tunnel intake section as seen from outside.....	14
Figure 6: Volkswagen Citi Golf Chico 1.3	15
Figure 7: Volkswagen Citi Golf Chico 1.3 side view	15
Figure 8: Volkswagen Citi Golf underhood	16
Figure 9: Vehicle parked in the tunnel with experimental apparatus in place.....	17
Figure 10: Schematic layout of the experimental wind tunnel (Kröger, 2004).....	18
Figure 11: Raytek Ti30 Thermoview thermal imager.....	18
Figure 12: Endress and Hauser Deltabar Pressure transducer	19
Figure 13: HP 34970A data-logger	20
Figure 14: Tufts taped to the Perspex sheet.....	20
Figure 15: Visualization of airflow via Perspex bonnet	21
Figure 16: Visualization of the airflow under the car	21
Figure 17: Heat exchanger experimental setup	23
Figure 18: Pressure drop versus velocity	24
Figure 19: Heat transfer versus velocity	24
Figure 20: Equipment connections	26
Figure 21: Thermocouple positions in the underhood.....	26
Figure 22: Pitot-static probe for velocity measuring.....	27
Figure 23: Thermal image of exposed exhaust manifold	28
Figure 24: Thermal image of the radiator through the grill	28
Figure 25: Thermal image of the radiator reservoir.....	28
Figure 26: A hardboard cover obstructing the thermal imager	30
Figure 27: Volkswagen Citi Golf Chico underhood environment.....	34
Figure 28: CAD model of the Volkswagen Golf Chico used for CFD	34
Figure 29: Volkswagen Golf Chico underhood layout for CFD.....	35
Figure 30: Front view of underhood environment with grill removed	35
Figure 31: Polyhedral mesh created during initial stages of the project.....	36

Figure 32: Transparent polyhedral mesh revealing the underlying geometry	37
Figure 33: Wire frame model of the CAD Geometry	38
Figure 34: Slice from the mesh generated from the geometry.....	38
Figure 35: Zoomed view of the underhood region	39
Figure 36: Zoomed view of the radiator and fan housing.....	39
Figure 37: Underhood boundary conditions with grill removed	40
Figure 38: Tunnel boundary conditions.....	41
Figure 39: Temperature distribution of a section through the fan	46
Figure 40: Velocity vectors of a section through the fan	46
Figure 41: Temperature distribution of a section through the air intake	47
Figure 42: Velocity vectors of a section through the air intake.....	47
Figure 43: Temperature distribution in a horizontal plane through the fan	48
Figure 44: Temperature distribution through the central plane.....	48
Figure 45: Temperature distribution through the central plane.....	50
Figure 46: Temperature distribution in a vertical plane through the fan	50
Figure 47: Velocity vectors in a vertical plane through the fan.....	51
Figure 48: Top view temperature distribution through the fan	51
Figure 49: Top view velocity distribution through the fan	52
Figure 50: Residuals for the final stationary solution	55
Figure 51: Residuals for the final moving solution	55
Figure 52: Field values from the final stationary simulation	56
Figure 53: Field values from the final moving case.....	57
Figure 54: Airflow profile in front of the vehicle for the stationary case	58
Figure 55: Airflow profile behind the vehicle for the stationary case	58
Figure 56: Airflow profile in the underhood for the stationary case	59
Figure 57: Airflow profile in front of the vehicle for the moving case	59
Figure 58: Airflow profile behind the vehicle for the moving case	60
Figure 59: Airflow profile in the underhood for the moving case	60
Figure 60: y^+ values in the underhood for the stationary case	61
Figure 61: y^+ values in front of the vehicle for the stationary case.....	62
Figure 62: y^+ value in the underhood for the moving case.....	62
Figure 63: y^+ values in front of the vehicle for the moving case.....	63

LIST OF TABLES

	Page
Table 1: Subsonic wind tunnel components.....	10
Table 2: Thermocouple positions	27
Table 3: Temperature measurements for experimentation	29
Table 4: Computer specifications	32
Table 5: Boundary conditions applied to the simulations	42
Table 6: Solver parameters.....	45
Table 7: Peak airflow speed through the fan shroud.....	64
Table 8: Comparison of numerical and experimental temperatures.....	65



NOMENCLATURE

3D	Three Dimensional
ABS	Anti-Lock Braking System
ASR	Acceleration Slip Regulation
CAD	Computer Aided Design
CAM	Computer Aided Manufacturing
CFD	Computational Fluid Dynamics
DPSS	Defence, Peace, Safety and Security
FEM	Finite element methods
IGES	Initial graphics exchange specification
LSV	Laser sheet visualisation
PBMR	Pebble Bed Modular Reactor
PDE	Partial differential equation
RNG	Reynolds normalisation group
SAE	Society of Automotive Engineers
VTMS	Vehicle thermal management systems
VW	Volkswagen
b_{fan}	Fan width
b_{rad}	Radiator width
r	Radius
T_{rad}	Radiator temperature
T_{env}	Environment temperature
u_i	Velocity in the i direction V_{mag} Velocity magnitude
V_{eq}	Equivalent velocity k Turbulence kinetic energy
α	Experimentally determined constant
β	Experimentally determined constant
ε	Turbulence kinetic energy dissipation rate
y^+	y -plus values used in boundary layer theory
ρ	Density of the air
ω	Angular velocity



1 INTRODUCTION

Since the birth of the automobile, people have improved its design to travel at higher velocities with greater acceleration. They advanced the suspension to improved comfort, manoeuvrability and safety and optimised the engines for increased fuel efficiency and power. Modern automobiles have produced outstanding results in these regards, but uncovered new challenges, which required electronics to solve. These included the engine control unit, which monitors and manages engine parameters to ensure low emissions and better fuel consumption, antilock braking systems (ABS) to improve braking capabilities, acceleration slip regulation (ASR) traction control for improved acceleration and reduced wheel slippage and stability control to prevent skidding during sharp turns.

Electronics solved most problems encountered thus far, but there are still problems that plague automobile designers. This is the fluid flow and thermal conditions through and over the automobile. This category branches into the air-conditioning within the passenger compartment, air intake and combustion processes, underhood thermal management and flow around the automobile body. This thermal management appears simple, but what happens when the engine compartment known as the underhood contains a large engine, clustered by many components. These components block the air-flow through the underhood resulting in extreme temperatures that negatively affect the electronics within. These effects include altering the thermal sensitive properties of the electronics, reducing the functionality and reliability.

To assist the designing of this complicated environment, engineers have turned to a technology known as computational fluid dynamics (CFD). This technology allows the flow field and heat transfer of a fluid to be numerically calculated using finite volume methods and numerical models to simulate effects such as turbulence and radiation. Many automobile manufacturers including Mercedes Benz, Ferrari, BMW, Ford, Daimler and Renault have successfully used the technology.

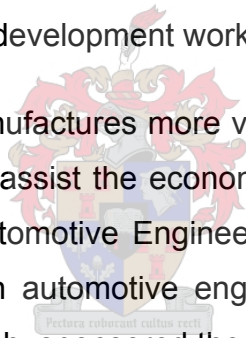
CFD is widely used internationally in the automotive field, but its automotive applications are limited and practised by few in South Africa. Attention to the development of such technology is required so that local manufacturers can modify and improve the automobiles to withstand South Africa's extreme climates.

The objective of this project was investigating the airflow and thermal processes that occur through an underhood by means of experimentation and numerical simulation. The goal was to develop a simple procedure for performing these types of simulations from computer aided design (CAD) models and demonstrate its application. This procedure includes the generation of a discretised mesh from a created CAD model and using a commercial CFD package to perform numerical simulations.

This procedure is common practise in the CFD community. However, as South Africa is still a developing country, research and development into such technology for automotive applications are of great importance if the country wishes to close the technology rift that has formed during past years. The advantages of such capability could result in South Africa expanding its own automotive industry, improving vehicles for the country.

While South Africa has successfully created an economic environment which makes it highly attractive for multi-national automotive companies to manufacture vehicles, only a limited amount of the associated development work is taking place in the country.

The idea is that South Africa manufactures more vehicles for its local market and international export. This will in turn assist the economic growth of the country. It was for this reason that Stellenbosch Automotive Engineering (Pty) Ltd, trading as Centre for Automotive Engineers (CAE), an automotive engineering research and development company initially from Stellenbosch, sponsored the work of this project.



2 LITERATURE REVIEW

2.1 Overview

This chapter briefly discusses the current South Africa situation with respects to the CFD community and describes previous research conducted in the international automotive field.

2.2 Objectives

The objective of the literature review was to understand the current situation in terms of CFD applications in South Africa.

The second goal was to obtain insight into the work performed in the automotive field with CFD as an analysis tool. This allowed a better understanding of the process required to conduct such numerical evaluations.

2.3 Present South Africa Situation

South Africa is a developing country with many untapped resources and technological gaps in the automotive industry. Although South Africa participates in the assembling of automobiles such as Toyota and Volkswagen, it still requires experience to conduct CFD simulations of automobiles to optimise them for harsh climates experienced in Southern Africa. South Africa currently has many types of CFD research projects undertaken at various institutions.

The Defence, Peace, Safety and Security (DPSS) division of the CSIR focuses mostly on large-scale simulations, including air ventilation through mines, missile aerodynamics, turbo machinery, supersonic waves and helicopter dynamics.

Aerotherm, an engineering consultancy company, focuses on large-scale commercial projects, including dam dynamics, chemical processes and hydroelectric power systems.

The North-West University in collaboration with the PBMR (Pty) Ltd Company currently conducts CFD research projects on the Pebble Bed Modular Reactor (PBMR), a new nuclear power station under development.

Many other smaller institutes such as Stellenbosch University and Cape Town University perform CFD simulations and research on a smaller scale.

Unfortunately, when compared to American and European countries, South Africa remains a small fish in the pond in terms of its automotive CFD applications. Companies such as Argonne National Laboratory, a transportation research and development laboratory in America conducts extensive research into all aspects vehicles and transportation. The Society of Automotive Engineers (SAE) collect and frequently releases papers and journals on all aspects related to automotive engineering with the goal of assisting the development self-propelled vehicles. InfoTech Enterprises Ltd. is another large automotive company with global offices based in India, Germany, Netherlands, United Kingdom, United States, Australia, Singapore and Dubai, which focuses on all aspects of automotive engineering.

2.4 Previous Work

Much work exists in the field of automotive engineering and the development of CFD models for underhood thermal management. These models allow the user to simulate the effects of the radiator and fan without requiring the geometric and computer intensive details of the fins, tubes and blades.

The following paragraphs mention some relevant work conducted over past years.

Winnard et al. (1995) conducted a study of the underhood thermal management of the Ford F-250 light truck with a 7.5 litre V-8 engine in a dynamometer, using cell blowers to simulate road speeds. The goal was to determine how the temperatures in the underhood could be reduced to the greatest extent. They investigated three options, namely; (1) diverting the radiator fan airflow from the engine compartment, (2) force air-cooling over the exhaust manifold with the manifold shielded and (3) the combination of the two methods. Their results indicated that diverting the radiator airflow away from the engine compartment had the dominating effect and that at high velocities the heat from the exhaust manifold is negligible compared to the radiator fan air.

Morris et al. (1997) experimentally investigated the directions and magnitudes of velocities in the wake of a truck fan. The fan was mounted directly on the engine with the radiator and shroud attach to the chassis. The nominal tip clearance was 25 mm, result-

ing in fan performance loss. The tests used a 457 mm fan with 10 blades, each having a chord length of 81 mm and a pitch angle of 41° . The velocity measurements were taken with an X-array hot-wire probe with tufts visually indicating flow directions. The result was a velocity profile, usable for further automotive fan research.

Abdul Ghani et al. (2000) discussed the design of a closed loop climatic wind tunnel. This tunnel presented possibilities for analysing vehicles under controlled environmental conditions such as varying rainfall type and wind directions. Fluent version 5.3.18 was used as a CFD tool to evaluate and optimise the key components of the tunnel. Well-established published data and laser sheet visualisation (LSV) data provided validation and verification of the CFD results. The result of the investigation was a compact wind tunnel with overall dimensions of approximately 3.0 m wide, 9.5 m tall and 9.5 m long.

Seider et al. (2001) developed an integrated numerical simulation strategy to analyse, optimise and control the highly coupled thermal systems of an automobile. These systems included the engine internal thermal system, coolant cycle, cooling module or radiator and a connected automatic transmission to the cooling cycle. The automobile used during this numerical investigation was the BMW 3-series compact car (E45/6) with a 2.5 litre, 6-cylinder inline engine (M54) and a ZF 5-speed automatic transmission (5HP-19). They used GT-Cool to model the performance maps of the cooling cycle and transmission and utilised CFD to determine the pressure drop through the cooling cycle. To perform the CFD analysis, they used ANSA to generate a CAD model, ICEM to create the discretised grids and STAR HPC version 3.050 as the CFD solver. This process resulted in the heat fluxes from the engine and transmission to be determined for slow uphill and high-speed horizontal travel.

Qian and Yuan (2001) used an integrated process of CFD analysis and design optimisation software to determine where an engine starter cap should be positioned in the underhood environment to minimise its temperature. They utilised Unigraphics to create the geometry, ICEMCFD to generate a discretised grid from the model, Fluent to perform the CFD simulations and iSIGHT to govern and optimise the process to obtain the best location for the starter cap. The result was a cap temperature of 117°C , compared to the initial temperature of 135.1°C . The measured temperature of the cap in the automobile was 130°C , which indicated that the vehicle had capacity for improvement.

Tzanos and Chien (2002) developed and validated a simple fan model for CFD investigations of the underhood thermal management. The objective involved implementing this model in a CFD code to represent the fan as a source of axial and circumferential body forces. Based on the actuator disk model, the fan model included blade and vortex theory. The STAR-CD CFD code provided validation for the model using the standard high Reynolds number $k-\epsilon$ model. The model proved to be a good compromise between accuracy and simulation time, with a maximum error of 14 %.

Mahmoud et al. (2003) developed a simulation-based vehicle thermal management system (VTMS), used to investigate the thermal systems of an automobile. These included passenger thermal comfort, power-train thermal behaviour and engine warm up rates. For the one-dimensional temperature analysis, they used AVL CRUISE to provide the load, operating and environmental conditions, along with controlling the data transfer between software packages. AVL BOOST simulated the gas circuits, while FLOWMASTER simulated the coolant and oil cycles. For the three-dimensional case, they used AVL FIRE coupled to the finite element packages, ABAQUS and MSC.NASTRAN to perform the analysis.

Shephard et al. (2003) discussed the missing components of the current technology for simulation-based design. He discussed efforts to develop the capabilities and integrate them with existing CAD models and computer aided engineering components. Simulation based design is a process in which simulation is the primary means of design evaluation and verification. Examples include CFD and finite element methods (FEM) as the computer aided engineering tool, using the geometry from the CAD model and discretised finite element or volume grids. This provides engineers with tools to analyse their data without unnecessary prototyping.

Carluccio et al. (2004) performed a numerical analysis of a cross-flow compact oil-air heat exchanger for vehicle applications. The objective was to determine its performance with relation to the heat transfer and pressure drop. They used Fluent version 6.1 to investigate the oil and airsides of the heat exchanger. Simulations conducted with and without fins, determined the effect the fins had on the flow characteristics. The numerical results and analytical solutions related and compared well.

Wang et al. (2005) did a numerical and experimental study on the 3-D flow field around a truck with a dome mounted on top of the cabin to determine whether it could reduce the drag and thus the energy required by it. This would streamline the airflow, in turn reducing the fuel consumption and allowing the vehicles to travel faster with less power requirements. They performed their analysis using the Reynolds normalisation group (RNG) $k-\epsilon$ turbulence model with grid size of up to 170 200 cells and a travelling velocity of 40 m/s (144 km/h). The result was a drag reduction of up to 21.5 %.

2.5 Discussion

The literature describes various aspects of the automotive design procedures and verifies that numerical simulations can represent complex environments such as the vehicle underhood with sufficient accuracy.

The general process deduced from the literature for performing numerical investigations can be summarised as follows. Firstly, the geometry is created using a CAD package. If automatic mesh generation is required, a program capable of creating the desired grid type is necessary. Finally, the CFD or FEM software performs the numerical analysis using the generated grids.

Assuming that the results from Winnard et al., (1995) are applicable to all automobiles, the effects of the exhaust manifold only account for a fraction of the heat transferred into the underhood environment. This allows a reasonable assumption that the radiation effects of the exhaust manifold and pipe effects are negligible.

The fan model developed by Tzanos and Chien (2002) and the experimental methods used by Morris et al. (1997) proved tempting to implement initially. Experimental investigation and initial simulations indicated that the effects of the fan could be captured by simpler methods. For this project, momentum sources in the axial and circumferential directions modelled the fan effects. Thus not requiring blade and vortex theory or enforcing a velocity profile within the simulations.

The idea from Abdul Ghani et al. (2000) of incorporating the wind tunnel geometry directly into the CFD simulations, side stepped the issues of tunnel blockage and additional wind tunnel compensations. This allows direct comparison of the numerical results to the experimental measurements.

The final deduction from the literature was the goal for the future of developing automobiles using only the simulation based design approach as indicated by Shephard et al. (2003). This would allow engineers to create the CAD and models using the computer aided engineering utilities such as FEM and CFD to evaluate their designs and eliminate the costly prototyping of each new model.



3 EXPERIMENTAL WORK

3.1 Overview

Experimental work provided additional information about the research problem and provided a basis for numerical evaluation. This section discusses the equipment and experimental procedures used to obtain acceptable results.

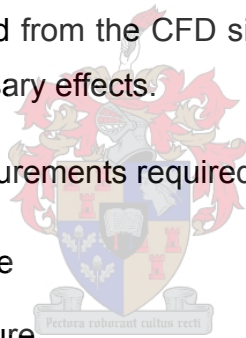
3.2 Objectives

The experimental work served two purposes. Firstly, to obtain an additional understanding of the underhood environment, determine the boundary conditions, momentum sources, momentum sinks and heat fluxes for use with the CFD simulations.

The second goal involved obtaining measurements to evaluate the numerical results to ensure that the solutions obtained from the CFD simulations were realistic and that the models used captured the necessary effects.

The list below indicates the measurements required for the numerical simulations:

- Engine surface temperature
- Radiator surface temperature
- Overflow reservoir temperature
- Exhaust manifold temperature
- Ambient air temperature
- Pressure drop over the radiator
- Airflow speed through the automobile fan
- Heat transfer through the radiator
- Airflow speed through the wind tunnel



The measurements taken for CFD verification purposes were:

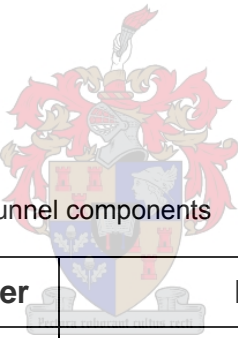
- Temperatures of the air at the four corners of the underhood envelope
- Temperatures before and after the radiator
- The inflowing velocity and temperature of the air from the radiator fan
- Visualizations of the airflow near the bonnet surface and under the automobile

3.3 Equipment

3.3.1 Subsonic wind tunnel

The subsonic wind tunnel situated at the Department of Mechanical Engineering in Stellenbosch was a critical component to this project. A schematic drawing provided in figure 1 indicates the various components of the wind tunnel. Table 1 provides a legend to these components.

Table 1: Subsonic wind tunnel components



Component Number	Description
1	Suction fan
2	Fan electrical drive motor
3	Flow regulation doors
4	Hydraulic pistons
5	Test section
6	Turbulence screens
7	Guide vanes
8	Pressure extraction points
9	Intake section
10	Diffuser outlet

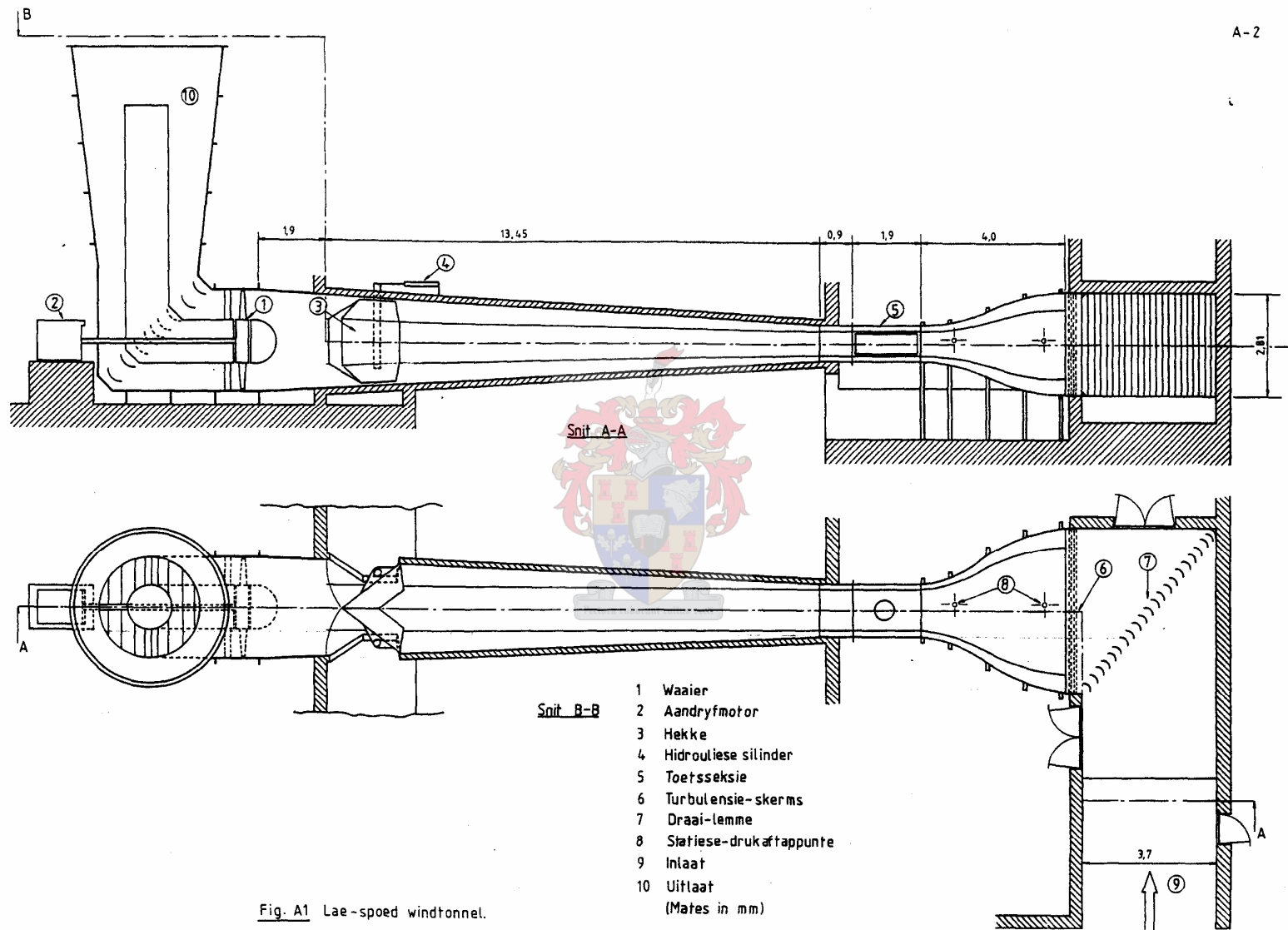


Fig. A1 Lae-spoed windtunnel.

Figure 1: Schematic layout of the subsonic wind tunnel (Stander, 2004)

In the following paragraphs, single digits in brackets refer to the component numbers provided in table 1 and figure 1.

The subsonic wind tunnel is an open circuit tunnel capable of producing average speeds of approximately 84 m/s (302 km/h) in the test section (5). The airflow for the tunnel is provided by a fan (1) consisting of 18 blades, with a length of 0.79 m and a fixed pitched angle of 50° relative to the fan axis. The steel fan has an overall diameter of 2.7 m. Powered by a 373 kW, 3-phase electric motor (2), the fan maintains a constant angular speed of 737 rpm. Figure 2 provides a view of the fan as seen from within the wind tunnel.

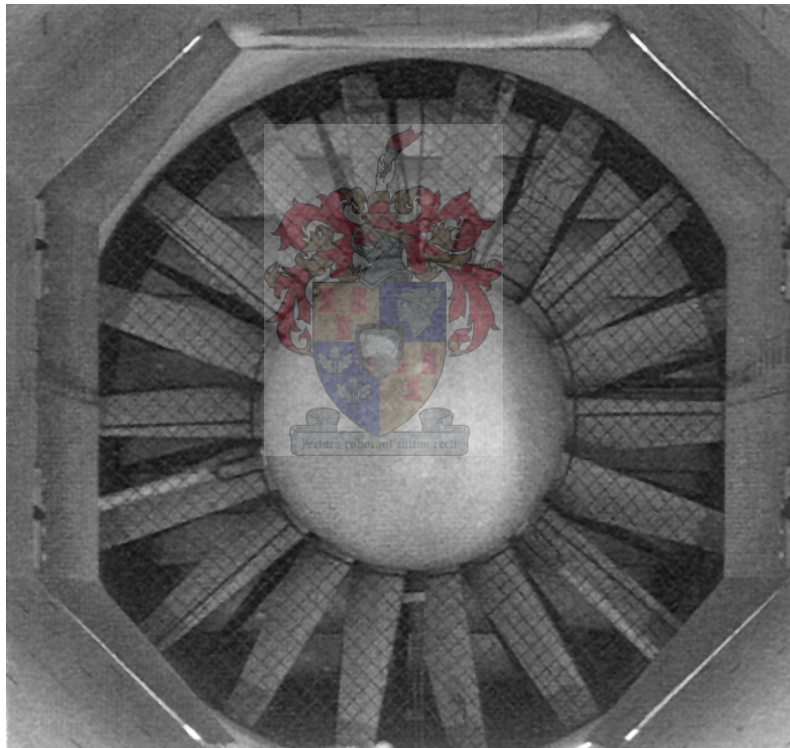


Figure 2: The suction fan of the wind tunnel

The airflow speed of the tunnel is controlled by two large steel doors (3) actuated using a hydraulic piston (4) situated above each door. The airflow can vary from approximately 0 m/s to 84 m/s, as the doors move from the closed to fully open positions. A remote control from within the tunnel test laboratory manipulates these doors. Figure 3 shows the doors in the closed position.



Figure 3: The hydraulic actuated doors in the closed position

This project forms part of a larger one known as “Project Cool”. The objective of the project is to utilise the intake of the wind tunnel for automotive tests to evaluate various aspect of test vehicles. These include its aerodynamics and underhood thermal management. The first part of the project entailed the construction of a ramp to allow vehicles to park in the intake section (9), parallel to the airflow. A student from the Mechanical Department designed and constructed this for his vacation training, Stander (2004). The effects of the installed ramp was an increase of the maximum tunnel airflow speed to approximately 90 m/s (324 km/h) and a boundary layer developing upon the ramp surface, which skewed the inlet profile to the test section (5). This distorted profile had little influence on this project as the vehicle underhood remained near the front of the ramp where the boundary layer had minimal thickness. Figure 4 and figure 5 provides views of the installed ramp as seen from inside and outside the tunnel intake.



Figure 4: Wind tunnel intake section as seen from within



Figure 5: Wind tunnel intake section as seen from outside

3.3.2 Vehicle

The automobile selected for the project was the 1996 model Volkswagen Citi Golf (also known as the Chico). It is front wheel driven, with a 1.3 litre, 48 kW, naturally aspirated 4-cylinder in-line engine. This engine lies transversely within the underhood and connects to a 5-speed manual transmission. Figure 6 and figure 7 provides a slanted and side view of the test vehicle respectively.



Figure 6: Volkswagen Citi Golf Chico 1.3



Figure 7: Volkswagen Citi Golf Chico 1.3 side view

This vehicle is one of the most popular vehicles found on the South African roads thus ensuring its availability. The advantages of this automobile was its simple underhood geometry, large ground clearance and compact size.

Figure 8 provides the vehicle underhood geometry. If the reader imagines the photo without all the cables and piping, it becomes clear that the remaining components form a simple layout easily represented with basic shapes. This simplification reduced the complexity of the underhood and served as a demonstration that these environments are analysable using CFD with only major components.

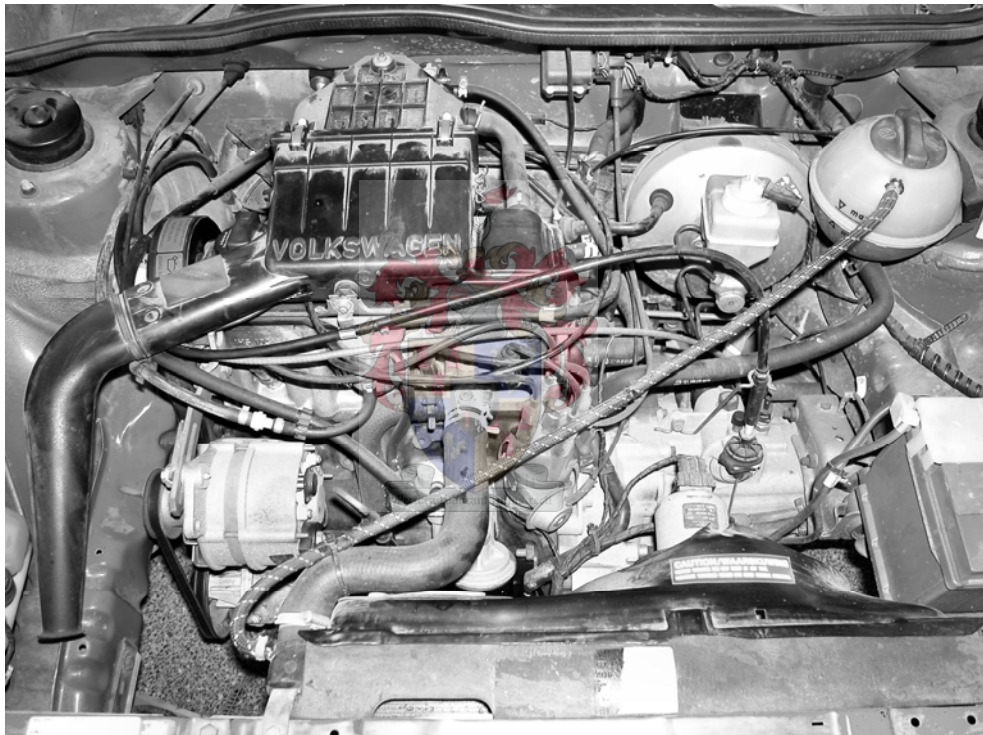


Figure 8: Volkswagen Citi Golf underhood

The large ground clearance of approximately 200 mm resulted in a large angle of departure. This allowed the vehicle to reverse into the wind tunnel without scraping the ground. Its compact size of; 3.815 m in length, 1.610 m in width and 1.410 m in height, allowed it to fit into the wind tunnel with dimensions of, 4.100 m in length, 3.700 m in width and 2.8 m in height as shown in figure 9.



Figure 9: Vehicle parked in the tunnel with experimental apparatus in place

3.3.3 Radiator test facility

Figure 10 provides a schematic representation of the radiator test facility situated in the thermodynamics laboratory at the Department of Mechanical Engineering at Stellenbosch (Kröger, 2004). The single digit numbers in brackets found in the following paragraphs refer to the component numbers in figure 10.

The installation of the test radiator (1) occurs at the entrance of the test tunnel. The air-flow speed through the radiator varies using a valve situated upwind of the centrifugal fan (8). The centrifugal fan, driven by an 11 kW electric motor, is capable of producing a maximum flow-rate of 3 m³/s and pressure rise of 2.0 kPa. The pressure drop over the nozzle (3, 7) determines the airspeed. Thermocouples placed upwind of the radiator measures the temperature of the air flowing into it with thermocouples positioned at (5) measuring the temperature of the air out of the radiator. An orifice plate and thermocouples respectively measured the mass flow rate and temperature of the hot water flowing in and out of the radiator. These measurements, along with the pressure differ-

ence over the radiator (3) provided the variables required for calculating the pressure drop and heat transfer characteristic curves of the radiator relative to the airflow velocity.

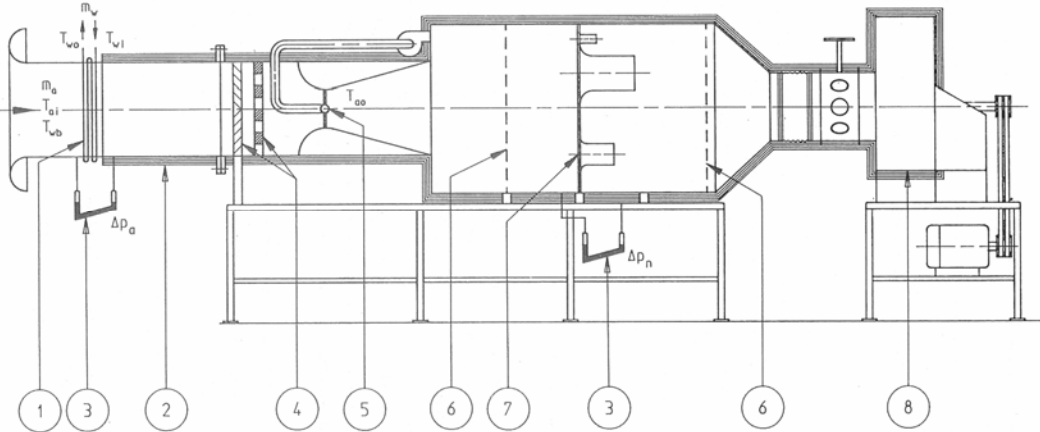


Figure 10: Schematic layout of the experimental wind tunnel (Kröger, 2004)

3.3.4 Measuring equipment

T-type thermocouples and a Ti30 Thermoview thermal imager from Raytek, presented in figure 11, measured the temperatures mentioned in section 3.2. The thermal imager has the ability of measuring surface temperatures between 0.0 °C and 255.0 °C with 2.0 % accuracy and repeatability of 1.0 %.



Figure 11: Raytek Ti30 Thermoview thermal imager

An Endress and Hauser Deltabar S pressure transducer, shown in figure 12, measured the dynamic pressure drop across a pitot-static probe, from which the velocity through the subsonic wind tunnel was calculated. Similar pressure transducers measured the differential pressure drops over the radiator and nozzles during the radiator tests. These pressure transducers are capable of measuring pressures between 0.0 kPa and 2.5 kPa with an accuracy of 0.075 %.

A TA5 hand held hot film anemometer from DP Measurement measured the air speed through the radiator fan and verified the wind tunnel air speed. The anemometer has a measurement range of 0.0 m/s to 30.0 m/s with an accuracy of approximately 2 %.

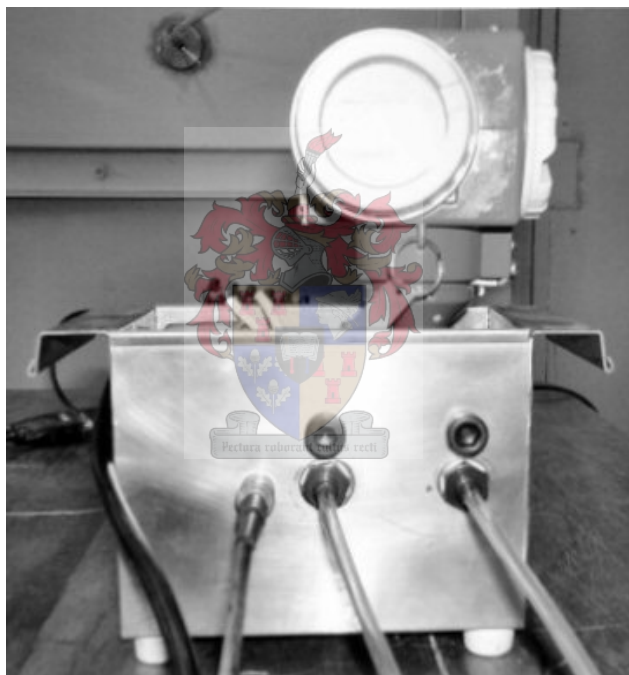


Figure 12: Endress and Hauser Deltabar Pressure transducer

A HP 34970A Data-logger, shown in figure 13, captured the pressure and temperature readings from the pressure transducer and nine thermocouples. An IBM ThinkPad R31 laptop recorded and processed the readings received from the data-logger. The Agilent Benchlink software accompanying the data-logger provided the connection between the two devices.



Figure 13: HP 34970A data-logger

A Perspex sheet taped with red tufts, shown in figure 14 and figure 15, helped visualise the airflow through the underhood. These tufts were only capable of indicating high flow and low flow regions. The flow patterns seen proved inconclusive and are not further discussed. Longer lengths attached to the vehicle skirting visualised the flow around the vehicle undercarriage, as seen in figure 16.

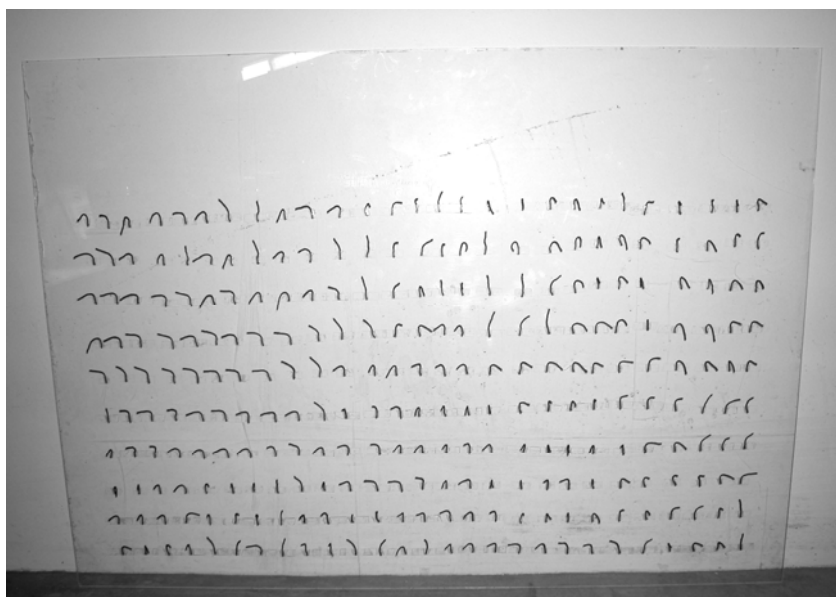


Figure 14: Tufts taped to the Perspex sheet



Figure 15: Visualization of airflow via Perspex bonnet



Figure 16: Visualization of the airflow under the car

3.4 Calibration

Before experimentation occurred, the equipment used required calibration. The instruments accepted to be correct were the Betz micro-manometer, thermal imager and hand held hot-wire anemometer. Comparing the thermal imager readings with known surface temperatures and the hand-held anemometer readings with the pitot-static

probe readings, verified their validity. The following paragraphs describe the methods used to calibrate the thermocouples and pressure transducers.

The nine thermocouples were calibrated under two conditions. The thermocouples were first placed together in a container of water at room temperature and then in a container of boiling water. The measurements from both cases indicated a maximum difference of 0.2 °C between the maximum and minimum readings. This was acceptable for the purpose of the project.

The pressure transducers were individually calibrated with a Betz micro-manometer 5000. The Betz micro-manometer 5000 has a range of -100 Pa to 5000 Pa with an accuracy of 0.04 % over its full-scale. The manometer reading was recorded along with the voltage reading obtained from the data-logger for each pressure induced. The result was a linear fitted curve through the data points, producing an equation for each pressure transducer to convert its voltage reading to pressure.

3.5 Radiator Tests



3.5.1 Procedures

The test facility discussed in section 3.3.3, was used to investigate the radiator of the vehicle. Single digit numbers in brackets in this paragraph refer to figure 10. The radiator (1) was attached to the inlet of the facility as shown in figure 17. Water at 80 °C was pumped through the radiator. The water temperatures entering and exiting the radiator and water flow rate were measured with thermocouples and an orifice plate. Further pressure transducers were used to measure the pressure before the nozzle (7) and pressure drops over the radiator and nozzle (3).

The radiator was tested at various velocities, resulting in the following useful data:

- average airflow speed through the radiator
- heat transfer by the radiator
- pressure drop across the radiator

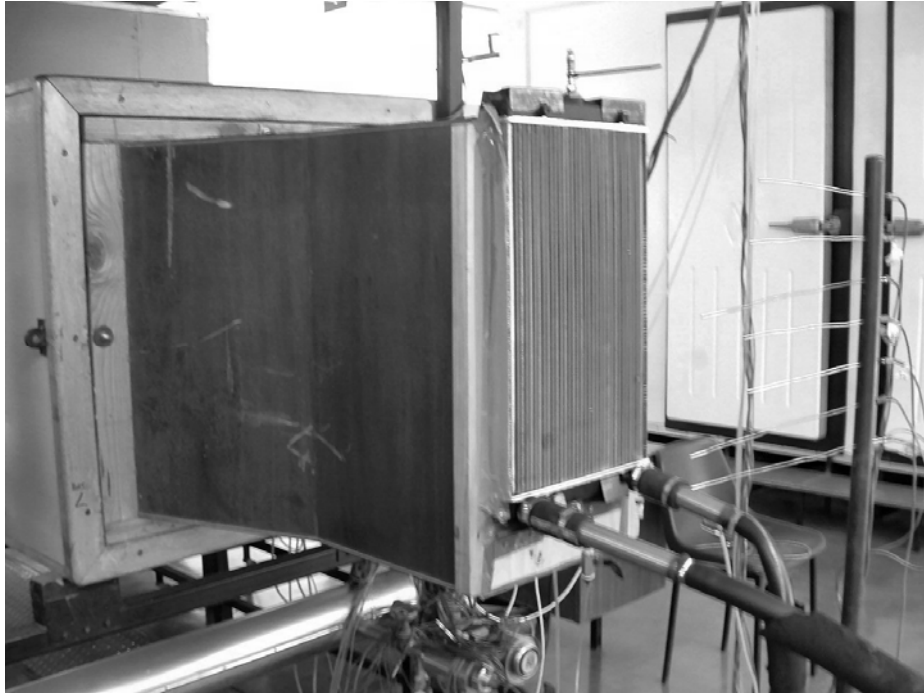


Figure 17: Heat exchanger experimental setup

3.5.2 Results

The results from the radiator tests are presented in figure 18 and figure 19. Figure 19 provides the pressure drop and figure 18 the heat transfer of the radiator versus the air speed through the radiator. Appendix B provides a sample calculations for these values.

The equations given in figure 18 and figure 19 describe the second and third order curve fits, which had regression coefficients of $R^2=0.9995$ and $R^2=0.9999$ respectively. The regression coefficients were determined using Microsoft Excel.

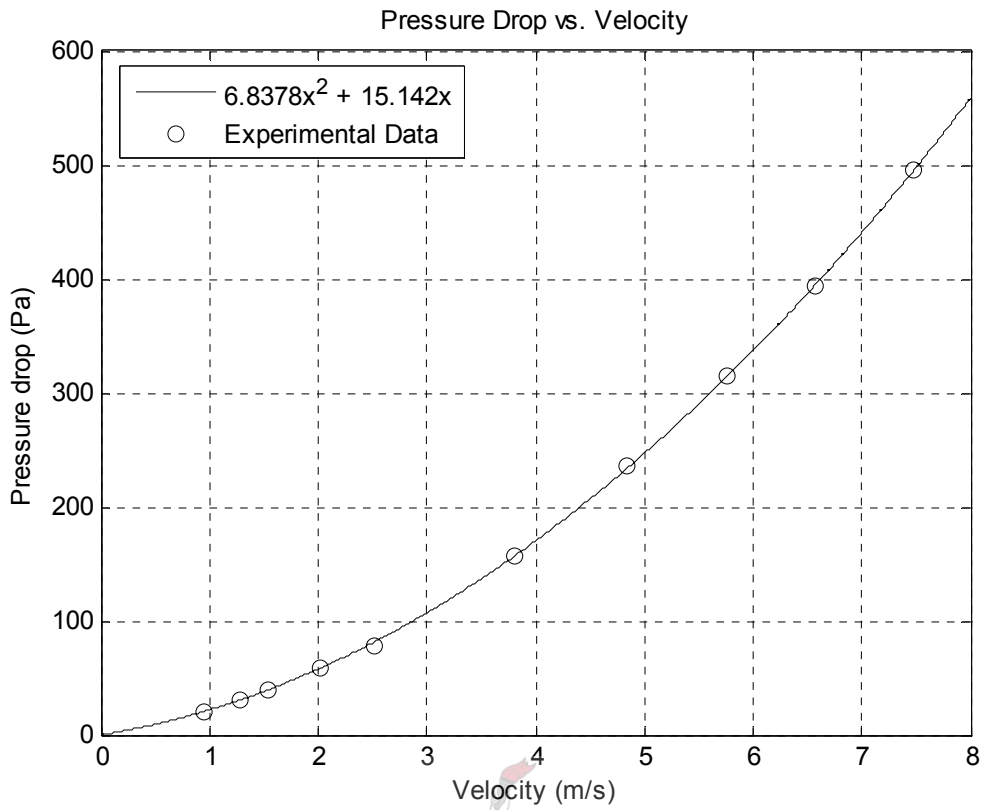


Figure 18: Pressure drop versus velocity

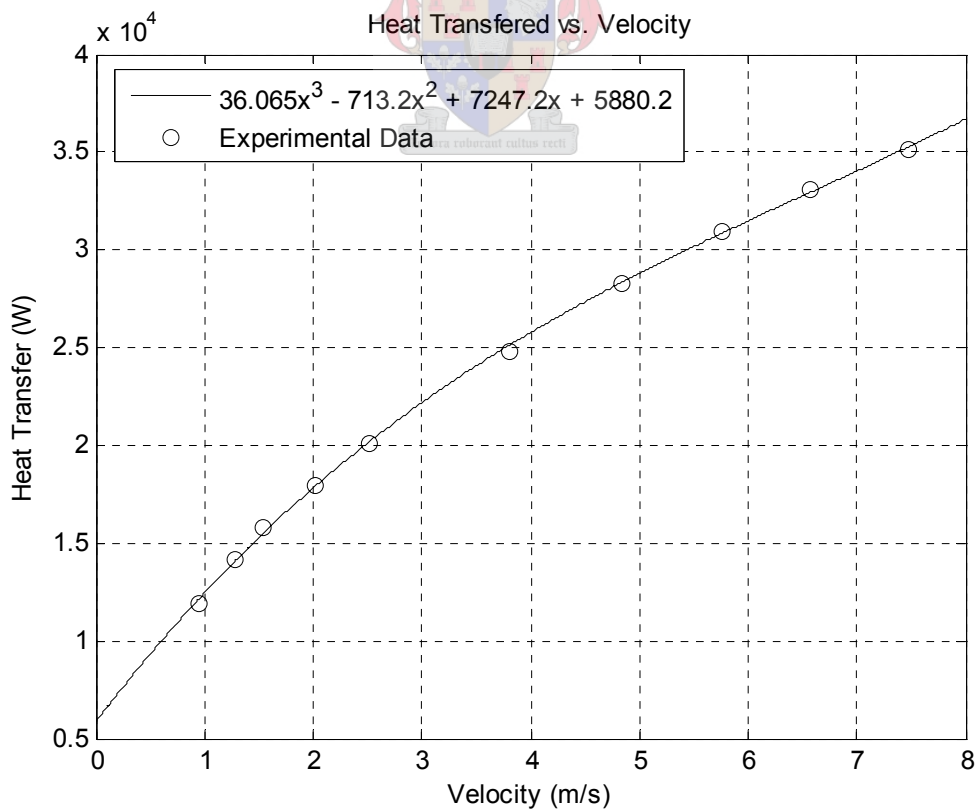


Figure 19: Heat transfer versus velocity

3.6 Underhood Tests

3.6.1 Procedures

Experimentally investigating two test cases eliminated coincidence from the numerical results. The first case consisted of the surrounding air of the subsonic wind tunnel remaining near stationary while the radiator fan ran continuously. This resulted in a steady state condition, meaning that small perturbations in the underhood were averaged to provide a single general solution. Henceforth this case is referred to as the “stationary case”. The second case involved drawing the air over the vehicle at approximately 5 m/s (18 km/h) with the wind tunnel. This case never required the radiator fan to run, also producing a steady state condition, henceforth referred to as the “moving case”.

There exist four definite differences between performing vehicle experiments in a wind tunnel and driving the vehicle on the road. The wind tunnel tests a boundary layer develops on the ground surface, which is not present on the road. The dimensions of the wind tunnel distort the flow patterns around the automobile known as blockage. The wheels do not turn while the vehicle is stationary in the wind tunnel and the road surface and car body do not move relative to each other. To account for these influences, the numerical simulations were performed to mimic the experimental tests.

Figure 20 provides a schematic representation of the experimental layout. The pitot-static tube was connected to the pressure transducer using rubber tubing. The pressure transducer along with nine thermocouples was further attached to the data-logger, which was linked to the laptop. The data-logger acquired the measurements from the pressure transducer and thermocouples and sent these measurements to the laptop for processing and storage.

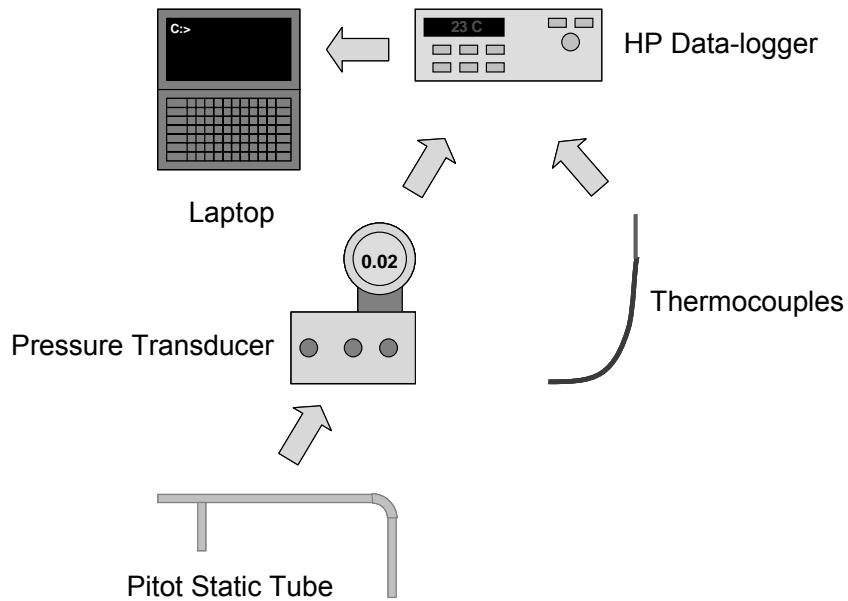


Figure 20: Equipment connections

The nine thermocouples were strategically positioned throughout the underhood to capture the temperatures of the engine block surface and surrounding air. Figure 21 indicates the positions of the thermocouples with numbered bubbles. Table 2 lists and describes these bubble positions.

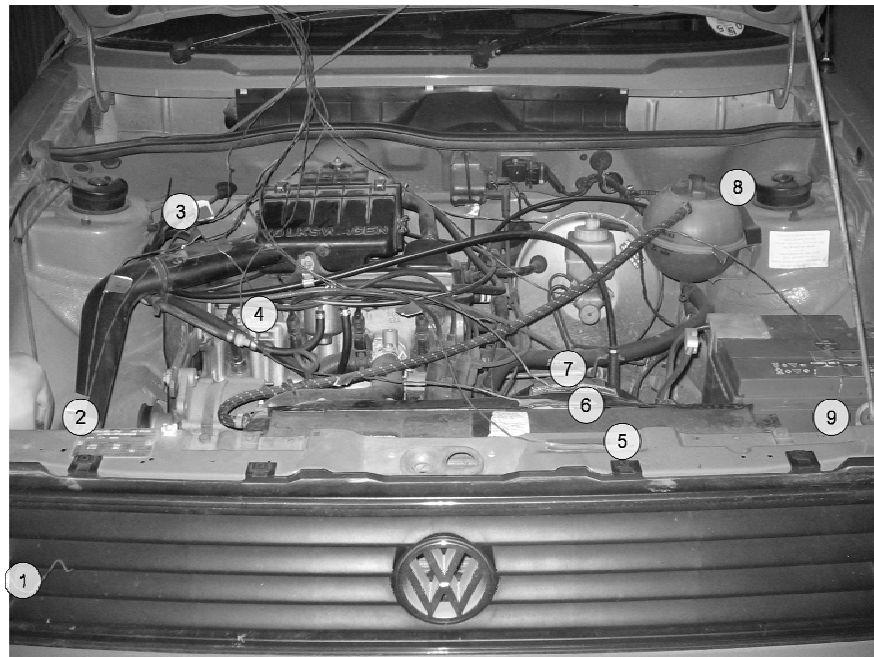
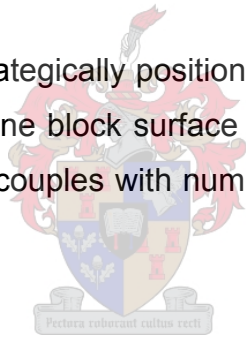


Figure 21: Thermocouple positions in the underhood

Table 2: Thermocouple positions

Position	Description
1	Ambient Air
2	Front Left Corner
3	Back Left Corner
4	Engine Surface
5	Radiator Inlet
6	Radiator Outlet
7	Fan Outlet
8	Back Right Corner
9	Front Right Corner

The Pitot-static probe used to measure the air speeds through the wind tunnel was positioned approximately 300 mm in front of the vehicle and 500 mm above the bonnet as indicated by the ellipse in figure 22. This position was selected because the airflow remained near uniform and not severely obscured by the vehicle.

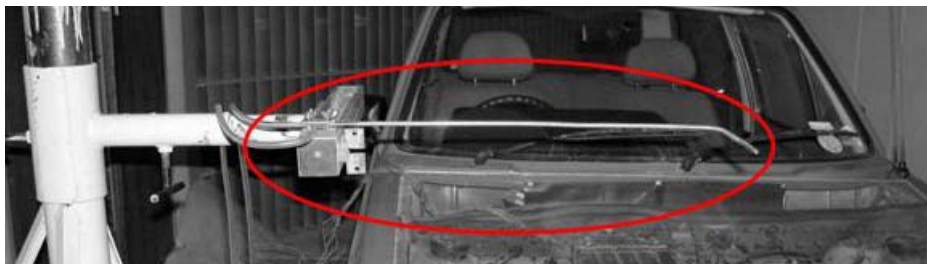


Figure 22: Pitot-static probe for velocity measuring

The Ti30 Thermoview infrared thermal camera was used to measure additional surface temperatures. These included the exposed exhaust manifold, radiator and radiator reservoir presented in figure 23, figure 24 and figure 25 respectively.

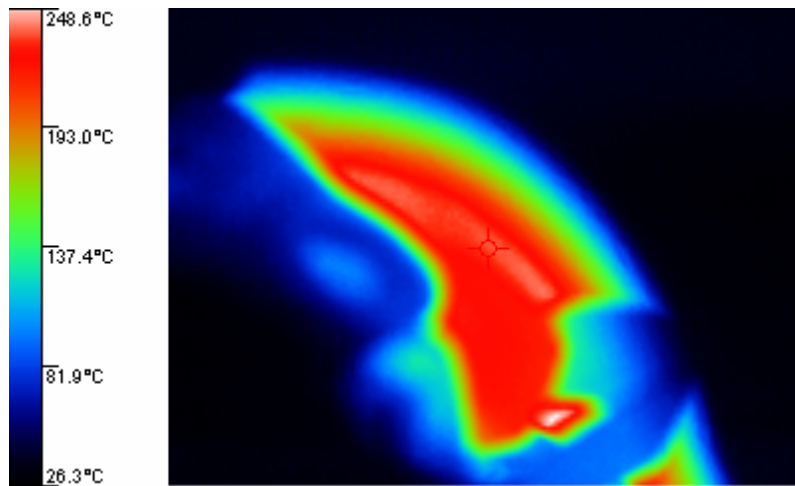


Figure 23: Thermal image of exposed exhaust manifold

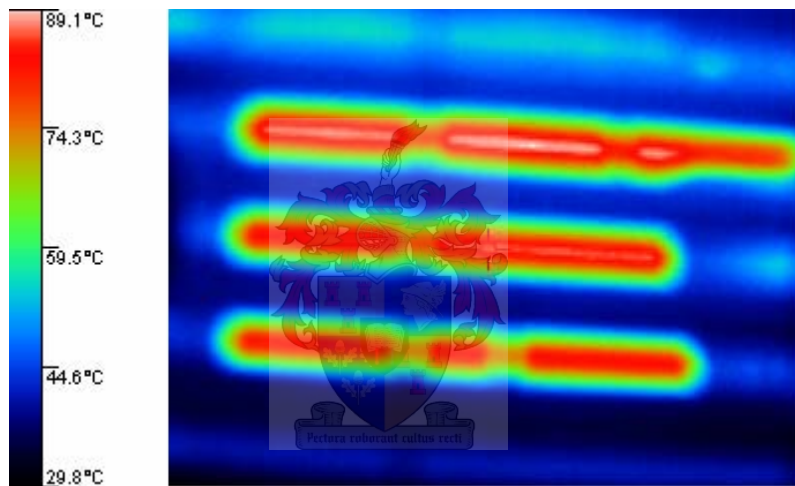


Figure 24: Thermal image of the radiator through the grill

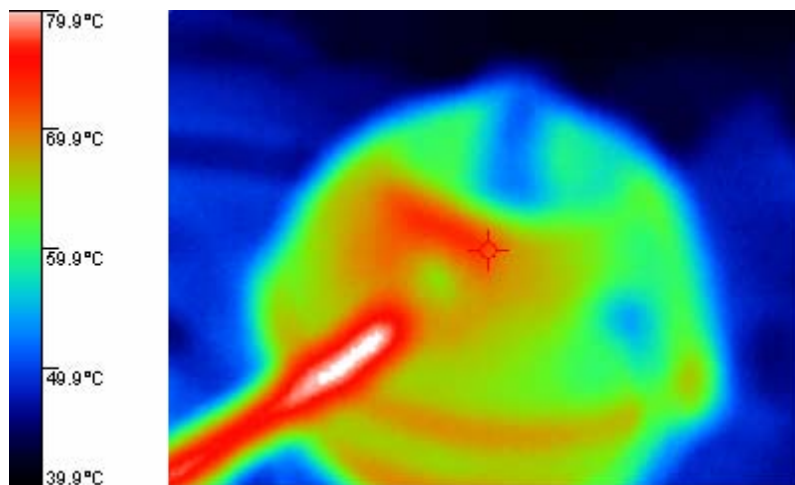


Figure 25: Thermal image of the radiator reservoir

3.6.2 Results

Ten tests were performed in total. They consisted of four stationary runs, two runs at 2 m/s and four runs at 5 m/s. The 2 m/s tests were not further investigated, as the results indicated a very dynamic and cyclic flow pattern. This pattern resulted from the automobile fan continuously switching on and off.

Table 3 provides the results from the processed thermocouples and infrared imager's surface temperature readings.

Table 3: Temperature measurements for experimentation

Position	Stationary	Moving
Ambient Air	24.0°C	23.5°C
Front Right	39.0°C	24.5°C
Back Right	42.0°C	29.0°C
Front Left	40.0°C	25.0°C
Back Left	40.0°C	33.5°C
Radiator Inlet	24.0°C	24.0°C
Radiator Outlet	36.5°C	73.0°C
Fan Outlet	36.0°C	64.5°C
Engine Surface	80.0°C	84.0°C
Exhaust Manifold Outlet	222.0°C	238.0°C
Radiator	25.0°C - 60.0°C	74.0°C

The flow through and around the vehicle was determined visually by means of tufts, which indicated flow activity and direction. The tufts indicated that while the radiator fan was active, the airflow near the fan outlet was high and very turbulent. Further, the air tended to flow out from under the vehicle near the front wheels during the stationary tests.

During the moving case, the tufts indicated high air speeds over and under the vehicle. These high velocities drew air out of the underhood, causing a small draft to exist through the grill and radiator.

3.7 Discussion

The radiator tests provided two characteristic curves, one for the heat transfer and the other for the pressure drop across the radiator as functions of the air speed through it. These curves were used to represent the radiator in the CFD model using FORTRAN version 8.2 for user coding. These codes are available in appendix B.

The data obtained from the vehicle tests were highly repeatable and remained approximately constant. This verified that the experimental data was representative of the processes occurring within the underhood environment. It also verified that the conditions investigated could indeed be modelled as steady state.

An interesting observation was made from figure 24, where there appears to be a cold spot in the lower right corner of the radiator. Further investigation revealed that a hardboard shield was present, indicated by the ellipse in figure 26, obscuring the view of the radiator from the thermal imager. This shield is probably intended for blocking the air-flow through the radiator near the thermostat, to allow it to obtain a better reading of the radiator water temperature.

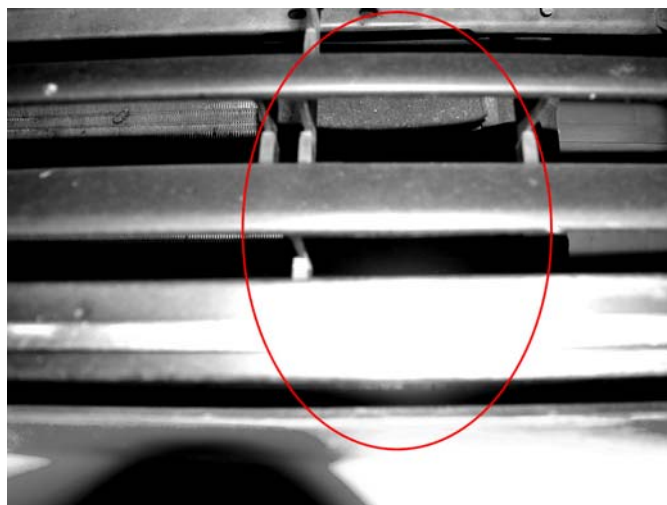


Figure 26: A hardboard cover obstructing the thermal imager

4 NUMERICAL WORK

4.1 Overview

This chapter discusses the processes followed to create the three-dimensional geometry of the vehicle, generate the discretised grids, perform the CFD simulations and extract the results.

4.2 Objectives

A foundation for the numerical modeling of thermal and flow processes that occurred in an automobile underhood formed the main objective.

This objective required the following procedures:

- Creating the geometry of the Volkswagen Citi Golf Chico 1.3 *litre*
- Generate a grid using an automatic mesh generator
- Applying the boundary conditions and solution parameters
- Implement fan and radiator models using user coding
- Extracting results for verification and experimental comparison

4.3 Equipment

To perform numerical simulations, requires computers, CAD software and a CFD analysis package. The following paragraphs describe each of these components.

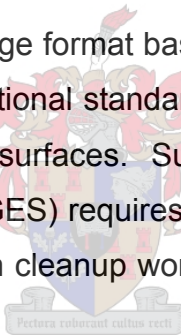
Table 4 provides the specifications of the two computers used to conduct simulations. The stationary case received the more powerful computer because it had a higher, more complex flow field through the underhood than the moving case.

Table 4: Computer specifications

Component	Specification	
	<i>Stationary</i>	<i>Moving</i>
Central Processing Unit (CPU)	Pentium® 4 CPU 3200 MHz	Pentium® 4 CPU 3200 MHz
Memory (RAM)	4096 MB	2048 MB
Hard drive	160 GB	120 GB
Motherboard (Intel)	D945GNT Neo	D865GLC

Solid Edge version 14 from EDS PLC solutions was the CAD software used to create the three-dimensional geometry of the vehicle. It produced files in the Parasolid format, which the automatic mesh generation software could import directly.

A Parasolid model is a data exchange format based on the Parasolid software package. This format has become an international standard and has the advantage of describing the geometry as a solid instead of surfaces. Surface based formats such as the initial graphics exchange specification (IGES) requires repair after importing. Thus, the Parasolid format eliminates the common cleanup work required to fix and stitch surfaces together after importing.



STAR-CD version 3.24 from CD-Adapco was the CFD software selected for the project. Although later versions of the code were available, version 3.24 proved to be the most stable. STAR-Design version 3.2 was the automatic mesh generation software selected. It is one of STAR-CD's companion codes.

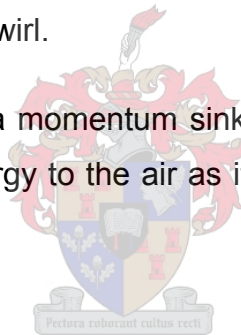
4.4 Assumptions

Before creating the numerical model, the geometry required simplification. The first reason for the simplification was the limited computational power available. Industrial simulations use high-resolution grids consisting of cells in excess of millions. The computers available at Stellenbosch could only handle lower-resolutions of 1.2 million tetrahedral cells. This project approached the CFD investigation as a demonstration of capability,

rather than investigating a particular thermal-flow component of the underhood. Thus, the analysis of the flow around the predominant features was satisfactory.

The following assumptions and simplifications limited the project requirements to a manageable scope.

- The network of cables and piping provided a negligible contribution to the thermal-flow analysis and were ignored.
- The underhood components geometries were simplified.
- Uniform temperature profiles represent the surface heat sources. These included the surfaces of the engine, gearbox, radiator reservoir, hot-water pipe and exhaust manifold.
- The fan behaved as a momentum source and accelerated the flow into the underhood while producing swirl.
- The radiator behaved as a momentum sink and a heat source, causing a pressure drop and adding energy to the air as it passed through the cells representing it.



4.5 Geometry

Figure 27 shows the geometry of the Volkswagen Citi Golf Chico 1.3 *litre* underhood environment. The underhood compartment has a simple layout, but contains a web of piping and wiring filling the spaces between major components.

Figure 28 to figure 30 shows the CAD geometry created for the numerical modeling. Figure 28 shows the complete car model. Figure 29 and figure 30 displays the underhood geometry with the bonnet removed to expose the individual. Figure 29 presents the top view of the underhood with all the major components and figure 30 shows the front view with the grill removed to reveal the radiator and fan as indicated.

The geometric model included the air-intake, engine, gearbox, battery, underhood outline, brake booster, radiator, fan, water bottle and radiator reservoir.



Figure 27: Volkswagen Citi Golf Chico underhood environment

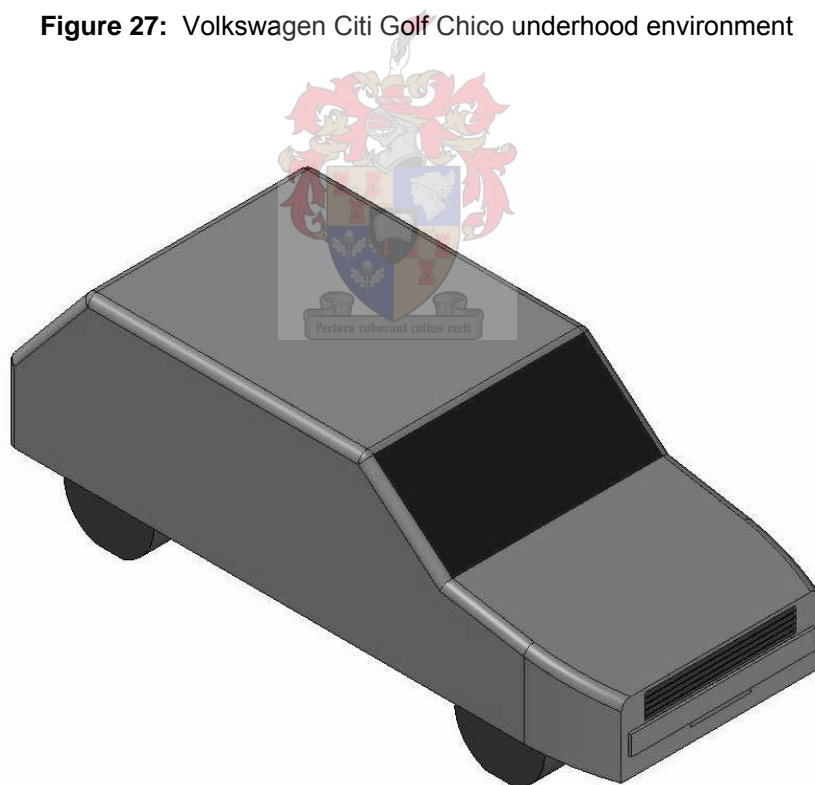


Figure 28: CAD model of the Volkswagen Golf Chico used for CFD

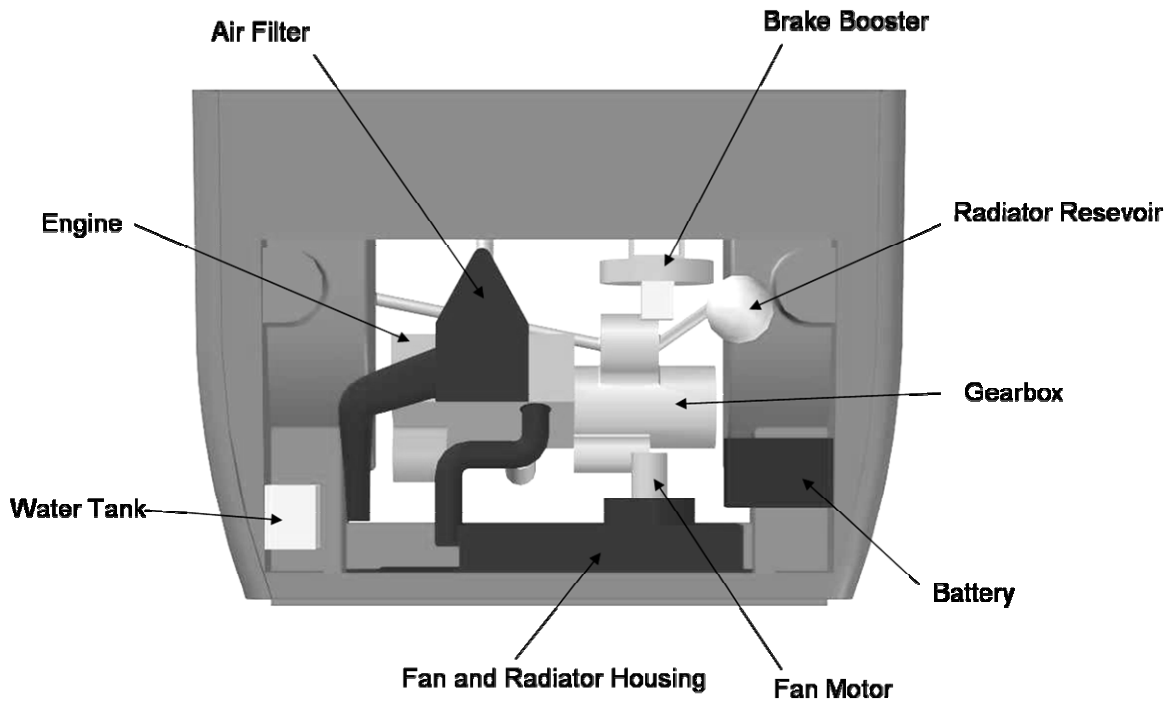


Figure 29: Volkswagen Golf Chico underhood layout for CFD

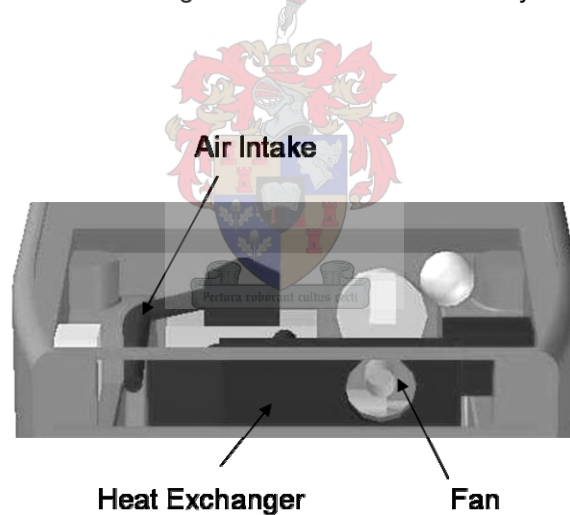


Figure 30: Front view of underhood environment with grill removed

4.6 Mesh Generation

The geometry discussed in the previous section formed the domain used to generate the meshes for the numerical simulations. The project initially opted for the polyhedral grid type, as it possesses many advantageous capabilities, particularly the reduction of false diffusion, thus requiring fewer cells to obtain a similar degree of accuracy as its tet-

rahedral counterpart. Another advantage of the polyhedral grid technology is its ability to eliminated mismatched cells. This is because the polyhedral cell type has no limit on its number of faces and simply treats mismatched cell faces the same as any other.

Previous experimentation with polyhedral technology was conducted on a low speed diffuser connected to a heat exchanger and nozzle, van Zyl (2006). The results proved that the technology worked with simple geometries. The mesh presented in figure 31 and figure 32 shows early attempts of using the polyhedral technology incorporated in the CFD software package STAR-CCM+ version 2.0. The author later determined that the beta version used still contained a number of critical bugs and lacked stability, indicating that the software had not yet matured to an acceptable level for use with this project.

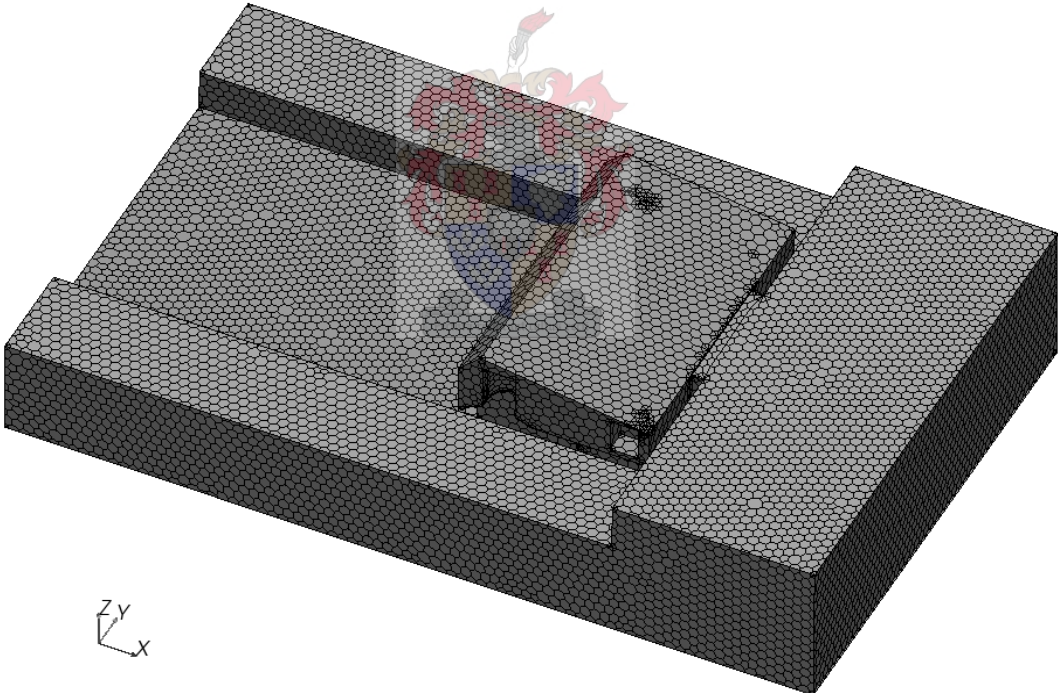


Figure 31: Polyhedral mesh created during initial stages of the project

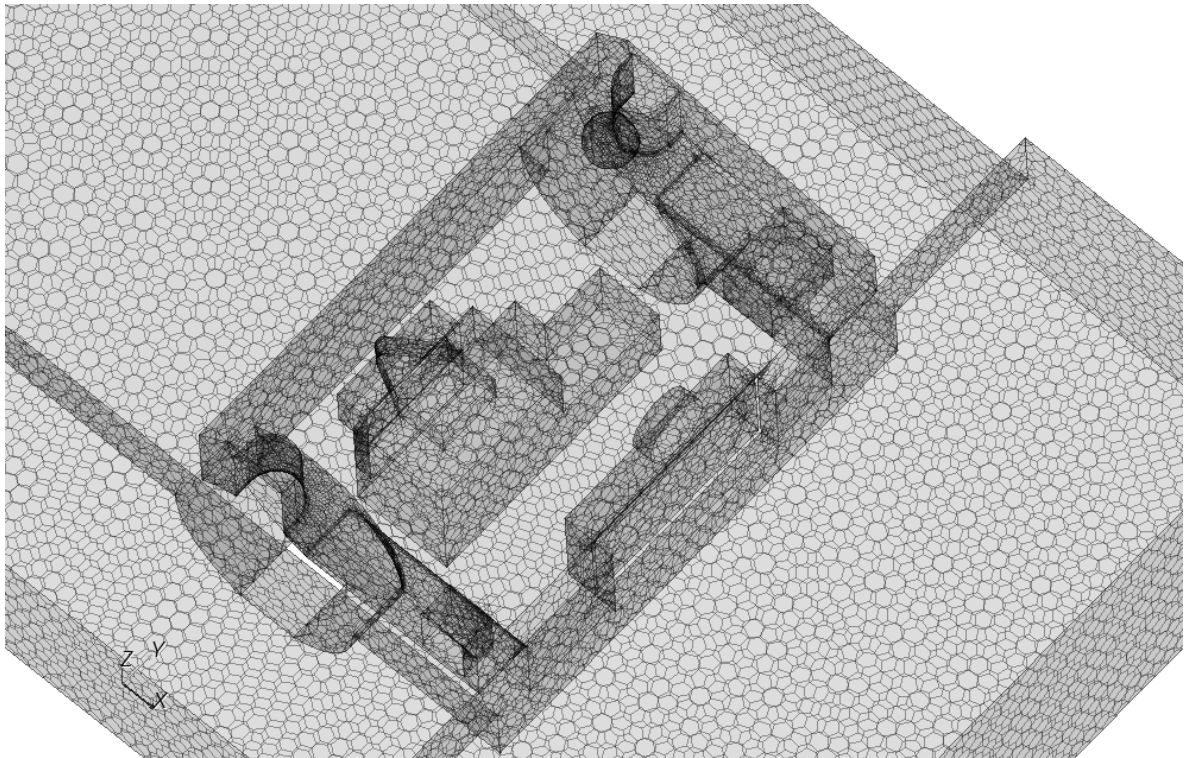


Figure 32: Transparent polyhedral mesh revealing the underlying geometry

Hexahedral grids appeared favourable after the polyhedral capable software proved insufficient. Although these cell types are numerically better than tetrahedral types in terms of false diffusion, convergence times and computational requirements, they continuously destroyed the surfaces of the geometry during the automatic meshing procedure. The tetrahedral cells types thus resulted as the only remaining option.

Figure 33 provides the geometric model used to generate the discretised grids. The model consists of a solid block with the automobile geometry cut from it, leaving only the air in and around the vehicle. Figure 34 presents a slice through the mesh generated using this method, making the automobile cut from a block analogy visible. Also visible in the figure are the various cells sizes. These ranged from the coarse (large) cells representing the airflow around the vehicle to the fine (small) cells representing the airflow through the smaller and more critical areas of the mesh.

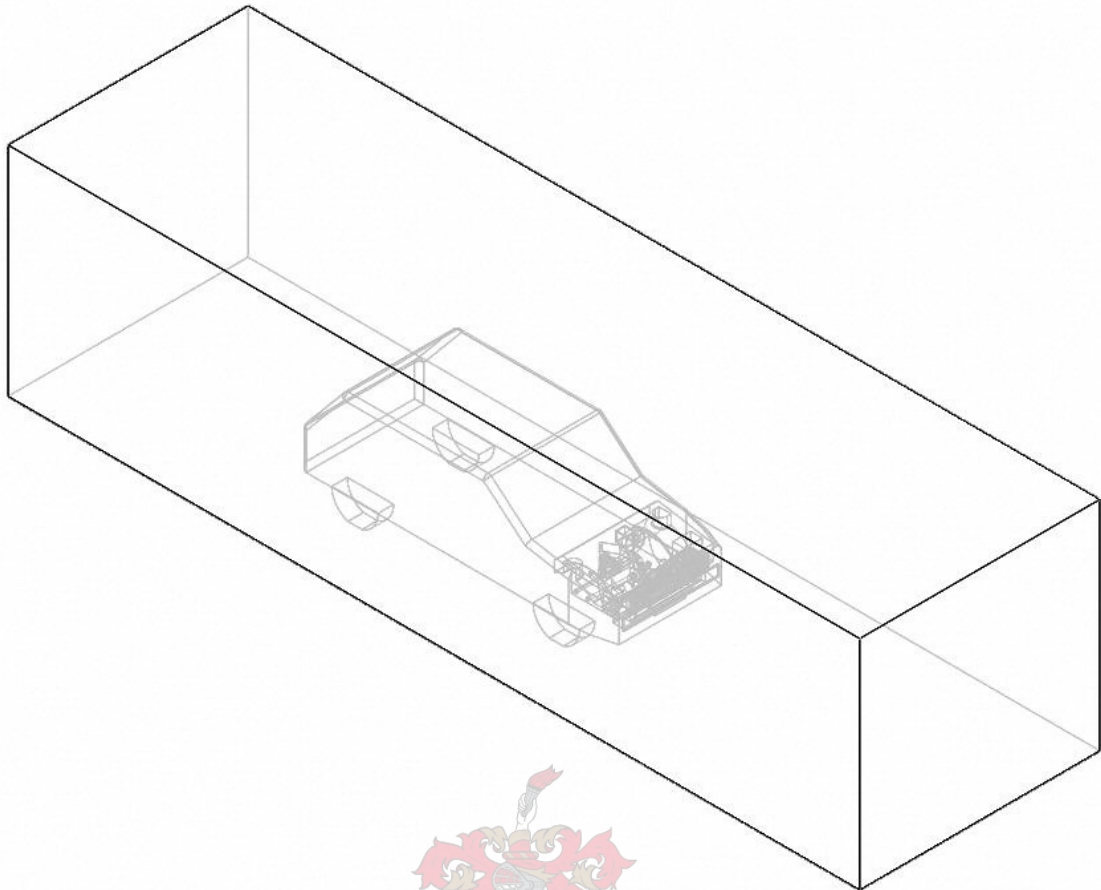


Figure 33: Wire frame model of the CAD Geometry

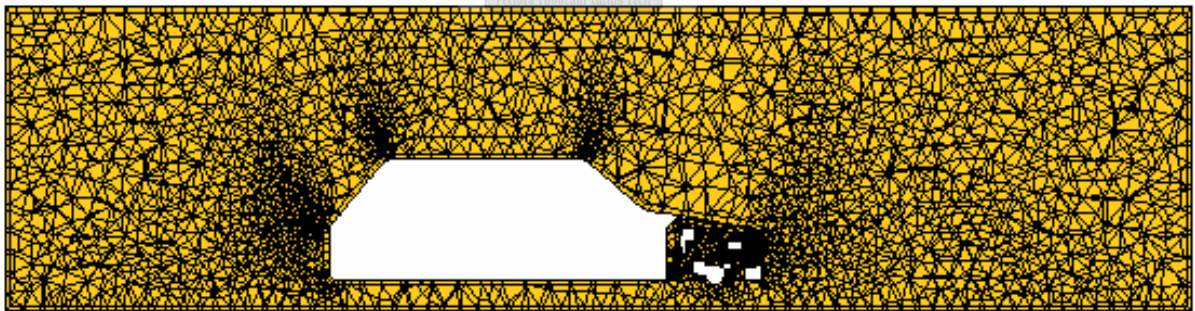


Figure 34: Slice from the mesh generated from the geometry

Figure 35 and figure 36 show magnified views of the underhood and radiator casing respectively. Figure 36 clearly shows the cells used to represent the fan (blue) and the radiator (green).

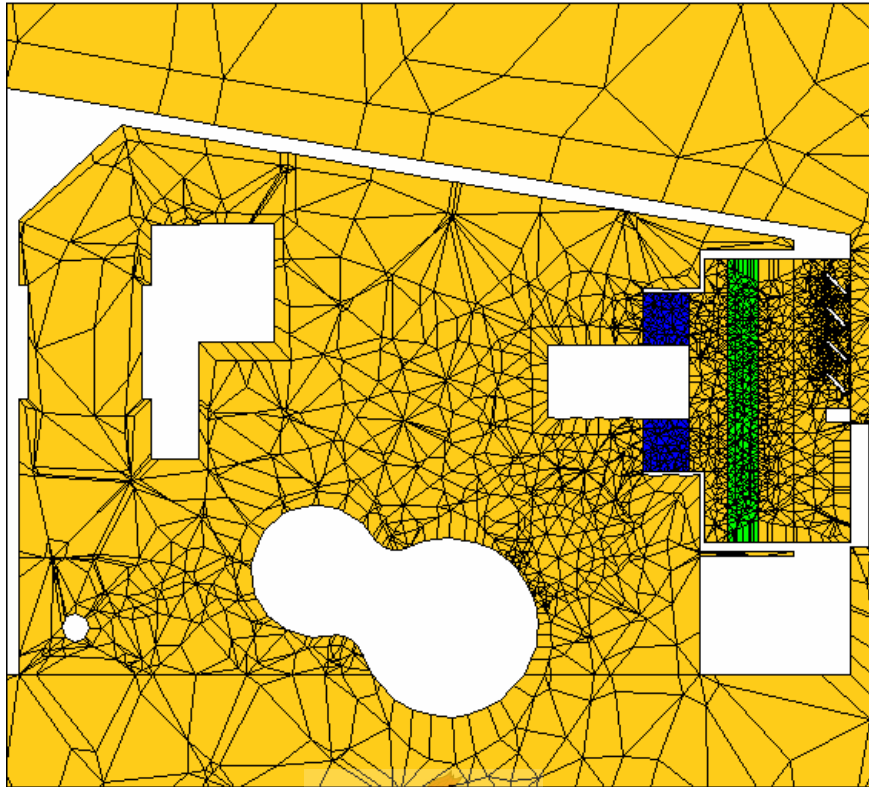


Figure 35: Zoomed view of the underhood region

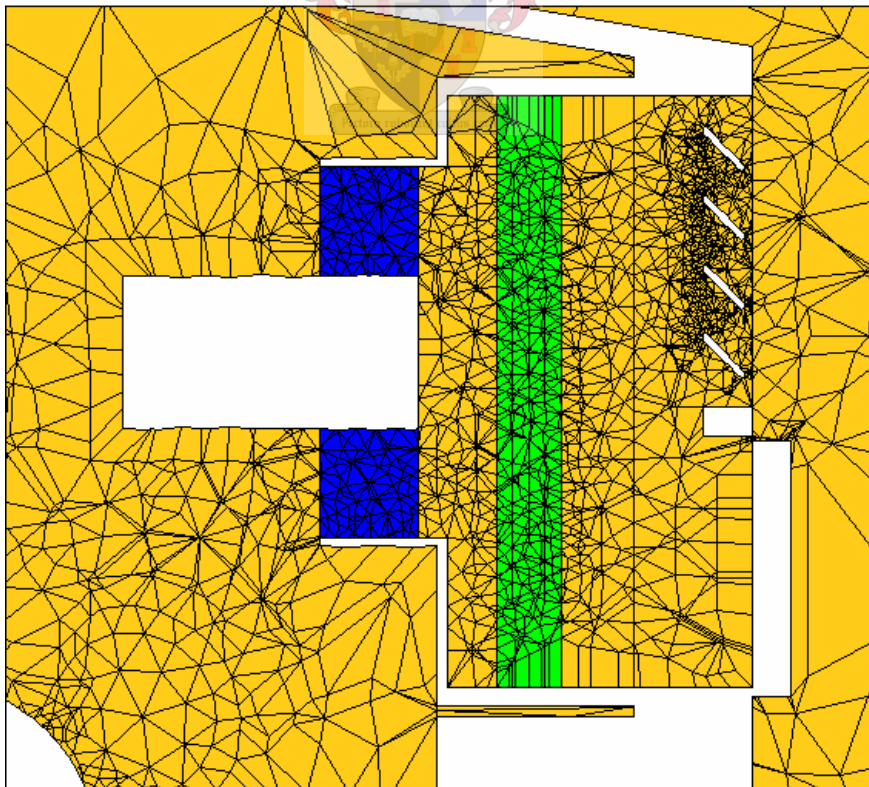


Figure 36: Zoomed view of the radiator and fan housing

4.7 Simulation Parameters and Models

The following paragraphs discuss the simulation parameters used in the modeling of the underhood environment. The investigation required the two cases addressed by the experimental test. To refresh the reader, the stationary case investigated the conditions where the vehicle remained stationary and the radiator fan provided the airflow through the underhood. The second case evaluated the condition where the wind tunnel drew air over the vehicle at 5 m/s (18 km/h) with the radiator fan never engaging.

Figure 37 indicates the positions of the temperature boundaries applied to selected surfaces in the underhood environment. The colour scheme represents a temperature range with the majority of the surfaces remaining adiabatic as indicated by silver. The coloured surfaces indicate the heat sources for the numerical model. Each colour indicates a respective temperature, thus the engine and water reservoir were determined to have similar temperatures and so forth.

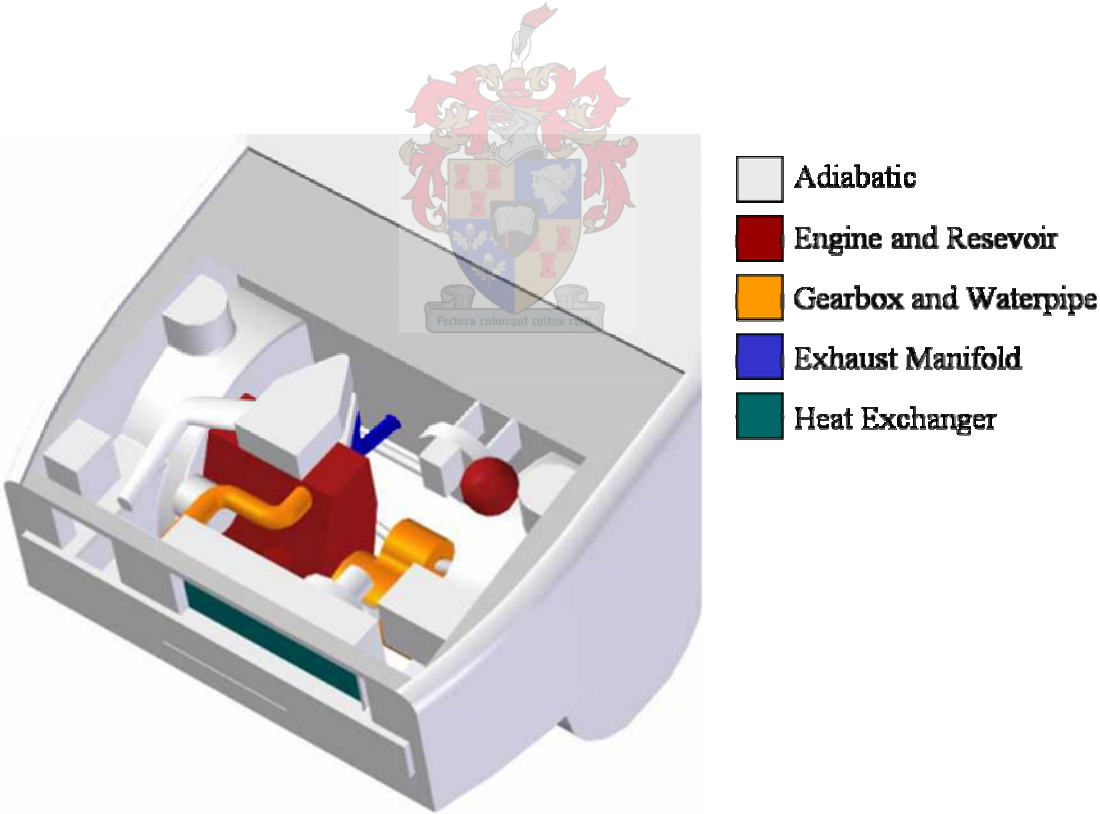


Figure 37: Underhood boundary conditions with grill removed

Figure 38 indicates the positions of the inlet and outlet boundary conditions for the wind tunnel. The inlet to the wind tunnel had a pressure profile applied using a pressure boundary. The pressure boundary requires the user to assign a specified pressure to all the cell nodes on the boundary. In this case, the pressure assigned was atmospheric. The outlet to the tunnel control volume has a velocity profile enforced by an inlet boundary. This boundary requires the user to apply a velocity profile to the cell nodes on the boundary. In this case, the velocity profile assigned represented the air drawn through and out of the tunnel. These conditions proved to represent the actual wind tunnel conditions most accurately.

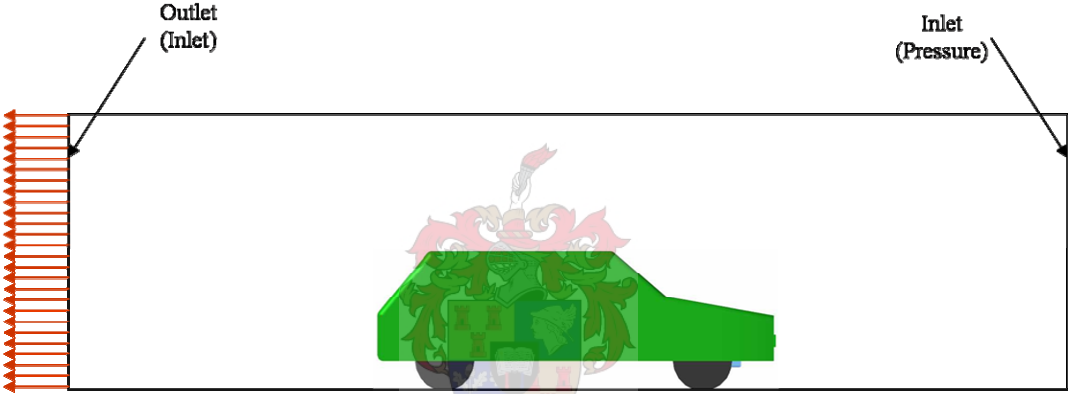


Figure 38: Tunnel boundary conditions

The turbulence model selected for the simulations was the high Reynolds number k-ε model with the standard log-law-of-the-wall boundary approximation. The requirement for the validity of this model is that the dimensionless parameter y^+ lies between 30 and 500.

Table 5 provides the boundary properties applied to the stationary and moving cases as illustrated by figure 37 and figure 38. The temperatures given in table 5 represent the surfaces of the heat sources experimentally determined, assuming that it remained constant. This resulted in the numerical solver determining the required heat fluxes from these temperatures.

Table 5: Boundary conditions applied to the simulations

Component or Position	Stationary		Moving	
	Boundary Type	Properties	Boundary Type	Properties
Engine Surface	Non-slip Wall	353.15 K	Non-slip Wall	357.15 K
Gearbox Surface	Non-slip Wall	333.15 K	Non-slip Wall	333.15 K
Exhaust Manifold Surface	Non-slip Wall	495.15 K	Non-slip Wall	511.15 K
Tunnel Wall Surface	Non-slip Wall	298.15 K	Non-slip Wall	298.15 K
Tunnel Entrance	Pressure	101 325 Pa	Pressure	101 325 Pa
Tunnel Exit	Inlet	-0.5 m/s	Inlet	-5 m/s
Hot Water Pipe	Non-slip Wall	333.15 K	Non-slip Wall	333.15 K
Water Reservoir	Non-slip Wall	353.15 K	Non-slip Wall	357.15 K

The turbulence of the incoming air was defined using turbulence intensity and turbulent length scale. For the stationary case the incoming air to the tunnel was assumed as zero, thus no turbulence was prescribed for this boundary. For the moving case, the air speed into the tunnel was 5 m/s. This resulted in a high turbulent flow and was assigned a turbulent intensity of 30 % with a length of 0.02 m.

The cells representing the fan in the domain had an additional momentum source term to simulate the effects of the radiator fan. The term increased the pressure from the inlet to the outlet of the fan, effectively forcing a rise in momentum and exit velocity of the fluid. This model allowed thermal energy to pass through the fan, density changes to occur and maintained continuity.

Initially an actuator disk model represented the fan, but was unable to capture all the effects necessary. Examining the assumptions accompanying an actuator disk model explains why it was not an acceptable option. These assumptions are:

- No rotation is imparted to the flow.
- Mach number is low, meaning that the flow behaves as an incompressible fluid.
- The flow imparts no work on the model.
- The flow is steady. Averaging out the moving blades so they become one thin steady disk with approximately the same effect on the flow as the moving blades.
- The pressure changes discontinuously across the actuator disk, but the velocity variation remains continuous.

It is thus clear that the actuator disk model would struggle to capture the effects required by this investigation. In particular, the density variation and energy transferred through it. The momentum source terms representing the fan in the axial and circumferential directions were:

$$S_{i,ax} = \frac{\rho V_{eq,ax}^2}{2b_{fan}} \quad (1)$$

$$S_{i,cir} = \frac{\rho(r\omega)^2}{2b_{fan}} \quad (2)$$

The cells representing the radiator contained an additional momentum sink and energy source term. The momentum sink caused the pressure drop of the radiator by removing momentum from the airflow as it passed through it. The same technique applied to directing the flow in only one direction through the radiator. The momentum sink term used in the flow direction was:

$$S_{i,rad} = (\alpha V_{mag} + \beta)u_i \quad (3)$$

Where α and β are experimentally determined constants.

An energy source term added to the enthalpy equations simulated the temperature rise in the radiator. Thus as the air passed through it energy was added resulting in a temperature rise of the air. The exit temperature is thus dependent on the airflow speed through the radiator. The energy source term used to accomplish this was:

$$s_h = \frac{H(T_{rad} - T_{env})}{b_{rad}} \quad (4)$$

$$\text{Where: } H = 1.7466u_i^3 - 41.982u_i^2 + 598.42u_i + 1796.9 \quad (5)$$

4.8 Solver

To refresh, the stationary and moving cases proved to be steady state and their domains meshed with tetrahedral cells. The solver selected for these problems was the SIMPISO solver. This steady state solver combines the best components from the SIMPLE and PISO solvers. It behaves very much like the steady state SIMPLE algorithm, but has an advantage over it with its increased stability with highly non-orthogonal cells. This increased stability derives from an additional pressure correction and under relaxation step in the method, which it derives from its transient PISO algorithm counterpart, which allows it to accommodate the non-orthogonal advection component present within the tetrahedral discretisation.

Table 6 presents under-relaxation and flux-blending parameters used. The under-relaxation factor reduces the amount of correction applied to the solution after every iteration. This allows the solving processes to apply smaller corrections, resulting in increased stability. The flux blending factors refer to the hybrid scheme used during the simulations. This scheme consists of central differencing, represented by a flux-blending factor of 1.0, and linear upwind differencing, represented by a flux-blending factor of 0.0. The central differencing scheme is second order accurate, but vulnerable to instability. The linear upwind differencing scheme on the other hand is only single order, but less vulnerable to instability. The combination of the two schemes, indicated by a value between 0.0 and 1.0, provides a good compromise between accuracy and stability.

Table 6: Solver parameters

Parameter	Under Relaxation	Flux Blending Factor
Momentum	0.5	0.7
Turbulence	0.7	0.7
Energy	0.7	0.7
Density	0.1	0.7
Viscosity	1.0	n/a
Pressure	0.1	n/a

4.9 Results

4.9.1 Stationary case

The stationary case represented the situation where the radiator fan situated behind the radiator produced the airflow in the underhood environment, while the doors of the wind tunnel remained closed. This approximated the condition where the vehicle was idling and the air around the vehicle remained near stationary. The following paragraphs discuss the results obtained.

The radiator fan produced airflow through the radiator where temperatures reached 40°C. This hot air entered the underhood environment through the fan, forcing it over the gearbox and against the brake booster. The combination of swirl introduced by the fan and the obstructions caused by the underhood components promoted the hot air to spread through the entire underhood, quickly lose momentum and energy. The complex airflow resulted in a temperature distribution throughout, with the warmest air detected at the back left corner where the airflow was slowest.

Buoyancy due to the temperature difference in the underhood caused the warm air to become trapped and further heated by the engine and exhaust manifold. The grill of the vehicle played a large role in trapping this warm air. This is because the grill has fins slanted upward towards the underhood compartment, causing the warm air to travel up from one fin to the next, preventing it from escaping the underhood environment. Figure 39 to figure 44 present typical results obtained from the final stationary simulation.

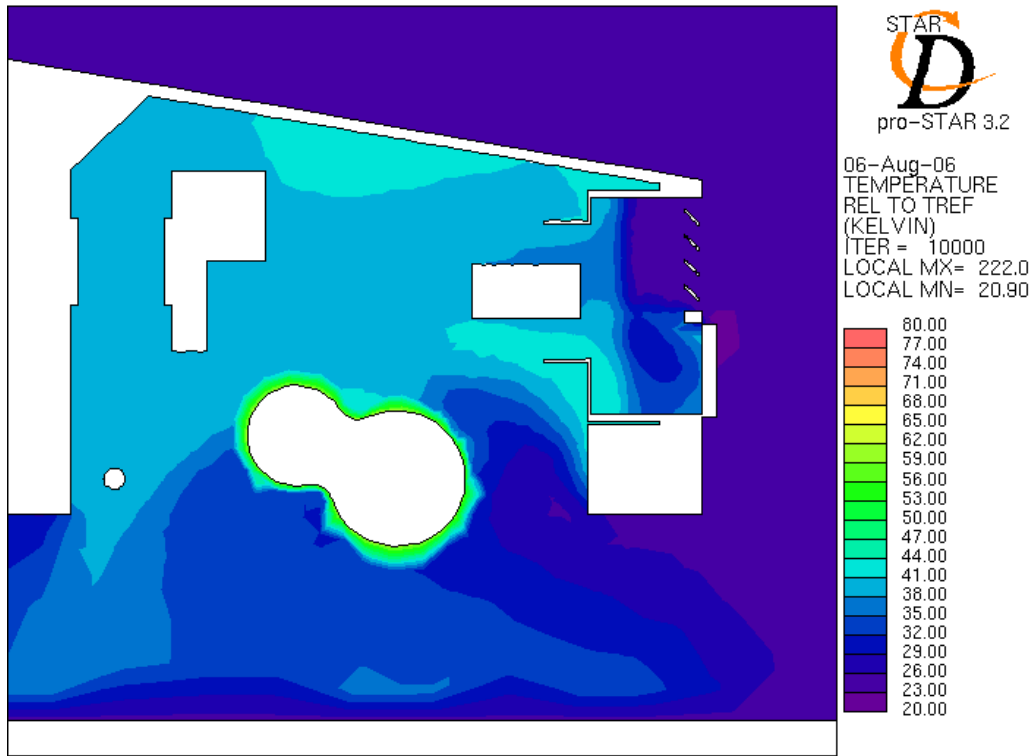


Figure 39: Temperature distribution of a section through the fan

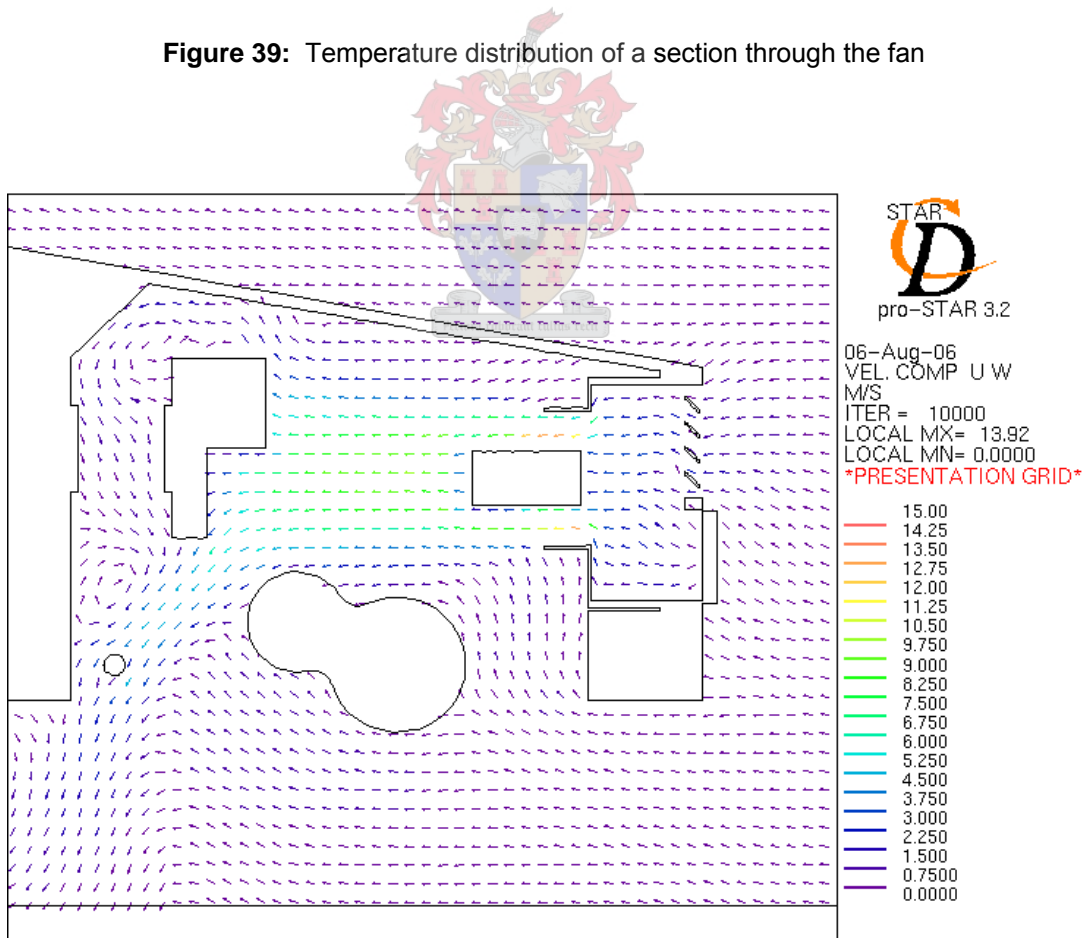


Figure 40: Velocity vectors of a section through the fan

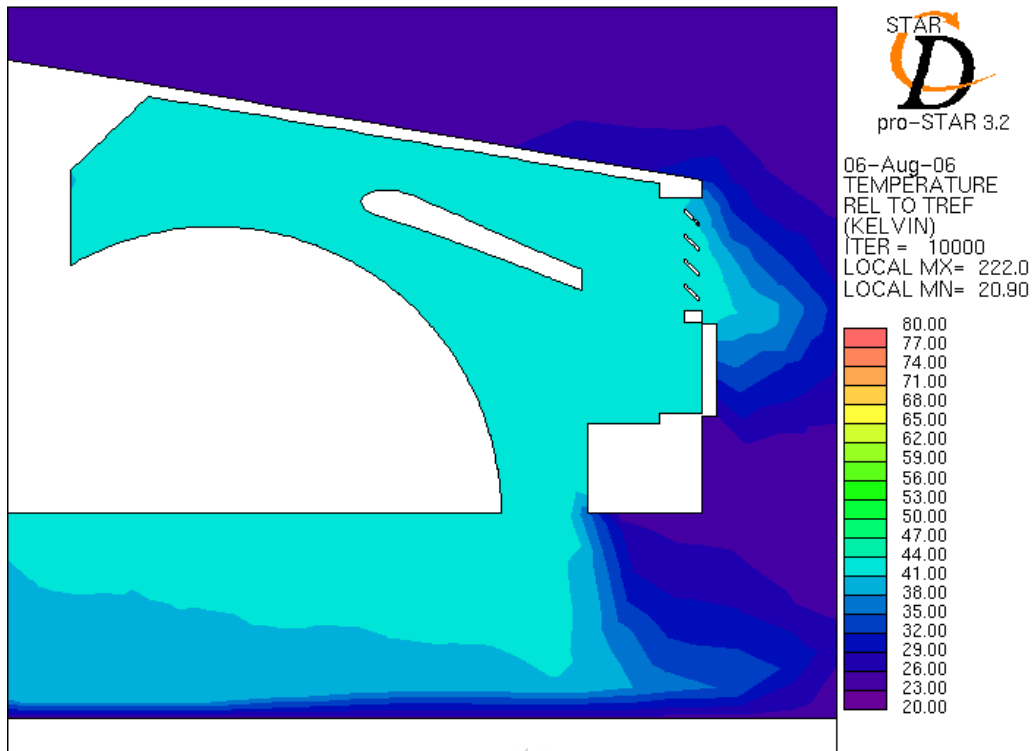


Figure 41: Temperature distribution of a section through the air intake

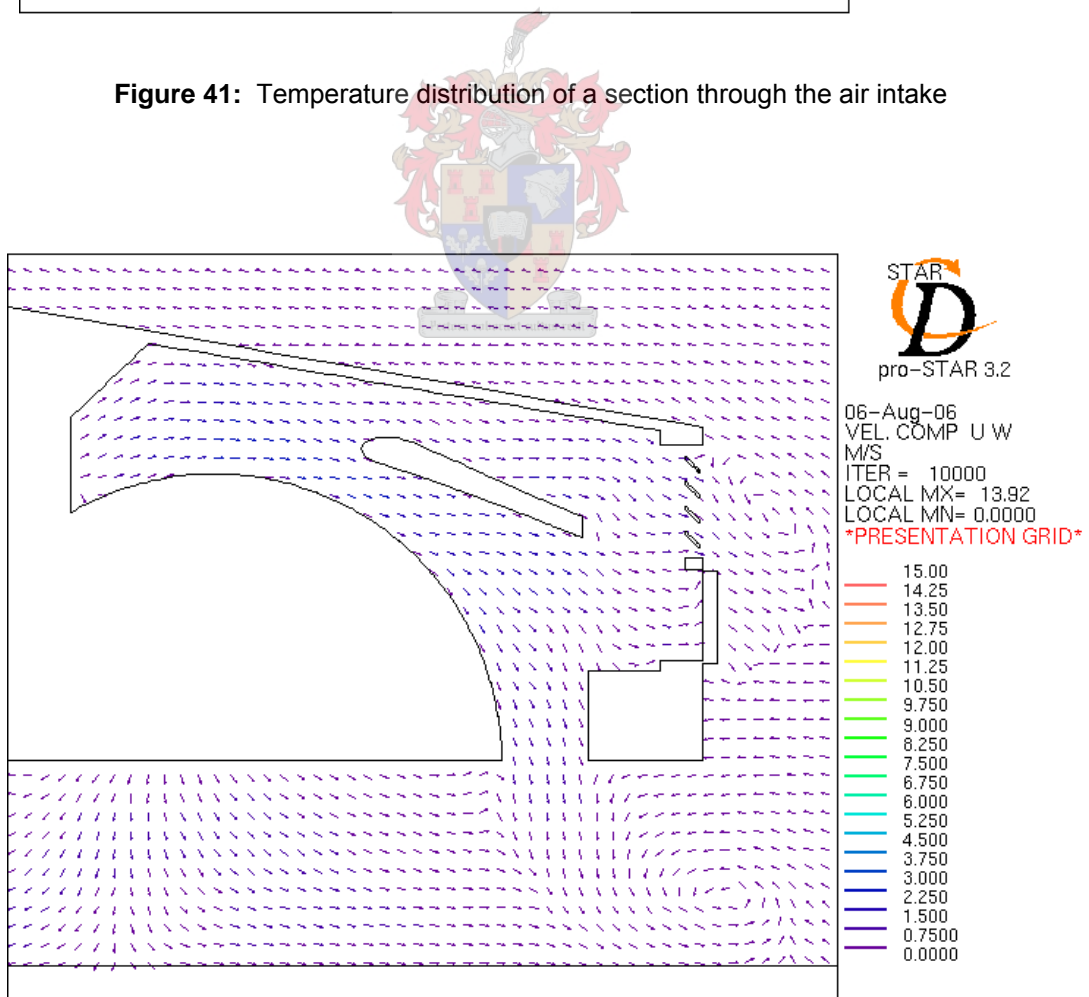


Figure 42: Velocity vectors of a section through the air intake

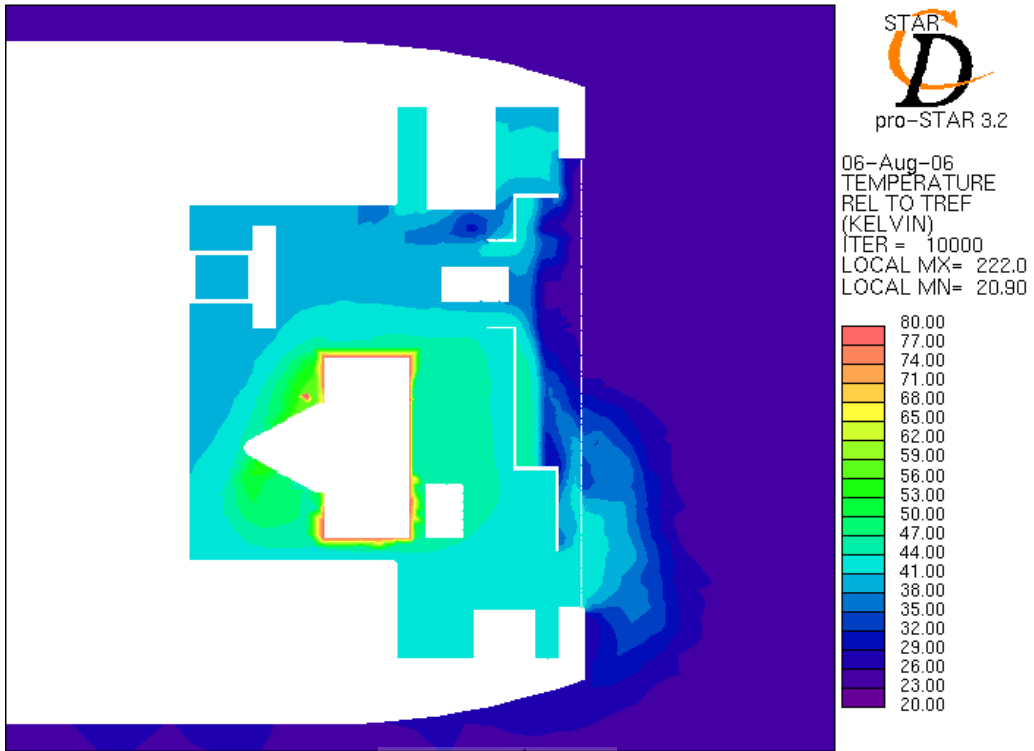


Figure 43: Temperature distribution in a horizontal plane through the fan

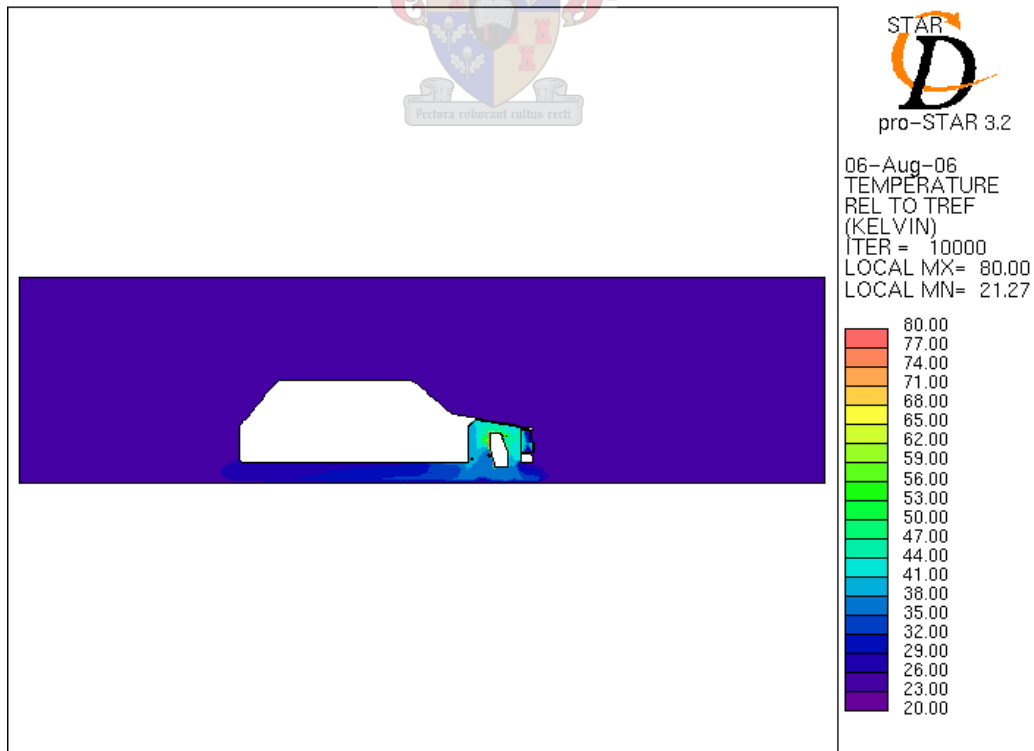


Figure 44: Temperature distribution through the central plane

4.9.2 Moving case

The moving case had the vehicle idling within the tunnel with airflow provided only by the wind tunnel fan. This had the effect of sucking air over the vehicle at approximately 5 m/s (18 km/h), measured approximately 300 mm in front of and 500 mm above the bonnet of the vehicle. This position allowed the pitot-static probe to measure the average wind tunnel air speed.

The results from the numerical simulations indicated that the air mostly passed over and under the vehicle. The airflow under the vehicle produced a low-pressure zone causing air from the underhood environment to join this air stream and subsequently facilitating low airflow through the grill and radiator into the underhood.

Another observation was that the lower airflow through the radiator caused the temperature of the air exiting the radiator to be much warmer, yet the underhood environment remained cooler than the stationary case discussed previously. The reason for this was that the radiator fan restricted the hot air from the radiator from entering the underhood environment. This low-speed hot air mixed with cooler air forced through the grill resulting in a lower mixture temperature.

Figure 45 to figure 49 provide some results obtained from the final moving case. It is clear to see here that the majority of heat came from the radiator.

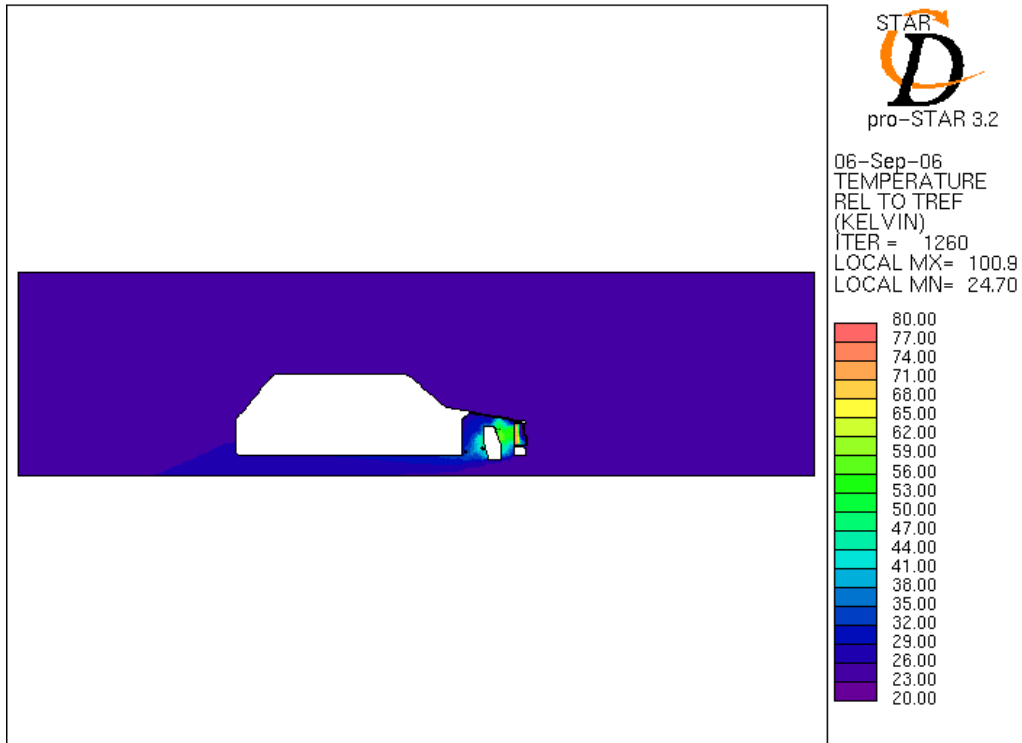


Figure 45: Temperature distribution through the central plane

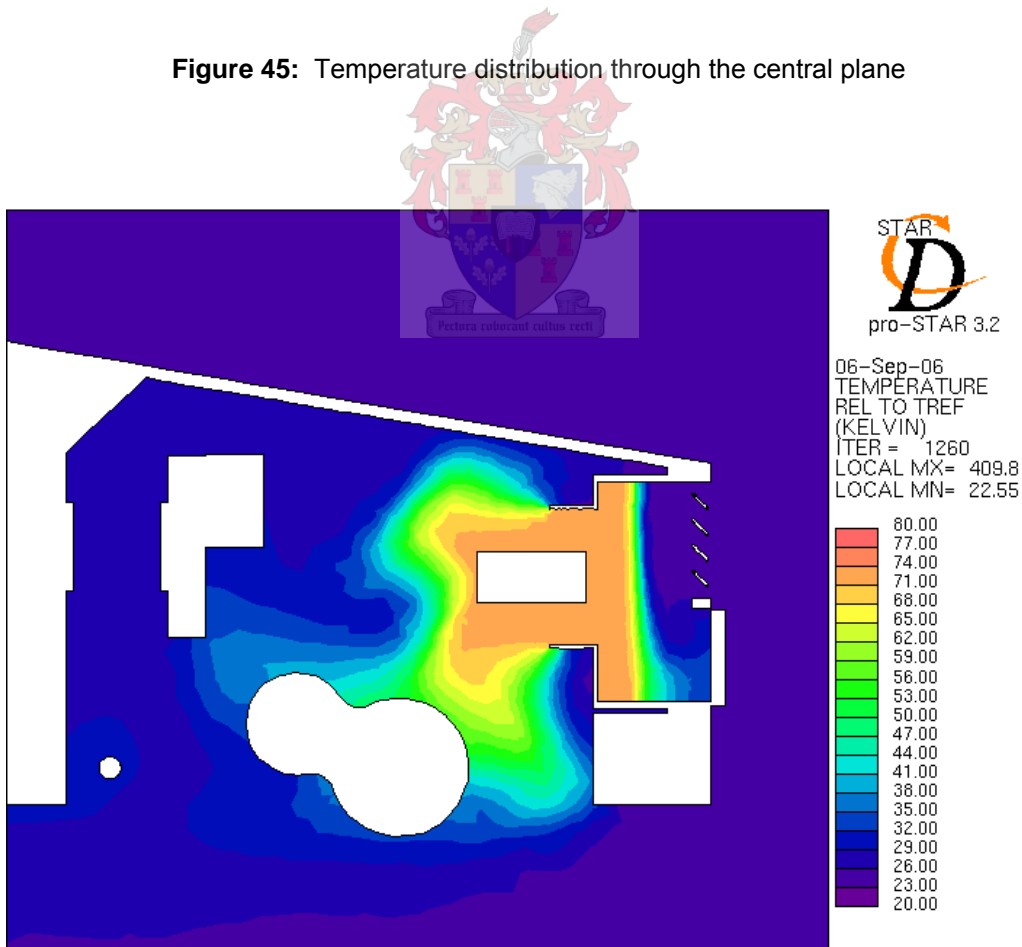


Figure 46: Temperature distribution in a vertical plane through the fan

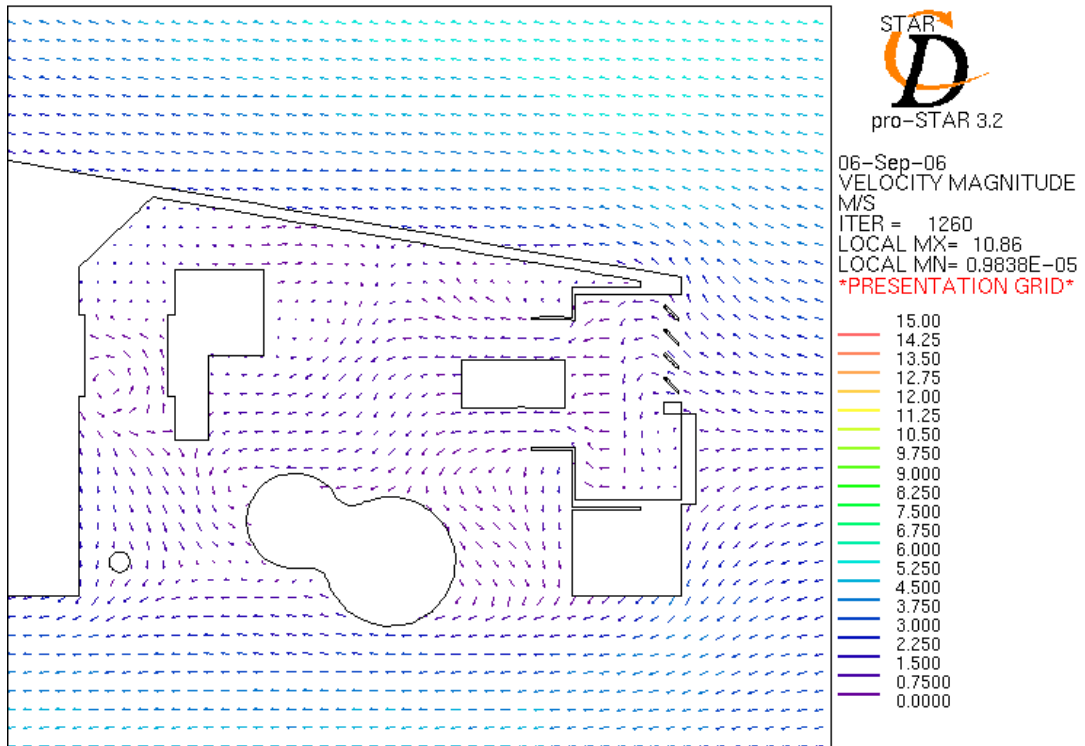


Figure 47: Velocity vectors in a vertical plane through the fan

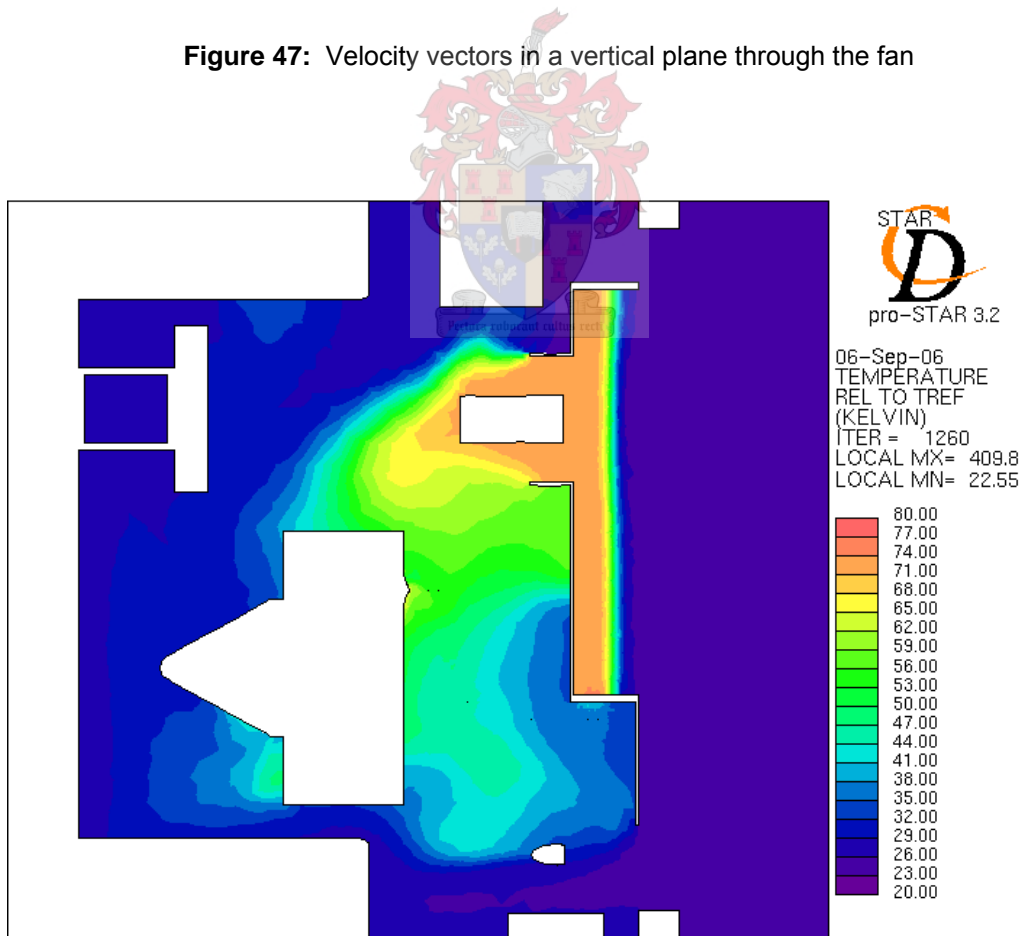


Figure 48: Top view temperature distribution through the fan

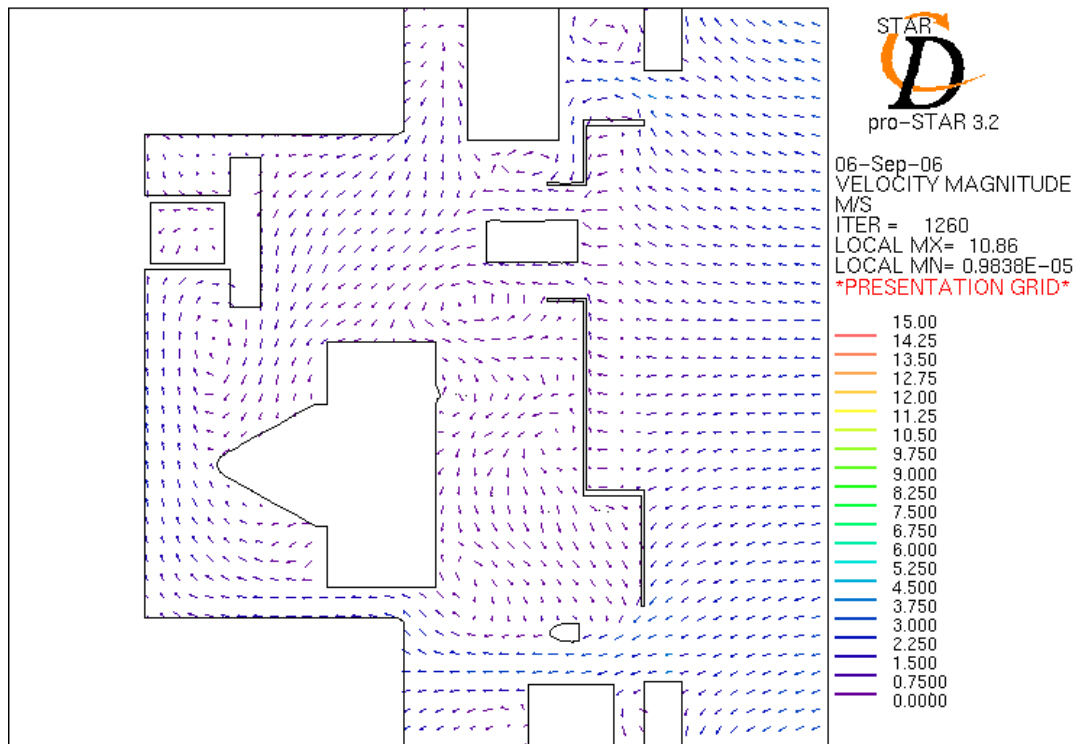


Figure 49: Top view velocity distribution through the fan

4.10 Discussion

The geometric CAD model used to generate the discretised grid contained the majority of the main components within the underhood environment.

The boundary conditions selected and applied to the numerical model, best represent the conditions present with the experimental tests. The wind tunnel section around the car was included to eliminate discrepancies related to the ground boundary layer and blockage of the airflow through the tunnel by the vehicle.

Comparing the results from the stationary and moving cases proved that the stationary case was the worst. It had average temperatures of approximately 40 °C, while the moving case had temperatures averaging at approximately 35 °C.

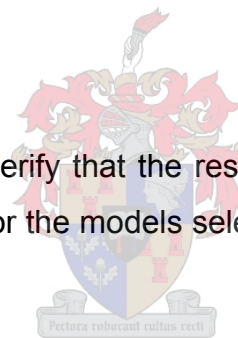
5 NUMERICAL VERIFICATION

5.1 Overview

CFD is a numerical method of solving a set of linearised partial differential equations (PDEs) describing the behaviour of fluids within a domain. A grid of discrete cells, each governed by the prescribed linear equations, represents this domain. The process of solving these equations is iterative. Thus, a sufficient amount of iterations is required to obtain a single converged solution. There are many factors, which may lead to an incorrect solution. These include modeling errors, discretisation factors and numerical errors. Each of these must be investigated to determine whether the solution obtained is correct. This chapter discusses the various evaluations performed to determine whether the solutions obtained were true representations of the underhood flow investigation.

5.2 Objectives

The aim of this chapter was to verify that the results obtained have indeed converged and that it satisfies the criterion for the models selected. This objective was sub-divided into the following.



- Check whether the solutions converge to a single solution
- Compare solutions from various grid resolutions to determine if grid independence had been achieved
- Investigate the y^+ values, to determine whether the turbulence model selected were valid

5.3 Numerical Evaluation

Modeling errors refers to the validity of the linear equations selected to describe the domain under investigation. A CFD simulation uses a combination of various models to approximate reality. These models include the Navier-Stokes equations, which describe the flow of the fluid, the energy equations, which represent the transfer of energy through the domain and the turbulence models, which accounts for the effects of turbu-

lence in the flow. Each model has a prescribed set of conditions for which the model is valid. Thus, caution should be exercised when selecting these models to ensure the correct problem definition is used.

After selecting the models for the simulation, the domain under investigation needs to be discretised. Selecting the cell size for the domain depends on various factors. Large cells produce low-resolution grids requiring less computing power and time, but are unable to capture finer details of the flow and tend to be unstable. Tiny cells produce stable high-resolution grids, which are more accurate, but require large amounts of computing power and time. Thus, different grid resolutions should be used to determine which is best for the problem under investigation.

After selecting the numerical models and grid resolution, the simulation is initiated. Determining when to stop this iterative process depends on when the solution has converged. Convergence is reached when a solution exactly satisfies all the PDEs governing the fluid. Although obtaining such an exact solution is highly improbable, good approximations are possible. A converged CFD solution is thus reached when it no longer changes a significant amount with ongoing iterations and satisfies the set of linear PDEs governing it.



5.3.1 Residuals

Residuals describe the rate at which the solution is changing. They provide a normalised indication to the correction being made to the previous iteration's solution. Ideally, all the residuals should continuously decrease to zero. Obtaining zero is impossible due to various factors, including numerical instability, computer round off errors and unsteady flow. Numerical instability occurs when perturbations in the solution are not bounded and damped out with continuous iterations, but compound together causing the solution to diverge. Computer round off errors occur due to the limited ability of computers to represent floating point number. An example is a 32-bit computer, which is capable of accurately calculating the seventh decimal place of numbers. Unsteady flow describes a situation where a steady state solver cannot resolve the flow of the problem under investigation. Unsteady flow problems are solved using a time dependent transient solver. Figure 50 and figure 51 present the residuals from the final stationary and moving CFD simulations respectively.

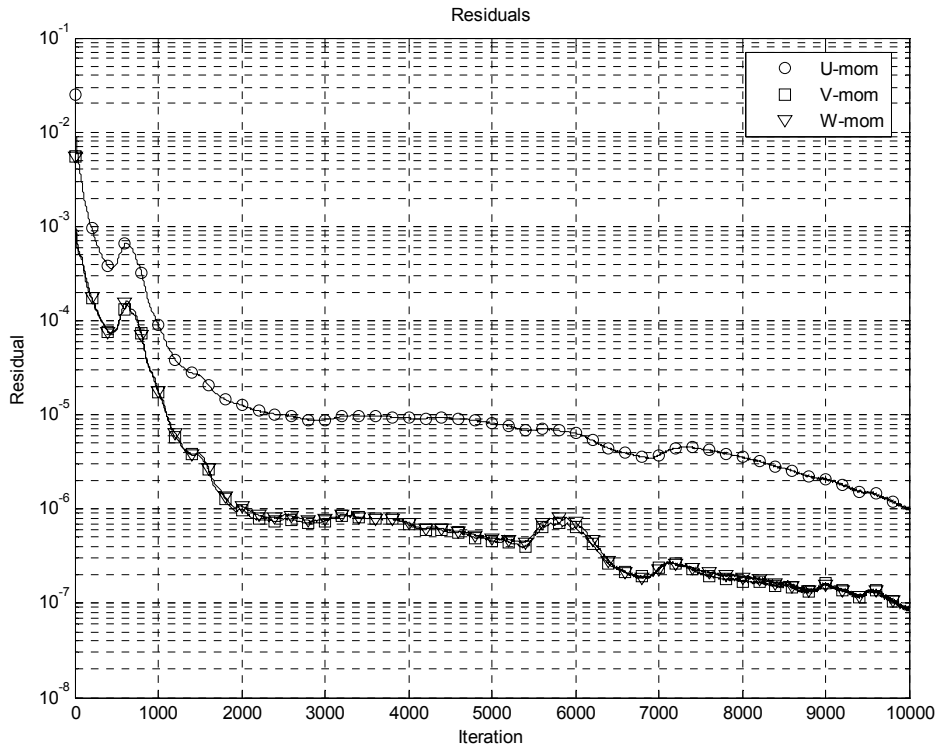


Figure 50: Residuals for the final stationary solution

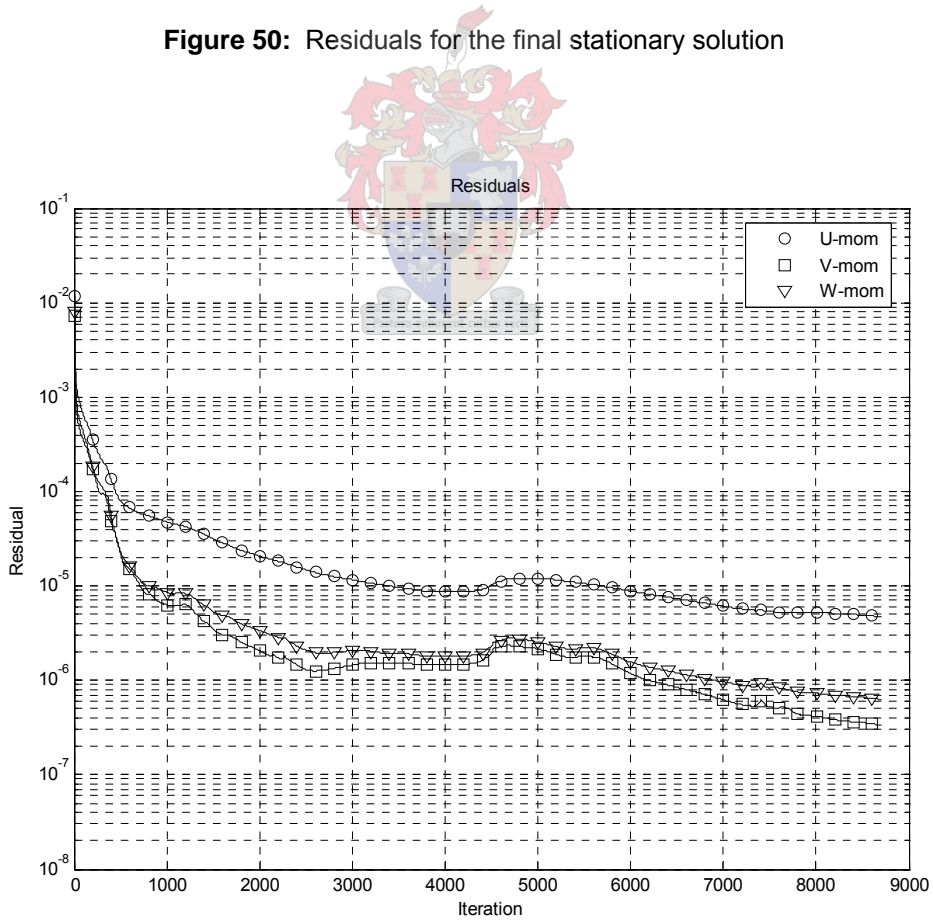


Figure 51: Residuals for the final moving solution

Although the residuals provide an indication to the changing rate of a solution between iterations, it is unable to indicate whether the solution has fully converged. For this, we examine the field values from a monitoring cell in the solution.

The field values are actual samples taken from the domain during the iterative process. They allow the CFD user to monitor the progress of the simulation. If the values remain constant for a large number of iterations, it signifies that the solution is not changing and the simulation can be stopped. Thus, the position of the monitoring point or cell should be placed at the point in the domain where convergence is expected last.

Figure 52 and figure 53 indicates the momentum field values from the final stationary and moving case simulations. The monitoring cell was placed in the wake of the vehicle. This position was chosen because it was the last place to reach convergence.

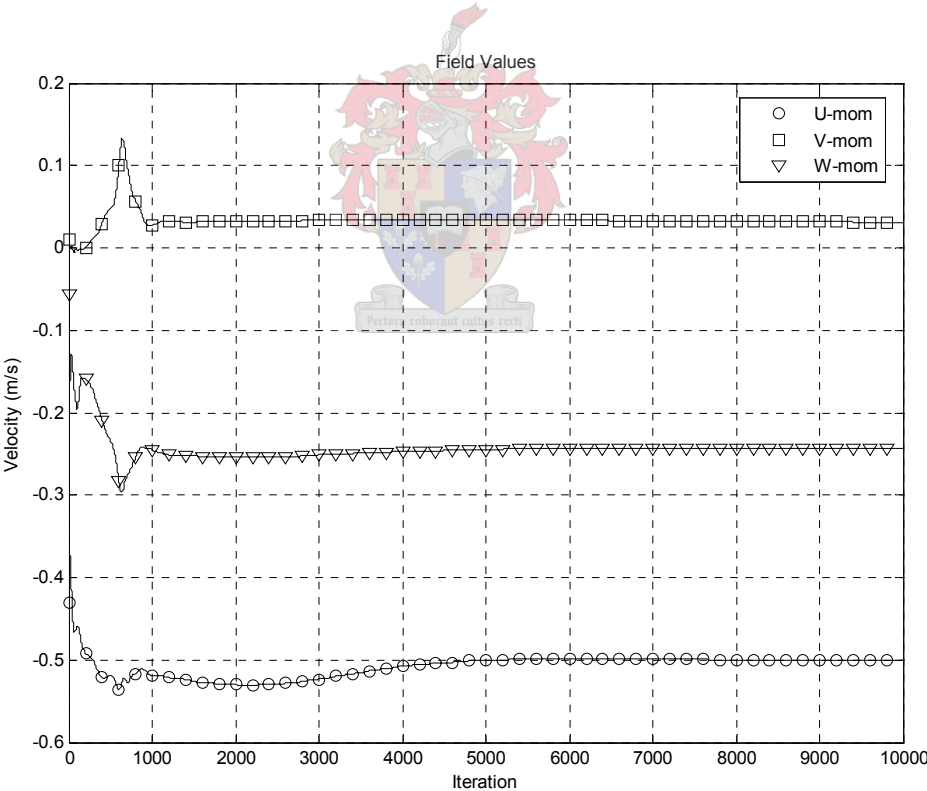


Figure 52: Field values from the final stationary simulation

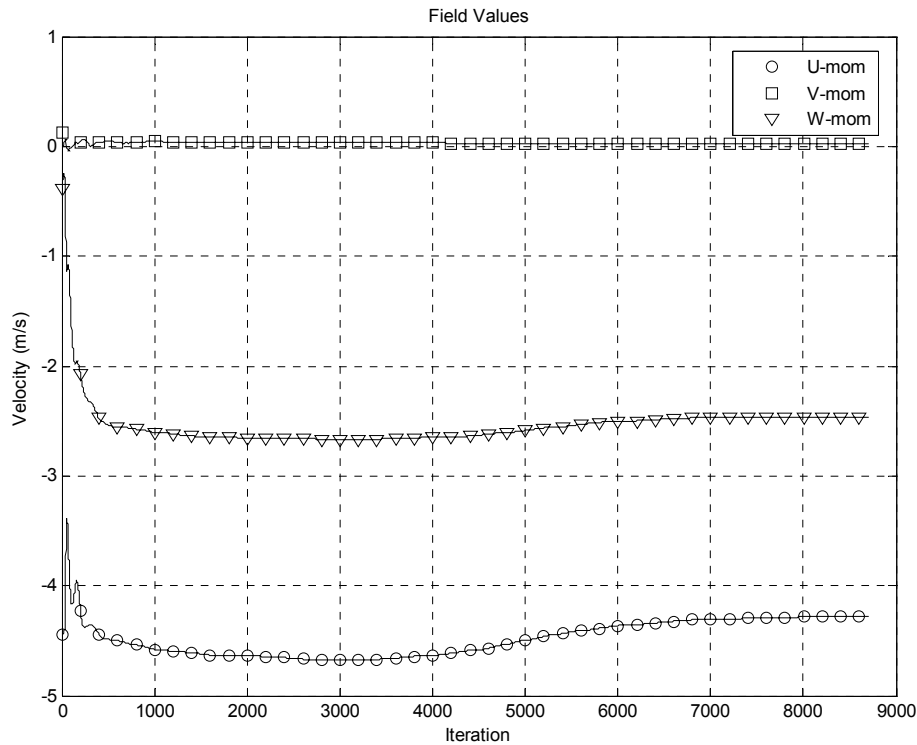


Figure 53: Field values from the final moving case

After obtaining a set of converged solutions for a given problem on different grid resolutions, they should be compared to each other. Comparing the solutions will indicate whether the solutions are grid independent. Grid independence is obtained when two or more simulations result in similar solutions at different grid resolutions. This ensures that errors due to the discretisation of the domain are eliminated, improving the accuracy of the solutions.

Figure 54 to figure 59 provide the airflow profiles for both the stationary and moving cases at approximately 500 mm in front of the vehicle, 300 mm behind the vehicle and horizontally through the underhood intersecting the wake of the fan respectively.

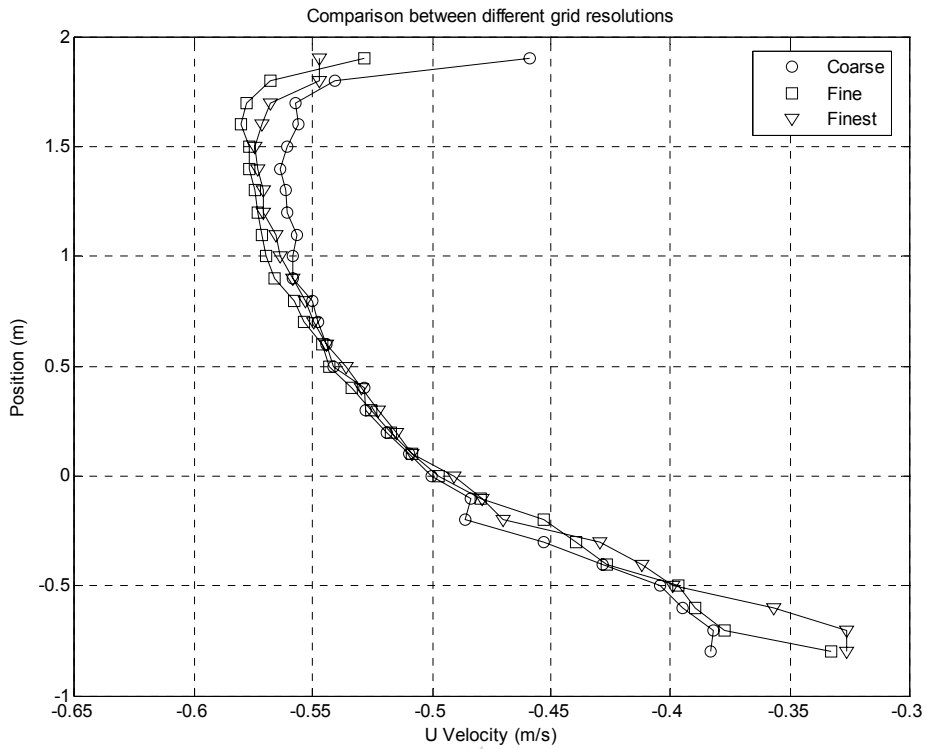


Figure 54: Airflow profile in front of the vehicle for the stationary case

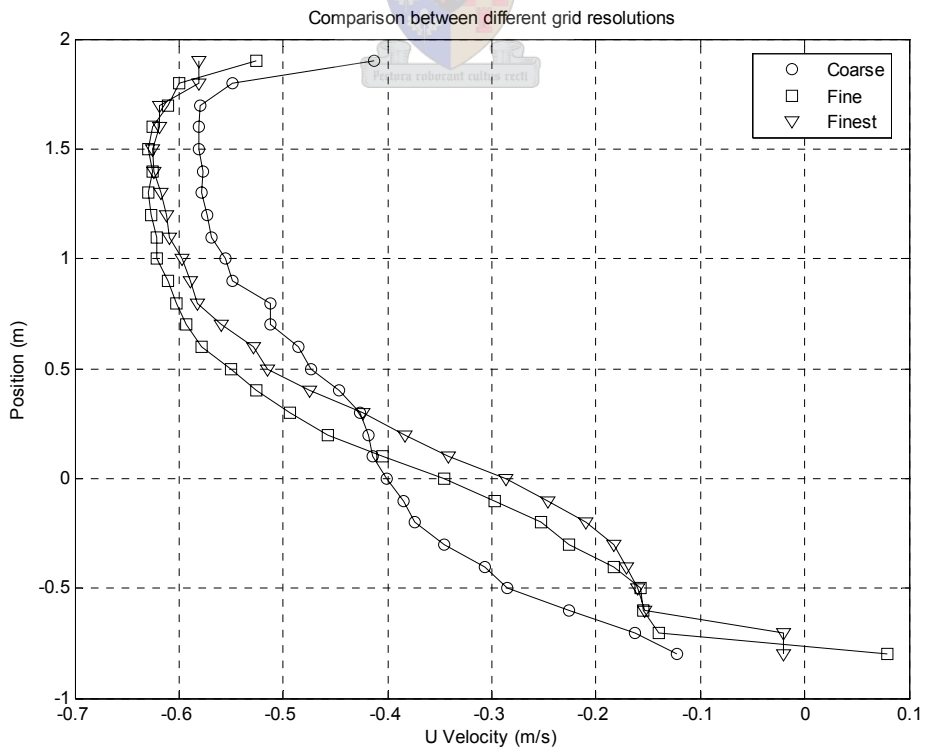


Figure 55: Airflow profile behind the vehicle for the stationary case

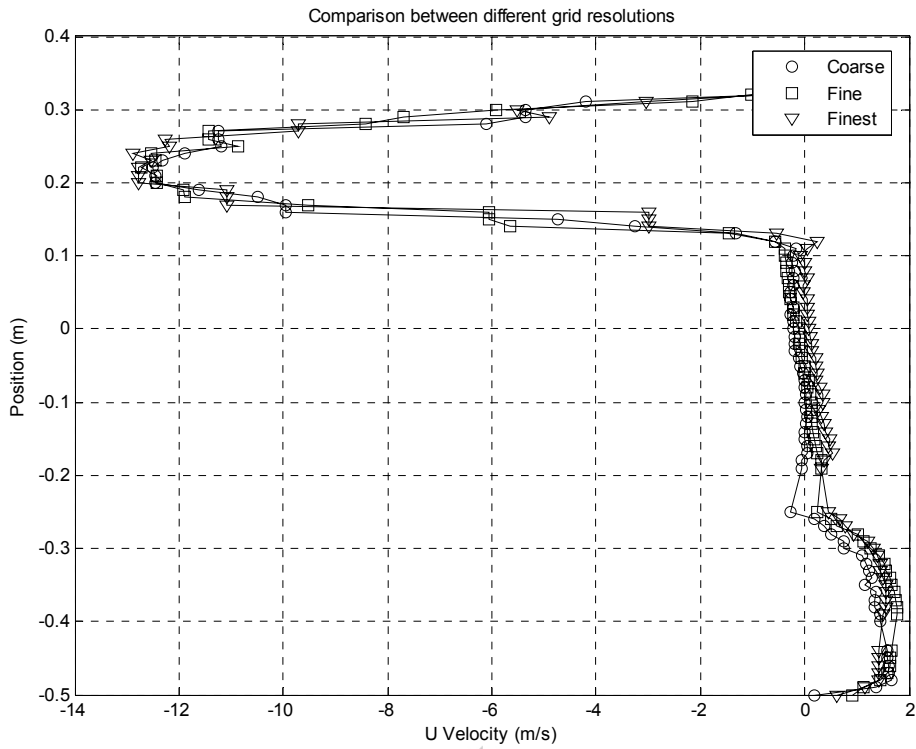


Figure 56: Airflow profile in the underhood for the stationary case

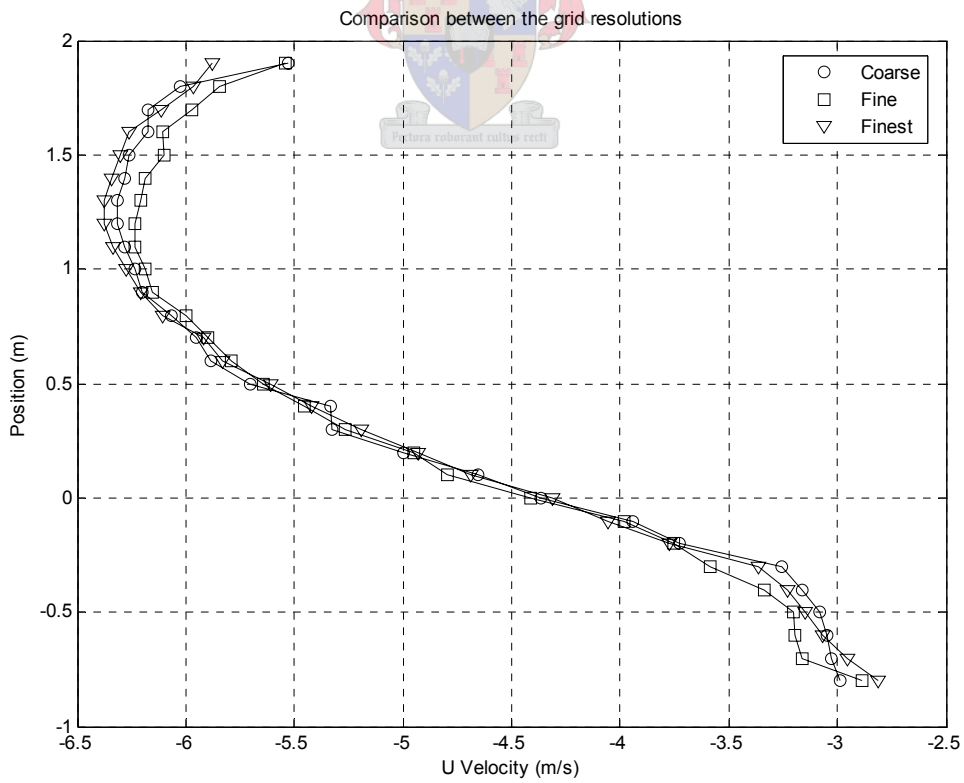


Figure 57: Airflow profile in front of the vehicle for the moving case

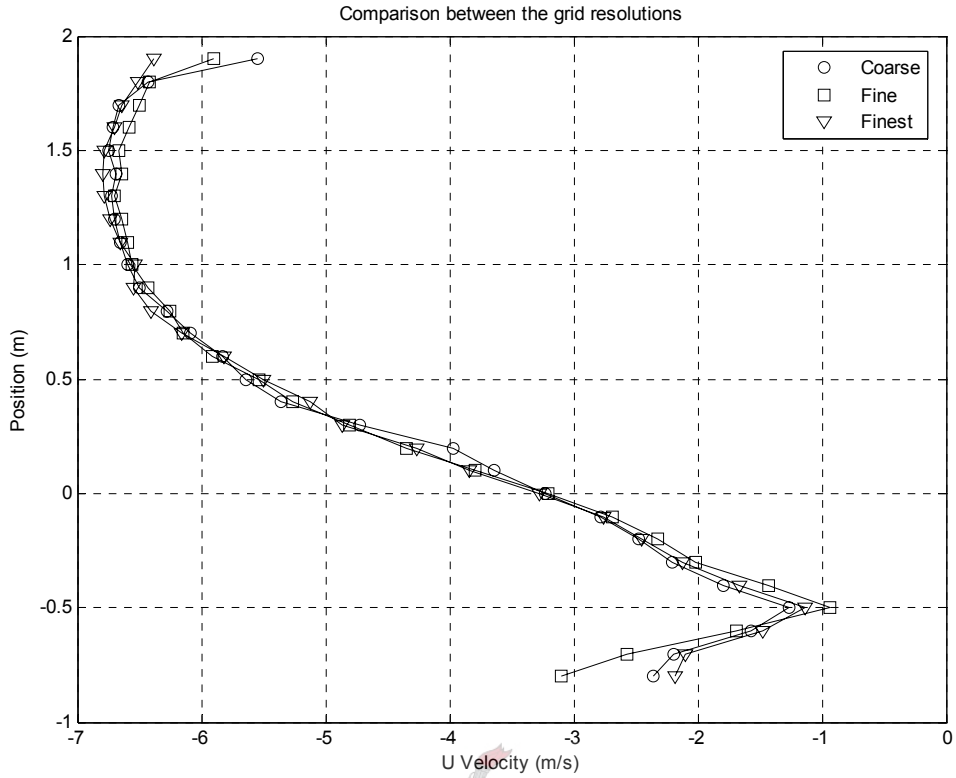


Figure 58: Airflow profile behind the vehicle for the moving case

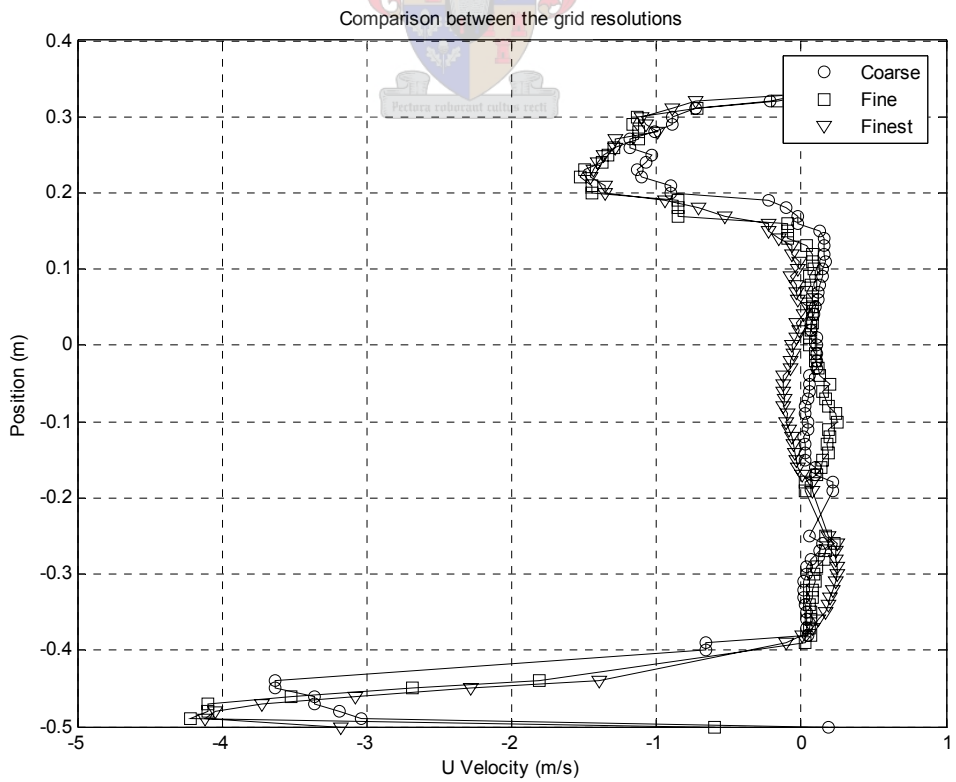


Figure 59: Airflow profile in the underhood for the moving case

The final numerical verification required was to ensure that the turbulence model selected is valid. A boundary layer consists of three regions, namely; the viscous sub-layer, buffer zone and logarithmic zone. The High-Reynolds $k-\epsilon$ turbulence model used in the project is only valid in the logarithmic zone, corresponding to y^+ values between 30 and 500.

Figure 60 to figure 63 provide the y^+ values obtained from the final simulations. With a limited number of cells as exception, the y^+ values in both the stationary and moving cases fell between with these values. This indicates that the High-Reynolds $k-\epsilon$ turbulence models used remained valid and that the results provided a good approximation of the governing equations.

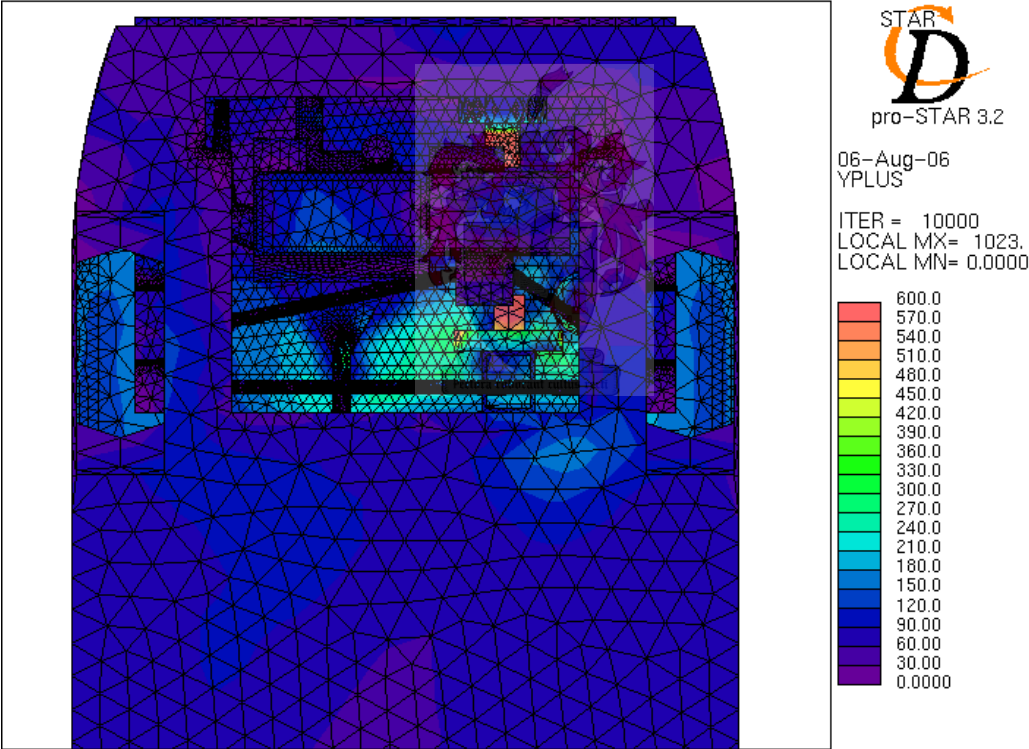


Figure 60: y^+ values in the underhood for the stationary case

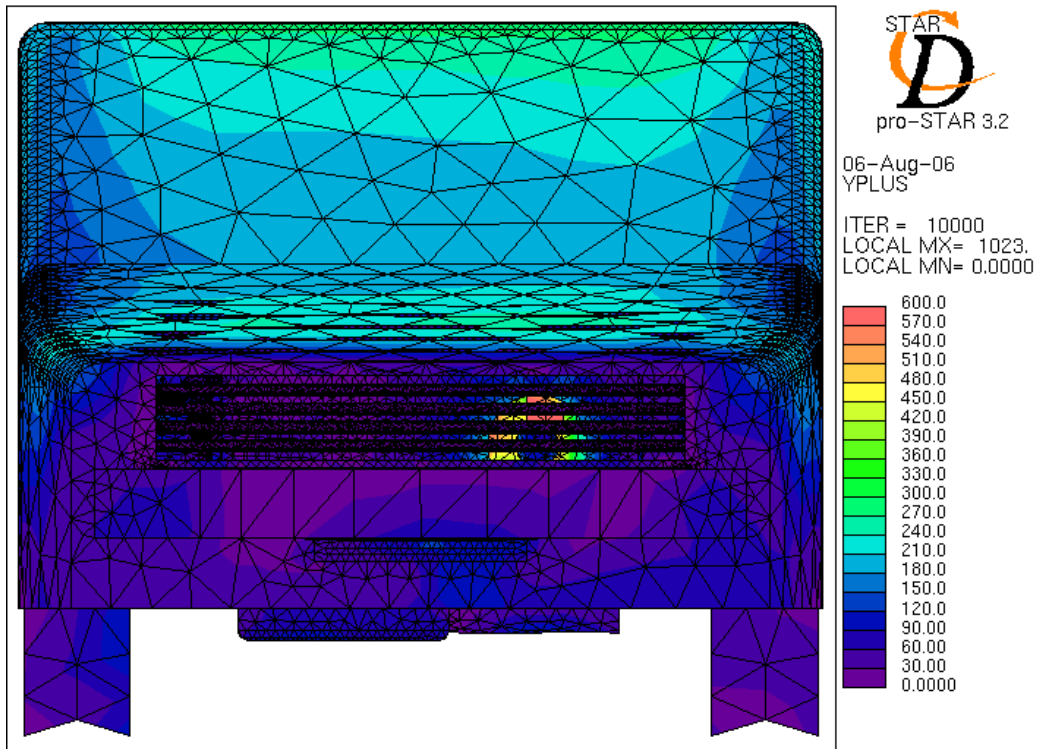


Figure 61: y^+ values in front of the vehicle for the stationary case

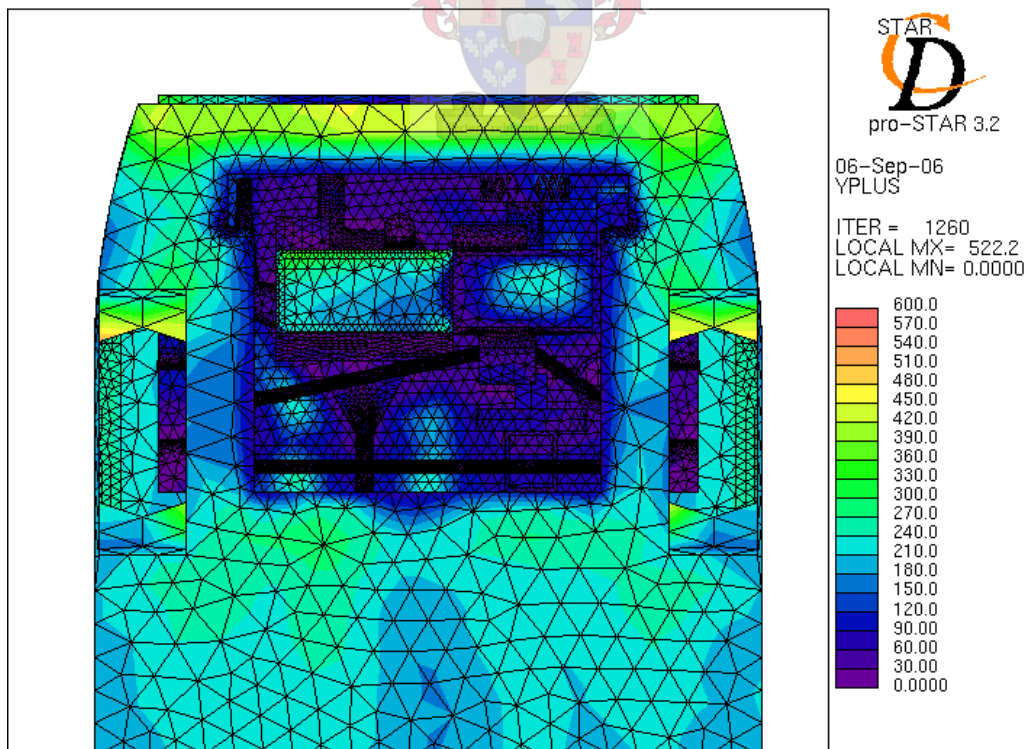


Figure 62: y^+ value in the underhood for the moving case

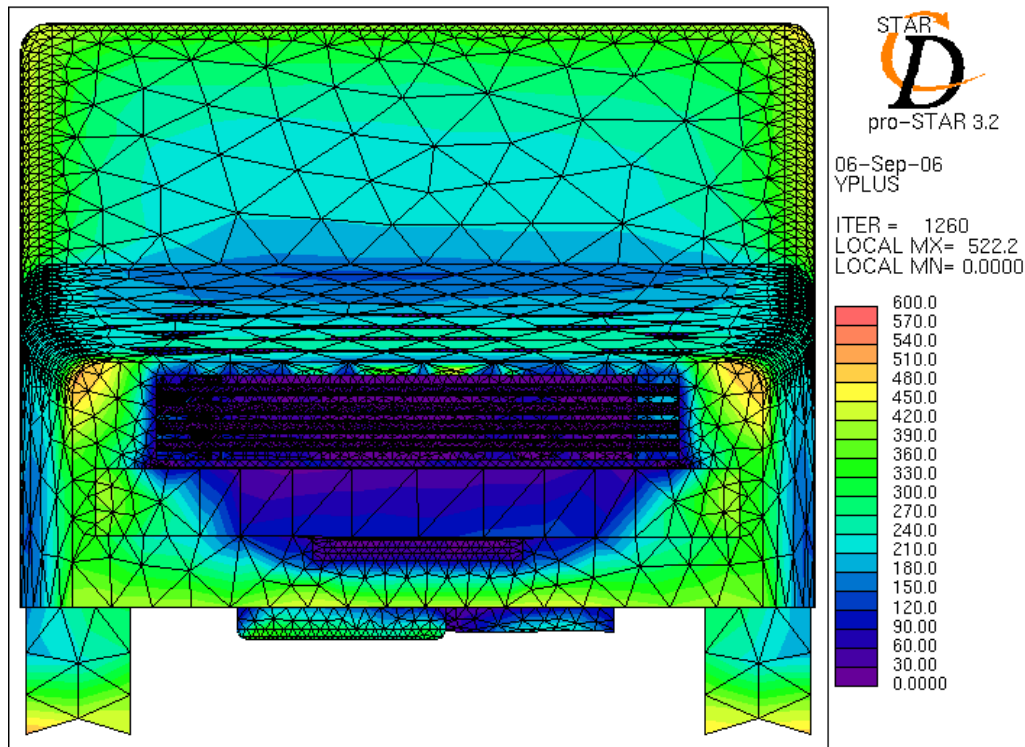


Figure 63: y^+ values in front of the vehicle for the moving case

5.4 Discussion

The residuals and field values of the simulations indicated that the solutions were indeed steady state, as all the field values converged to a single value and the residuals decreased by at least four magnitudes.

Grid independence was evaluated by comparing the solutions from three different grid resolution and three grid positions. The result was that all solutions from each independent case produced similar results with little variance. It was thus confirmed that the solutions were grid independent.

The evaluation of the y^+ values indicated that the centre nodes of the cells positioned adjacent to the wall boundaries, were situated within the logarithmic zone. This produced y^+ values between 30 and 500, proving that the High-Reynolds $k-\epsilon$ turbulence model selected was valid.

6 EXPERIMENTAL COMPARISON

6.1 Overview

This chapter compared the numerical solutions to the experimental measurements. The comparison of the two results indicated how accurate the numerical model represented the experimental conditions.

6.2 Objectives

The goal of this section was to compare the numerical temperatures and fan velocities results to the experimental values measured in the wind tunnel.

6.3 Experimental comparison

Table 7 provides the peak air speeds through the fan. For the stationary case, the fan model accurately simulated the fan producing an air speed of 13 m/s. For the moving case, the fan blocked the airflow through itself. The numerical fan was model as a momentum sink, reducing the air speed, but in reality the fan deflects the flow. This resulted in the numerical fan over-predicting the air speed by approximately 0.65 m/s. This indicates that the fan model requires improvement to allow it to represent the effects of the fan deflecting the airflow.

Table 7: Peak airflow speed through the fan shroud

Stationary		Moving	
Experimental	Numerical	Experimental	Numerical
13 m/s	13 m/s	0.76 m/s	1.4 m/s

To compare the experimental temperature measurements with the numerical solutions, sensors were placed in similar positions in the numerical domain. These sensors interpolated between the values of the nearby cells providing a good indication of the temperatures. Table 8 provides temperatures from the experimental and numerical results.

As indicated in table 8, the numerical solutions compared very closely with the experimental readings. The temperature difference of 3.5 °C in the moving case was caused by the fan velocity difference between the numerical and experimental readings.

The shaded blocks indicate numerical values or conditions enforced upon the numerical simulations. The numerical solver calculated all other temperatures.

Table 8: Comparison of numerical and experimental temperatures

Position	Stationary		Moving	
	Experimental	Numerical	Experimental	Numerical
Ambient Air	24.0 °C	25.0 °C	23.5 °C	25.0 °C
Front Right	39.0 °C	40.5 °C	24.5 °C	25.7 °C
Back Right	42.0 °C	39.4 °C	29.0 °C	27.2 °C
Front Left	40.0 °C	41.4 °C	25.0 °C	27.0 °C
Back Left	40.0 °C	44.0 °C	33.5 °C	33.4 °C
Radiator Inlet	24.0 °C	25.0 °C	24.0 °C	25.0 °C
Radiator Outlet	36.5 °C	38.6 °C	73.0 °C	73.3 °C
Fan Outlet	36.0 °C	37.8 °C	64.5 °C	68.0 °C
Engine Surface	80.0 °C	80.0 °C	84.0 °C	84.0 °C
Exhaust Manifold	222.0 °C	222.0 °C	238.0 °C	238.0 °C
Radiator	25.0 °C - 60.0 °C	45.0 °C	74.0 °C	74.0 °C

6.4 Discussion

The majority of experimental and numerical results compared well. The difference of 0.65 m/s in the peak air speeds from the fan indicates that the numerical solution requires improvement.

7 CONCLUSION AND RECOMMENDATIONS

The project lasted 14 months, with the experimental and numerical evaluation completed and the thesis submitted in September 2006. The following sections discuss the conclusions derived from the project and recommendations for further research in the field.

7.1 Conclusions

Literature reviewed, indicated that South Africa was not actively involved in CFD applications on automobile underhood thermal environments. The current economic status of South Africa is attracting the interests of multi-national companies, which intend to promote an increase in vehicles manufactured in the country. This requires the development of skills and experience into associated work, including the capability of the CFD underhood thermal analysis.

The experimental data obtained from the stationary and moving cases were assumed as steady state. The numerical solutions confirmed the validity of this assumption and provided results that differed by less than 10 % from the experimental data.

The simple fan and radiator models simulated as either a momentum and energy source or sink captured the effects of these components well. The only discrepancy was the fan air speed in the moving case, which was over-predicted by 0.65 m/s.

The numerical simulations indicated that the stationary case suffered from the highest underhood temperatures. These high temperatures were caused by the radiator fan blowing hot radiator air into the underhood. This air became trapped and heated further by the engine.

The numerical evaluation process investigated the convergence, grid independence and validity of the High-Reynolds $k-\epsilon$ turbulence model in terms of the y^+ values. The result of the investigation indicated that the numerical solutions had converged, was grid independent and that the turbulence was valid.

The project was a success, in terms of laying the foundation for automotive underhood thermal management studies in South Africa and demonstrating its validity.

7.2 Recommendations

The work presented for this thesis forms the foundation for future projects and improvements to be researched and developed.

The model for the fan was very simple to capture the effects it had on the flow of the air. There is much room for improvement and the employment and perhaps development of more advanced and accurate models as presented by Tzanos and Chien (2002) are necessary.

The radiator model was also very simple with only the momentum loss and heat generation taken into account. Further model development is required to address effects such as surface temperature changes on the airside, which could lead to improved predictions for the heat transfer and increase accuracy.

The model created in this project investigated the effects of major obstructions and heat sources. Due to insufficient computing power, radiation was not included in the simulations, but these effects should further be investigated. The assumption that radiation effects in the underhood environment are negligible was based on the small temperature differences present. The only region where the radiation effects could be substantial is the exhaust manifold and pipe, but according to Winnard et al. (1995), the effects from these components only amount to approximately 1/3 of the energy introduced by the radiator.

Other effects not included in the analysis were those produced by the alternator, piping, wiring, fan belts, exhaust pipe under the carriage of the automobile and blockage by smaller components. These components include the horn, lights, alternator and support brackets.

The resolution of the solutions and investigations remained course as to remain within the computer capability of the facilities here at Stellenbosch University. With the increase in computing power over following years, improved resolutions will be achievable to allow for acceptable turnover times between these large simulations.

The geometry of the vehicle was relatively simple, but measuring parameters within sufficient accuracy remained difficult. Thus, vehicles that are more complex can be mod-

elled if the geometry and component characteristics are available to the analyst beforehand.

The use of modern technology will allow polyhedral cell types to reduce the required cells for any desired accuracy.

The instalment of the ramp in the subsonic wind tunnel intake resulted in a boundary layer forming on its surface. This distorted the velocity profile through the test section of the subsonic wind tunnel. A possibility for overcoming this issue would be to insert a groove near the end of the ramp with a suction fan situated below it, which draws air down into the groove. This in turn destroys the boundary layer and may restore the original velocity profile.

Numerical results indicated that the underhood of the Volkswagen Citi Golf Chico acts as a heat reservoir, trapping large amounts of energy causing high temperatures. A possible solution to this problem could entail the addition of vents to the highest positions on the side panels adjacent to the underhood compartment. This would allow the hot air to escape, possibly reducing the underhood temperatures significantly.

The turbulence intensity of 30 % used during for the moving case is excessively high. Although it was found to have little effect on the results from the underhood environment by means of comparing the numerical and experimental results to each other, this value should be measured and corrected to improved accuracy.

8 REFERENCES

- Abdul Ghani SAA, Aroussi A, Rice E (2000) Simulation of road vehicle natural environment in a climatic wind tunnel, *Simulation Practice and Theory*, vol.8, pp. 359-375.
- Carluccio E, Starace G, Ficarella A and Laforgia D (2004) Numerical analysis of a cross-flow compact heat exchanger for vehicle applications, *Applied Thermal Engineering*, vol.25, pp. 1995-2013.
- Kröger DG (2004) *Air-cooled Heat Exchangers and Cooling Towers – Thermal-Flow Performance Evaluation and Design*, Penn Well Corp., Tulsa, Oklahoma.
- Mahmoud KG, Loiber E, Wiesler B, Samhaber C and Kußmann Ch (2003) Simulation-based vehicle thermal management system – concept and methodology, *Society of Automotive Engineers*, Paper 2003-01-0276.
- Morris SC, Good JJ and Foss JF (1997) Velocity measurement in the wake of an automotive cooling fan, *Experimental Thermal and Fluid Science*, vol.17, pp. 100-106.
- Qian C and Yuan C (2001) an integrated process of CFD analysis and design optimization with underhood thermal application, *Society of Automotive Engineers*, Paper 2001-01-0637.
- Seider G, Bet F, Heid T, Hess U, Klein T and Sauer J (2001) A numerical simulation strategy for complex automotive cooling systems, *Society of Automotive Engineers*, Paper 2001-01-1722.
- Shephard MS, Beall MW, O'Bara RM and Webster BE (2003) Toward Simulation-Based Design, *Finite Elements in Analysis and Design*, vol.40, 1575-1598.
- Stander JN (2004) the evaluation of the flow characteristics of a newly installed test ramp, University of Stellenbosch, Report for vacation training.
- Tzanos CP and Chien T (2002) a simple fan model for underhood thermal management analyses, *Society of Automotive Engineering*, Paper 2002-01-1025.

van Zyl JM, Wipplinger KPM, Harms TM and Taylor AB (2006) CFD investigation of an experimentally detected heat transfer phenomenon, *South African Association of Computational and Applied Mechanics*.

Wang D, Du G and Wu J (2004) Numerical experimental study on the 3-D flow field around a van with a dome for energy saving, *Energy Conversion and Management*, vol.46, 833-846.

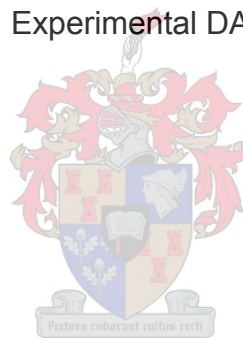
Winnard D, Venkateswaran G and Barry RE (1995) Underhood thermal management by controlling airflow, *Society of Automotive Engineers*, Paper 951013.

Xie X, Huang Z, Wang J and Xie Z (2005) Thermal effects on vehicle emission dispersion in an urban street canyon, *Transportation Research Part D*, vol.10, 197-212.



APPENDIX A

Experimental DATA



The data presented in this appendix was the experimental data recorded by the computer. This data was used to determine the conditions of the underhood environment and served as a method of comparison to evaluate the numerical data obtained through simulations.

Three cases were initially investigated. These cases were the stationary case where the wind tunnel was switch off and the automobile internal fan thermostat bypassed to provided continuous airflow for the radiator. This provided a steady state condition and is subsequently referred to as the 'stationary' case.

The second and final case evaluated was the case where the wind tunnel fan drew air at approximately 5 m/s resulting in the vehicle fan not engaging. This condition was evaluated as a steady state condition, because the fluctuations seen were caused by the wind tunnel, due to the velocity not being very controllable. This state is subsequently referred to as the 'moving' case

The third case was conducted with the wind tunnel fan drawing air at approximately 2 m/s through the tunnel while the thermostat was reactivated. This resulted in a very dynamic case where the conditions under the underhood would continuously in a cyclic manner. This case confirmed the expectation of the extreme dynamics of the underhood thermal environment. This case was not further investigated as transient simulations required a much larger amount of processing time and computer capacity, which was outside the current capability of the project computing facilities.

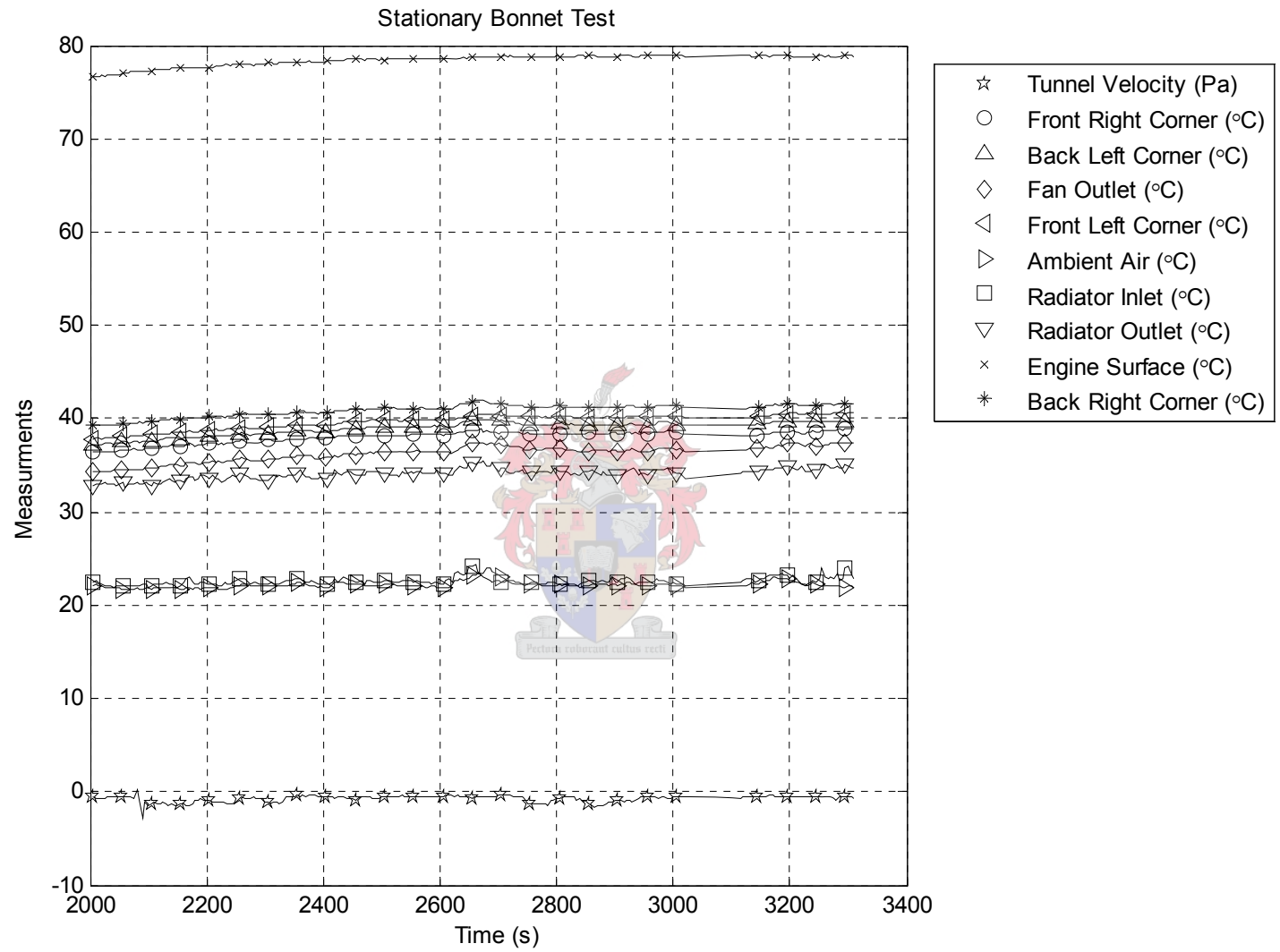


Figure A-1: Experimental data set 1

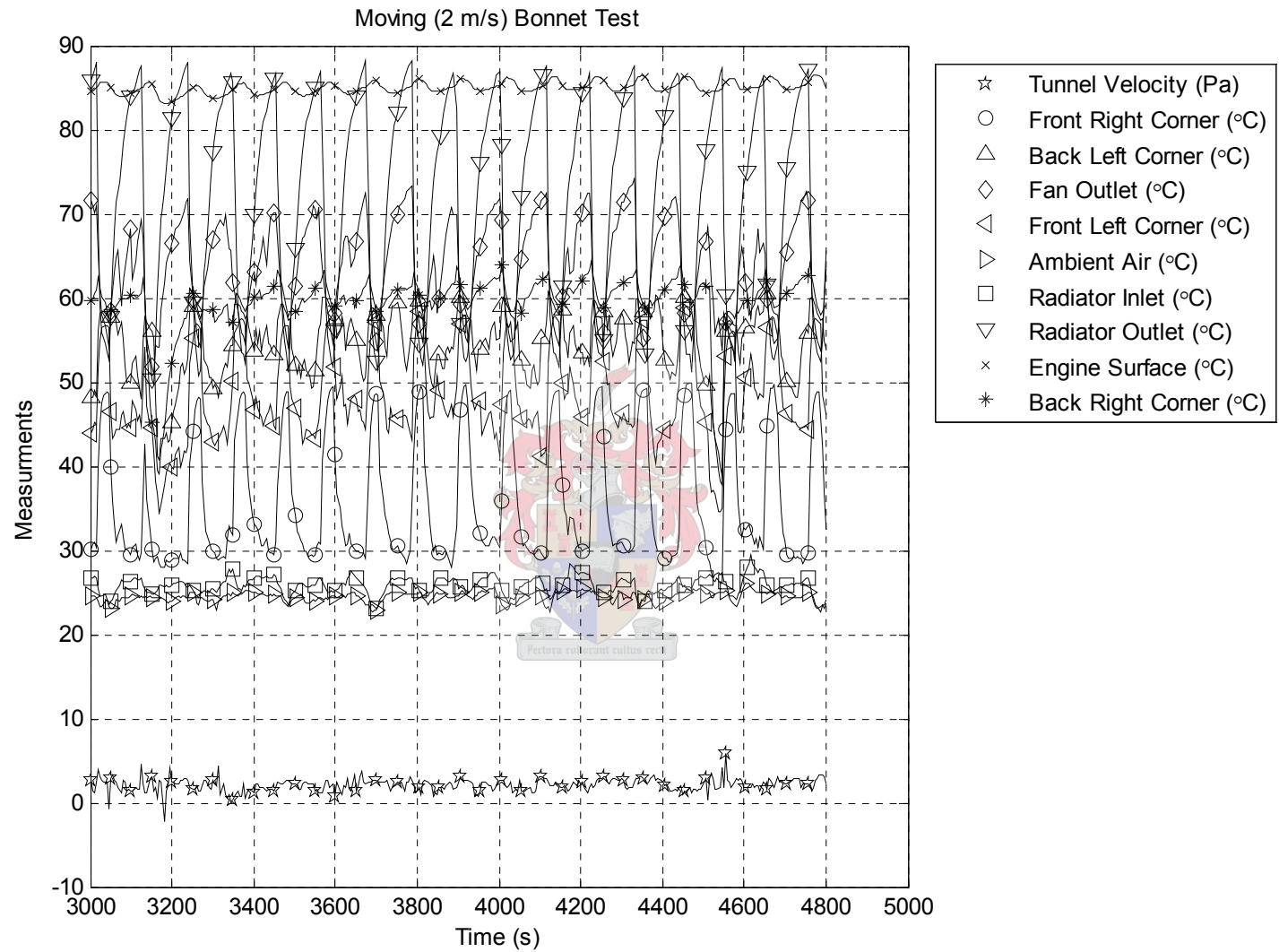


Figure A-2: Experimental data set 2

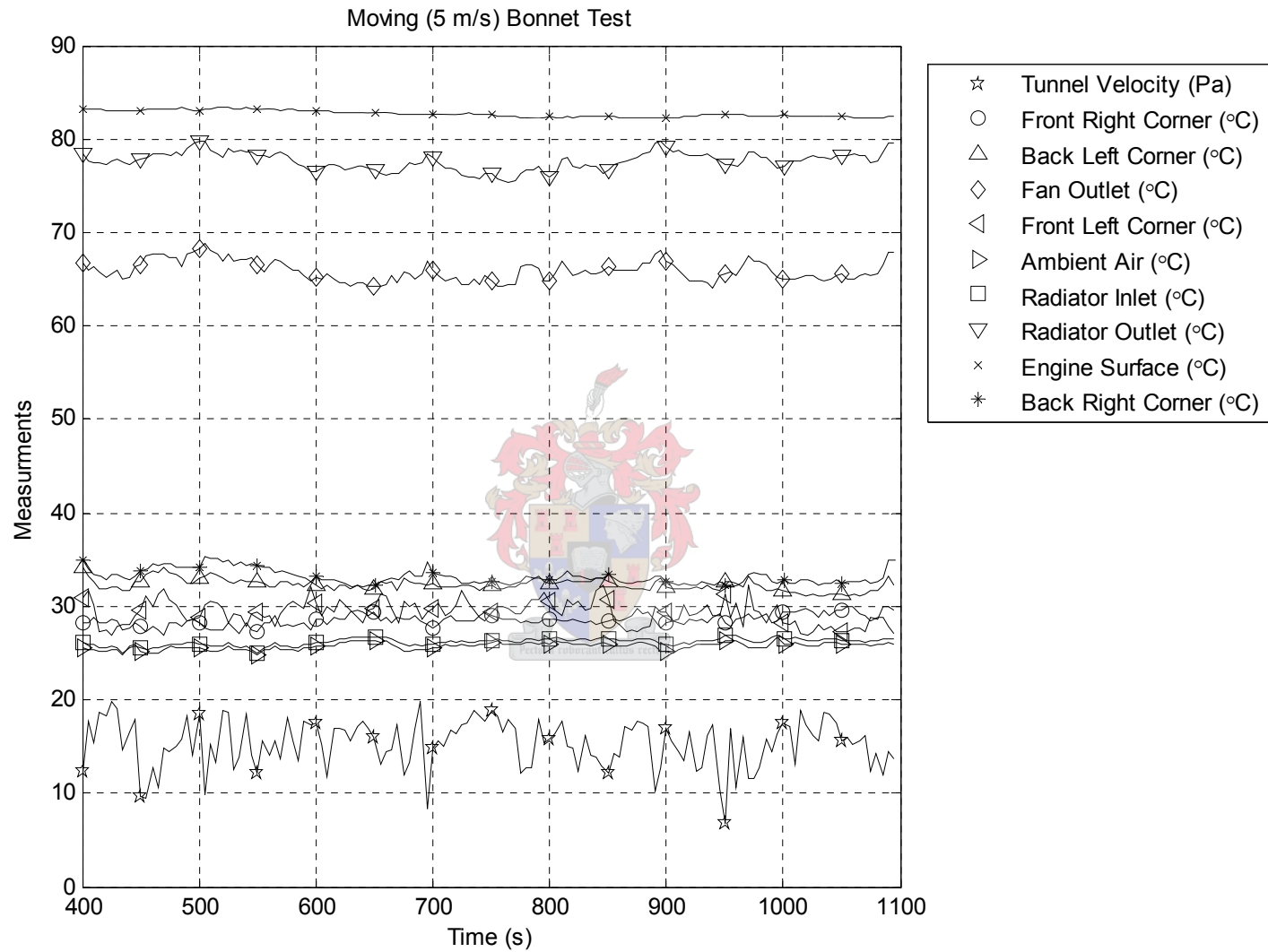


Figure A-3: Experimental data set 3

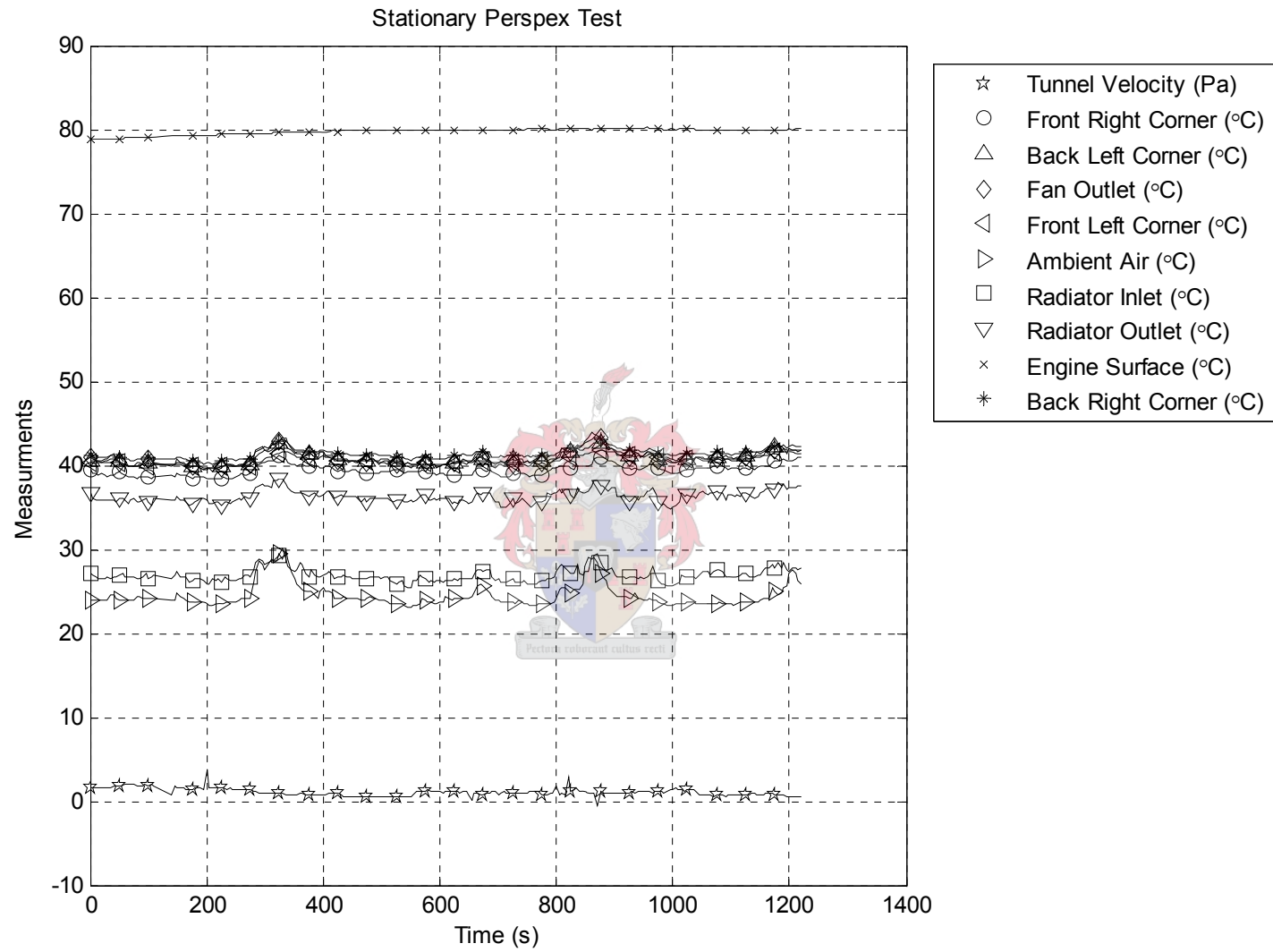


Figure A-4: Experimental data set 4

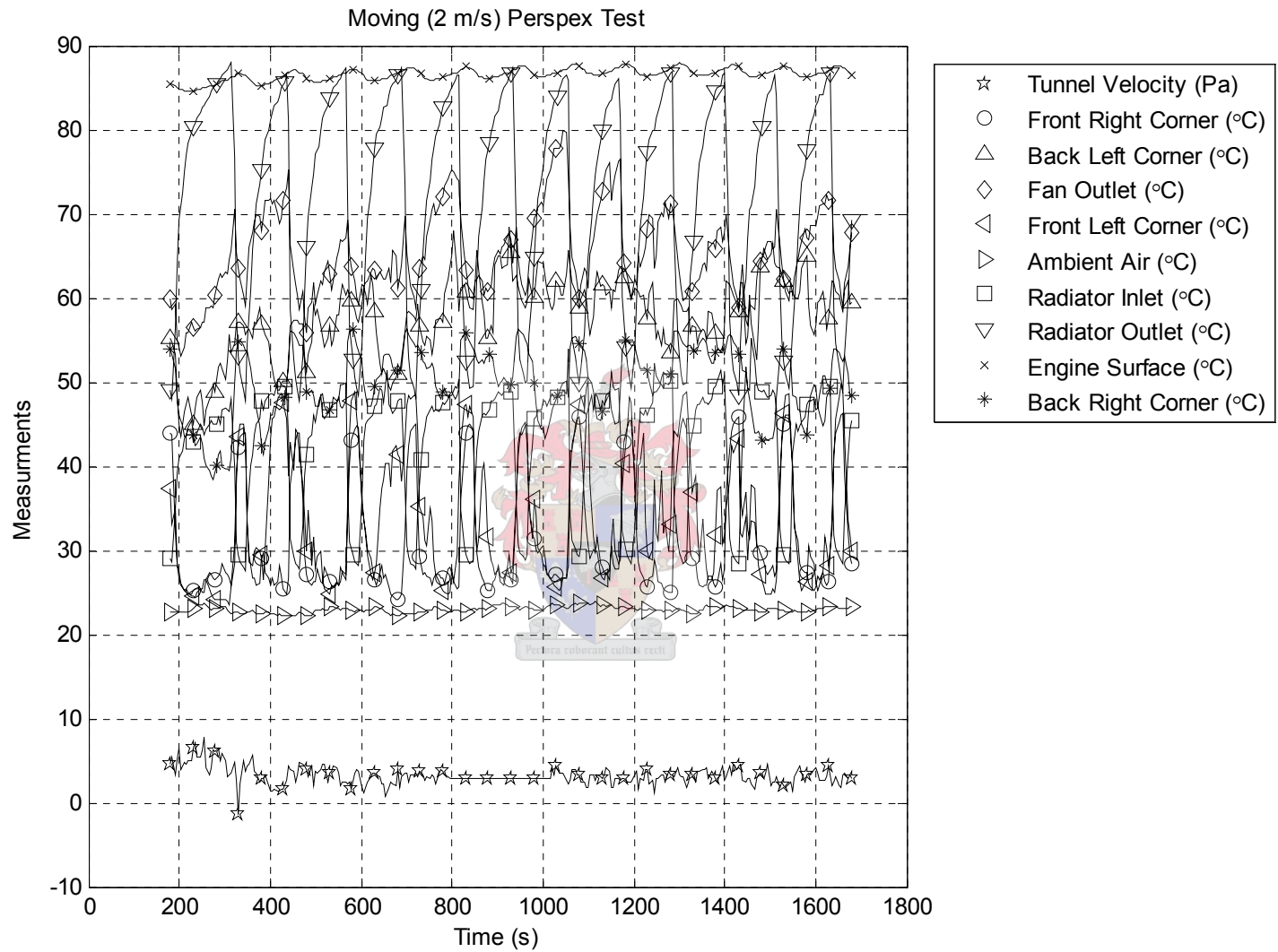


Figure A-5: Experimental data set 5

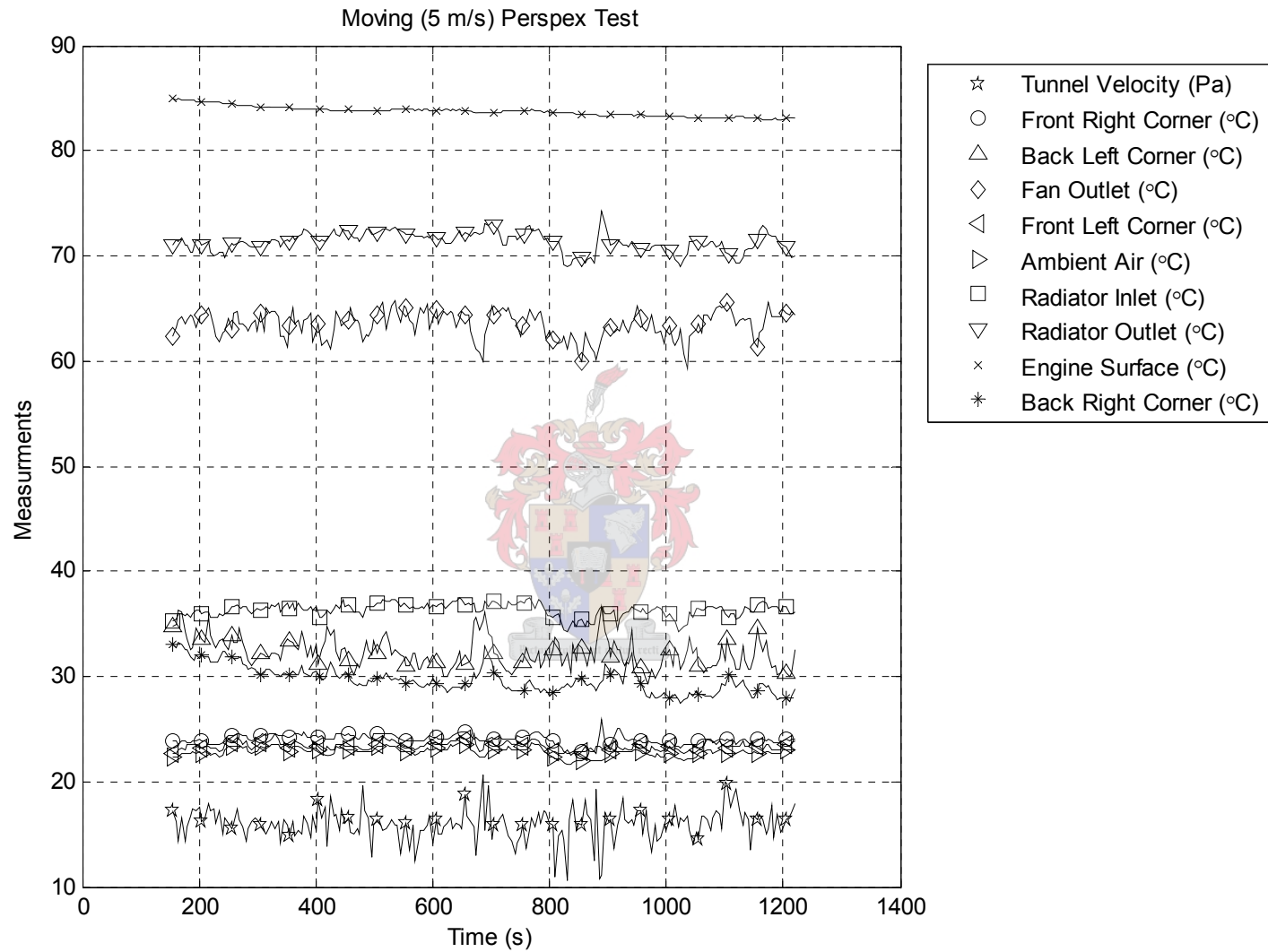


Figure A-6: Experimental data set 6

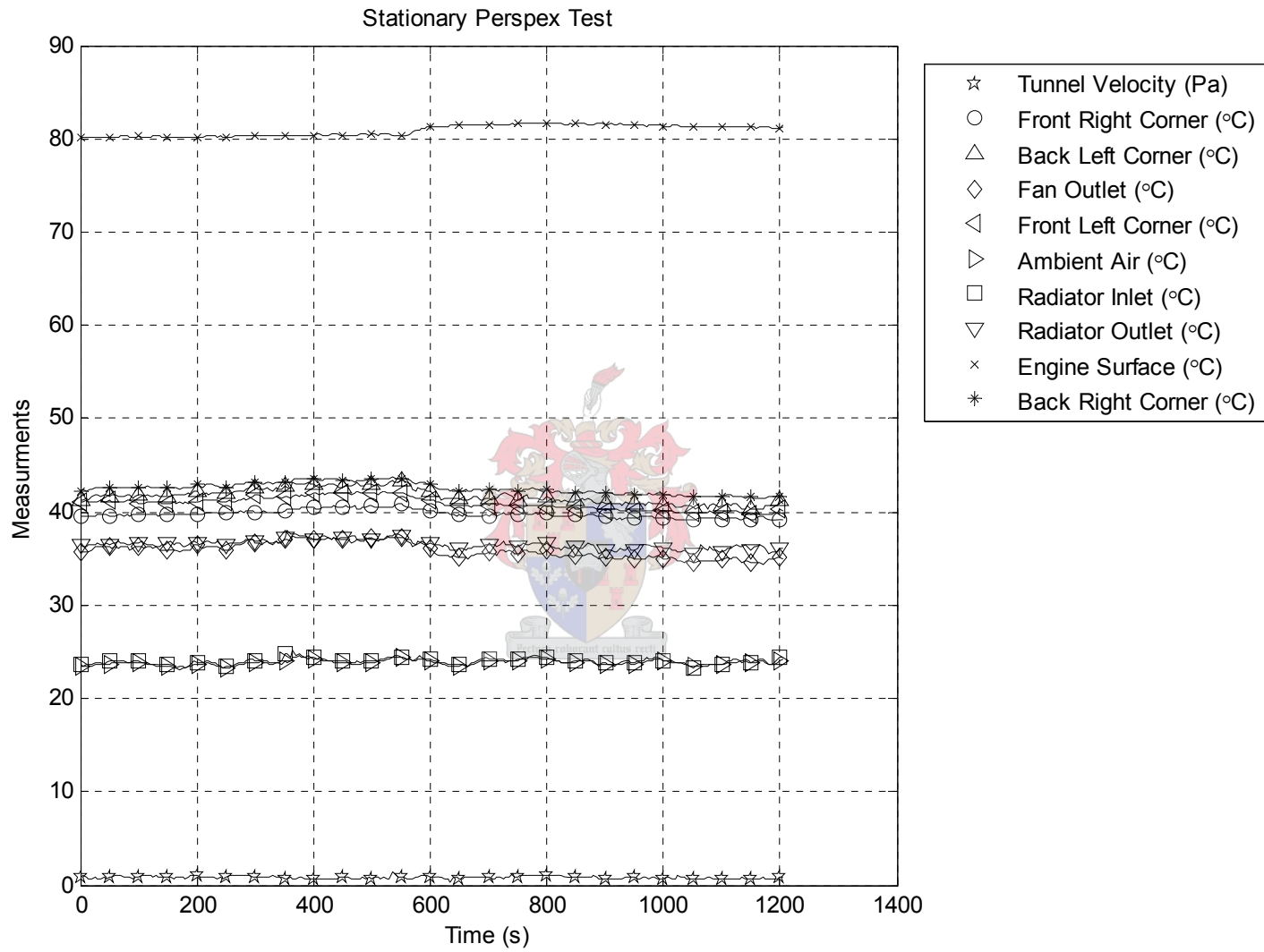


Figure A-7: Experimental data set 7

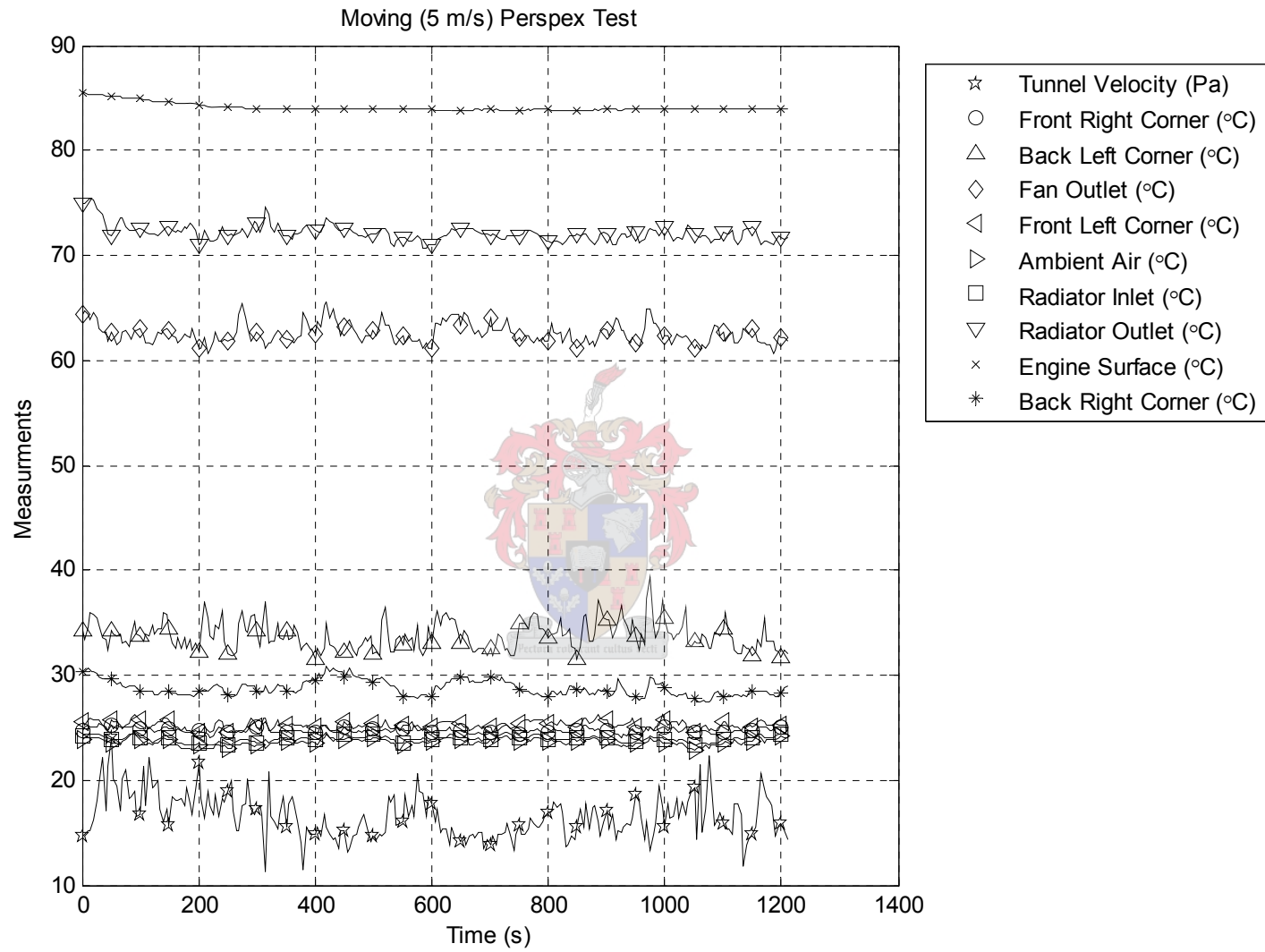


Figure A-8: Experimental data set 8

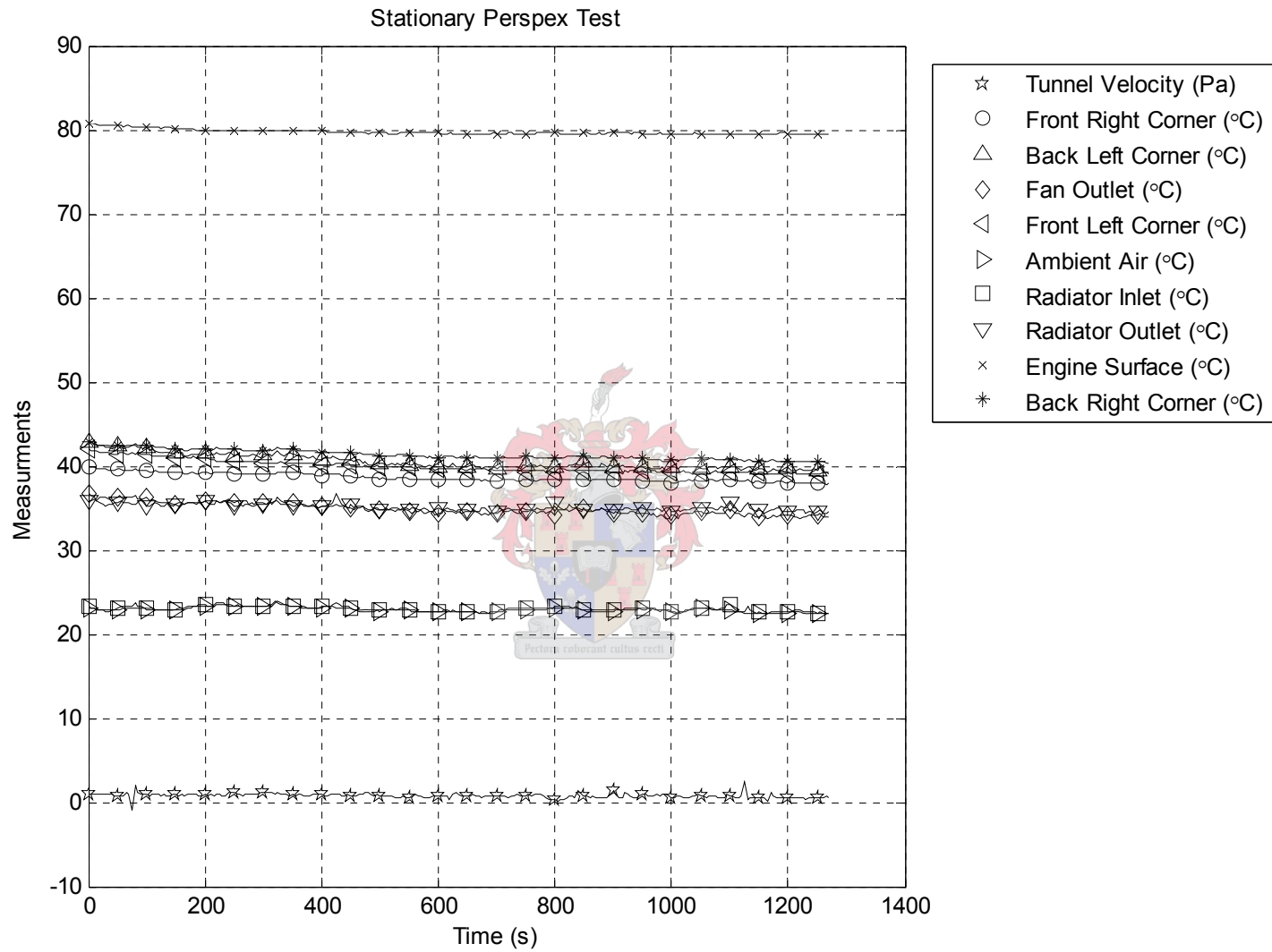


Figure A-9: Experimental data set 9

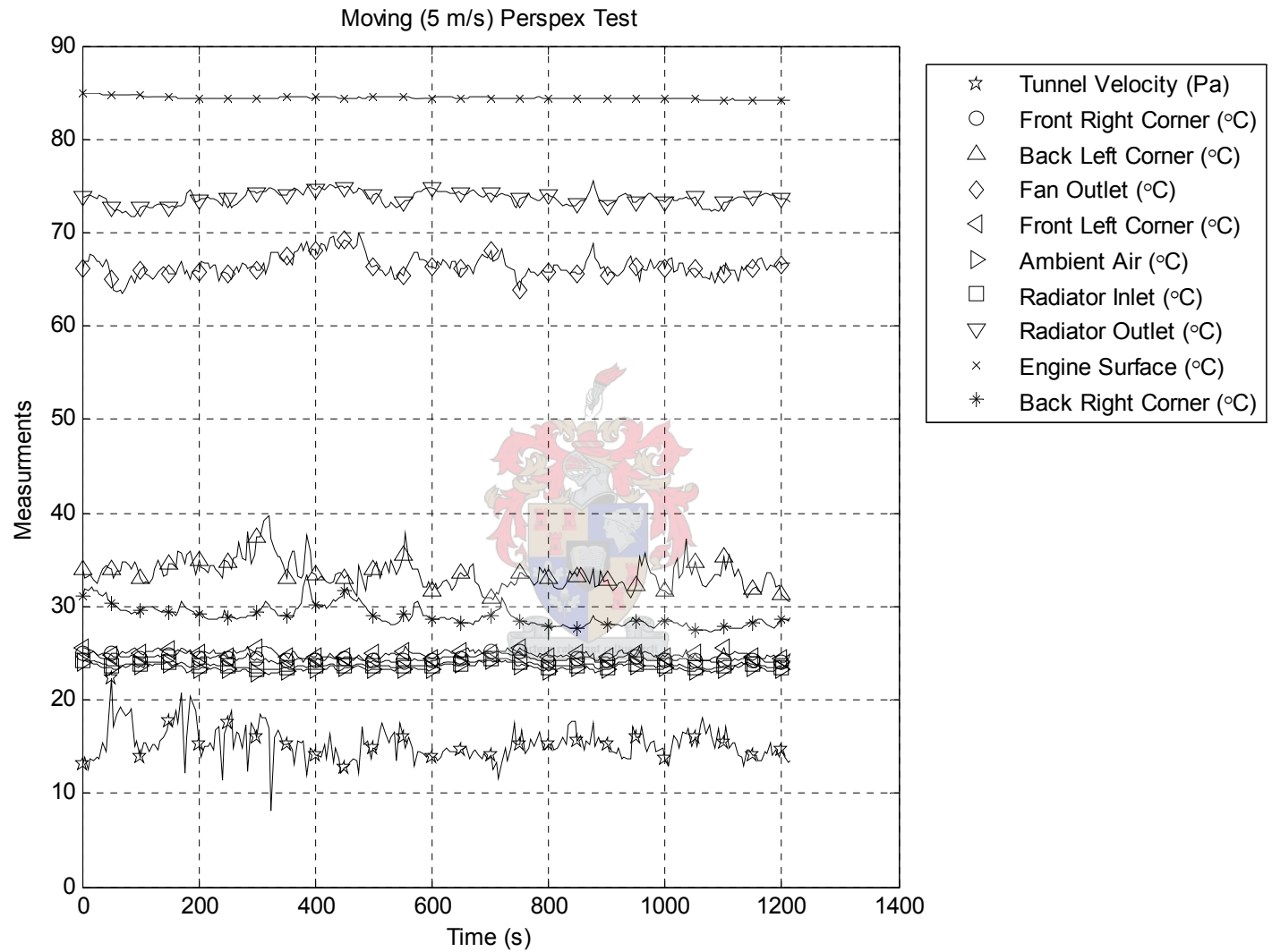


Figure A-10: Experimental data set 10

APPENDIX B

Radiator Test Sample

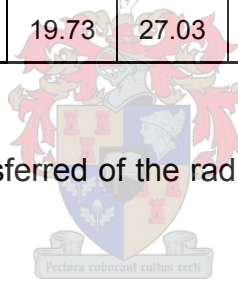


Table B-1 presents a sample of the experimental data obtained from the radiator test.

Table B-1: Experimental data from the radiator tests

T_{ai}	T_{ao}	T_{wi}	T_{wo}	m_w	dP_{heat}	dP_{inl}	dP_{noz}	A_{rad}	P_{atm}	D_{noz}	b
[°C]	[°C]	[°C]	[°C]	[kg/s]	[Pa]	[Pa]	[Pa]	[m ²]	[kPa]	[m]	[m]
18.27	39.34	79.34	71.46	1.04	494.76	850.93	1039.10	0.17	100.50	0.20	0.03
17.99	40.91	79.40	71.97	1.04	393.79	669.82	805.81	0.17	100.50	0.20	0.03
17.93	42.38	79.45	72.46	1.03	314.76	529.76	620.77	0.17	100.50	0.20	0.03
17.73	44.26	79.44	73.04	1.03	235.79	391.08	442.75	0.17	100.50	0.20	0.03
17.84	47.10	79.44	73.80	1.03	157.77	255.75	274.90	0.17	100.50	0.20	0.03
17.59	52.35	79.55	75.05	1.04	78.23	121.37	121.72	0.17	100.50	0.20	0.03
17.69	54.84	79.57	75.53	1.03	58.41	88.56	248.60	0.17	100.50	0.15	0.03
17.67	58.41	79.63	76.12	1.05	39.04	57.24	146.24	0.17	100.50	0.15	0.03
17.64	60.92	79.70	76.53	1.04	29.96	42.89	102.83	0.17	100.50	0.15	0.03
17.63	64.91	79.75	77.08	1.04	19.73	27.03	57.41	0.17	100.50	0.15	0.03

The pressure drop and heat transferred of the radiator was calculated from this data as follows.



The pressure in front of the nozzle is calculated as:

$$\begin{aligned}
 P_{noz} &= P_{atm} - dP_{inl} \\
 &= 100500 - 850.93 \\
 &= 99649.07 [Pa] \\
 &= 99.65 [kPa]
 \end{aligned}
 \tag{B. 1}$$

From which the air density is calculated as

$$\begin{aligned}
 \rho_{noz} &= \frac{P_{noz}}{R_{air} T_{ao}} \\
 &= \frac{99649.07}{287 \times (273.15 + 39.34)} \\
 &= 1.11 [kg / m^3]
 \end{aligned}
 \tag{B. 2}$$

and the nozzle velocity as

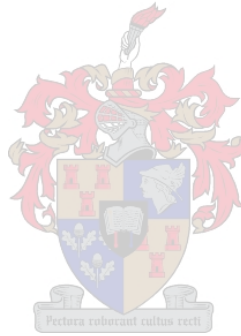
$$\begin{aligned}
V_{noz} &= \sqrt{\frac{2dP_{noz}}{\rho_{noz}}} \\
&= \sqrt{\frac{2 \times 1039.10}{1.11}} \\
&= 43.27 [m/s]
\end{aligned}
\tag{B. 3}$$

thus the mass flow through the tunnel is:

$$\begin{aligned}
\dot{m}_{air} &= \frac{V_{noz} \rho_{noz} D_{noz}^2 \pi}{4} \\
&= \frac{43.27 \times 1.11 \times 0.2^2 \pi}{4} \\
&= 1.51 [kg/s]
\end{aligned}
\tag{B. 4}$$

This mass flow remains constant through the test facility is thus used to determine the velocity through the radiator as follows.

$$\begin{aligned}
\rho_{rad} &= \frac{P_{atm}}{R_{air} T_{ai}} \\
&= \frac{100500}{287 \times (273.15 + 18.27)} \\
&= 1.20 [kg/m^3]
\end{aligned}
\tag{B. 5}$$



therefore:

$$\begin{aligned}
V_{rad} &= \frac{\dot{m}}{\rho_{rad} A_{rad}} \\
&= \frac{1.51}{1.2 \times 0.17} \\
&= 7.4 [m/s]
\end{aligned}
\tag{B. 6}$$

The heat transfer of the radiator was done by examining the energy loss from the water and the energy added to the air.

$$\begin{aligned}
Q_{water} &= \dot{m}_w c_{p,w} (T_{wi} - T_{wo}) \\
&= 1.04 \times 4182 \times (79.34 - 71.46) \\
&= 34272.3 [W] \\
&= 34.27 [kW]
\end{aligned}
\tag{B. 7}$$

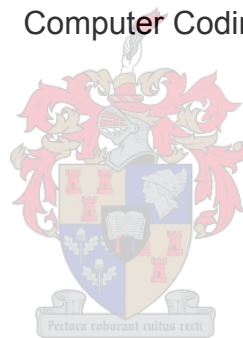
$$\begin{aligned} Q_{air} &= \dot{m}_{air} c_{p,air} (T_{ao} - T_{ai}) \\ &= 1.51 \times 1005 \times (39.34 - 18.27) \\ &= 31974.7 \text{ [W]} \\ &= 31.97 \text{ [kW]} \end{aligned} \tag{B. 8}$$

The difference between the two heat transfers of the water and the air is attributed to energy loss to the environment as the radiator was not completely insulated to not affect the pressure drop readings. The heat transferred of the water was used in the CFD simulations as the radiator is encapsulated in the vehicle improving the insulation of the radiator.



APPENDIX C

Computer Coding



Momentum source for the stationary runs

```
INCLUDE 'comdb.inc'


COMMON/USR001/INTFLG(100)

INCLUDE 'usrdat.inc'
DIMENSION SCALAR(50)
EQUIVALENCE( UDAT12(001), ICTID )
EQUIVALENCE( UDAT03(001), CON )
EQUIVALENCE( UDAT03(006), G1 )
EQUIVALENCE( UDAT03(007), G2 )
EQUIVALENCE( UDAT03(008), G3 )
EQUIVALENCE( UDAT03(019), VOLP )
EQUIVALENCE( UDAT04(001), CP )
EQUIVALENCE( UDAT04(002), DEN )
EQUIVALENCE( UDAT04(003), ED )
EQUIVALENCE( UDAT04(005), PR )
EQUIVALENCE( UDAT04(008), TE )
EQUIVALENCE( UDAT04(009), SCALAR(01) )
EQUIVALENCE( UDAT04(059), U )
EQUIVALENCE( UDAT04(060), V )
EQUIVALENCE( UDAT04(061), W )
EQUIVALENCE( UDAT04(062), VISM )
EQUIVALENCE( UDAT04(063), VIST )
EQUIVALENCE( UDAT04(007), T )
EQUIVALENCE( UDAT04(067), X )
EQUIVALENCE( UDAT04(068), Y )
EQUIVALENCE( UDAT04(069), Z )

IF (ICTID.EQ.6) THEN
  VMAG=SQRT(U**2+V**2+W**2)
  ALPHA=217.15
  BETA=454.04

  S1U=0
  S1V=0
  S1W=0
  S2U=ALPHA*VMAG+BETA
  S2V=1000*ALPHA*VMAG+1000*BETA
  S2W=1000*ALPHA*VMAG+1000*BETA
END IF

IF (ICTID.EQ.7) THEN
  VEL=19
  S1U=-DEN*(VEL**2)*0.5/0.05
  S2U=0
  OMEGA=30 ! RAD/S
  R=SQRT((Y-0.220)**2+(Z+0.25505)**2)
  S1V=DEN/(2*0.05)*OMEGA**2*(Z+0.25505)*ABS(Z+0.25505)
  S2V=DEN/(2*0.05)*OMEGA*ABS(Z+0.25505)
  S1W=-DEN/(2*0.05)*OMEGA**2*(Y-0.220)*ABS(Y-0.220)
  S2W=-DEN/(2*0.05)*OMEGA*ABS(Y-0.220)
END IF
RETURN
END
```



Enthalpy source for the stationary model

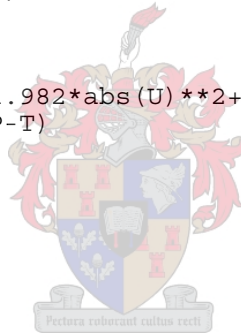
```
REAL*8 H
INCLUDE 'comdb.inc'

COMMON/USR001/INTFLG(100)

INCLUDE 'usrdat.inc'
DIMENSION SCALAR(50)
EQUIVALENCE( UDAT12(001), ICTID )
EQUIVALENCE( UDAT03(001), CON )
EQUIVALENCE( UDAT03(019), VOLP )
EQUIVALENCE( UDAT04(001), CP )
EQUIVALENCE( UDAT04(002), DEN )
EQUIVALENCE( UDAT04(003), ED )
EQUIVALENCE( UDAT04(004), HP )
EQUIVALENCE( UDAT04(006), P )
EQUIVALENCE( UDAT04(008), TE )
EQUIVALENCE( UDAT04(009), SCALAR(01) )
EQUIVALENCE( UDAT04(059), U )
EQUIVALENCE( UDAT04(060), V )
EQUIVALENCE( UDAT04(061), W )
EQUIVALENCE( UDAT04(062), VISM )
EQUIVALENCE( UDAT04(063), VIST )
EQUIVALENCE( UDAT04(007), T )
EQUIVALENCE( UDAT04(067), X )
EQUIVALENCE( UDAT04(068), Y )
EQUIVALENCE( UDAT04(069), Z )

TEMP=318.15
IF (ICTID.EQ.6) THEN
  H=1.7466*abs(U)**3-41.982*abs(U)**2+598.42*abs(U)+1796.9
  S1P=(H/(0.032))*(TEMP-T)
  S2P=0
END IF

RETURN
END
```



Momentum source for the moving runs

```
C*****
      SUBROUTINE SORMOM(S1U,S2U,S1V,S2V,S1W,S2W,POROS)
C      Source-term for momentum
C*****
C-----*
C      STAR VERSION 3.24.000
C-----*
      INCLUDE 'comdb.inc'

      COMMON/USR001/INTFLG(100)

      INCLUDE 'usrdat.inc'
      DIMENSION SCALAR(50)
      EQUIVALENCE( UDAT12(001), ICTID )
      EQUIVALENCE( UDAT03(001), CON )
      EQUIVALENCE( UDAT03(006), G1 )
      EQUIVALENCE( UDAT03(007), G2 )
      EQUIVALENCE( UDAT03(008), G3 )
      EQUIVALENCE( UDAT03(019), VOLP )
      EQUIVALENCE( UDAT04(001), CP )
      EQUIVALENCE( UDAT04(002), DEN )
      EQUIVALENCE( UDAT04(003), ED )
      EQUIVALENCE( UDAT04(005), PR )
      EQUIVALENCE( UDAT04(008), TE )
      EQUIVALENCE( UDAT04(009), SCALAR(01) )
      EQUIVALENCE( UDAT04(059), U )
      EQUIVALENCE( UDAT04(060), V )
      EQUIVALENCE( UDAT04(061), W )
      EQUIVALENCE( UDAT04(062), VISM )
      EQUIVALENCE( UDAT04(063), VIST )
      EQUIVALENCE( UDAT04(007), T )
      EQUIVALENCE( UDAT04(067), X )
      EQUIVALENCE( UDAT04(068), Y )
      EQUIVALENCE( UDAT04(069), Z )

      IF (ICTID.EQ.6) THEN
          VMAG=SQRT(U**2+V**2+W**2)
          ALPHA=217.15
          BETA=454.04

          S1U=0
          S1V=0
          S1W=0
          S2U=ALPHA*VMAG+BETA
          S2V=1000*ALPHA*VMAG+1000*BETA
          S2W=1000*ALPHA*VMAG+1000*BETA
      END IF

      IF (ICTID.EQ.7) THEN
          VEL=4.7
          S1U=0.5*DEN*(VEL**2)/0.05
          S2U=0
      END IF

      RETURN
      END
```



Enthalpy source for the moving model

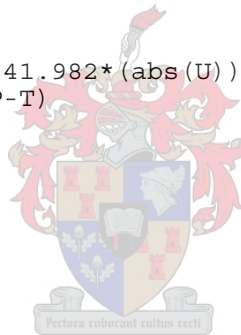
```
REAL*8 H
  INCLUDE 'comdb.inc'

  COMMON/USR001/INTFLG(100)

  INCLUDE 'usrdat.inc'
  DIMENSION SCALAR(50)
  EQUIVALENCE( UDAT12(001), ICTID )
  EQUIVALENCE( UDAT03(001), CON )
  EQUIVALENCE( UDAT03(019), VOLP )
  EQUIVALENCE( UDAT04(001), CP )
  EQUIVALENCE( UDAT04(002), DEN )
  EQUIVALENCE( UDAT04(003), ED )
  EQUIVALENCE( UDAT04(004), HP )
  EQUIVALENCE( UDAT04(006), P )
  EQUIVALENCE( UDAT04(008), TE )
  EQUIVALENCE( UDAT04(009), SCALAR(01) )
  EQUIVALENCE( UDAT04(059), U )
  EQUIVALENCE( UDAT04(060), V )
  EQUIVALENCE( UDAT04(061), W )
  EQUIVALENCE( UDAT04(062), VISM )
  EQUIVALENCE( UDAT04(063), VIST )
  EQUIVALENCE( UDAT04(007), T )
  EQUIVALENCE( UDAT04(067), X )
  EQUIVALENCE( UDAT04(068), Y )
  EQUIVALENCE( UDAT04(069), Z )

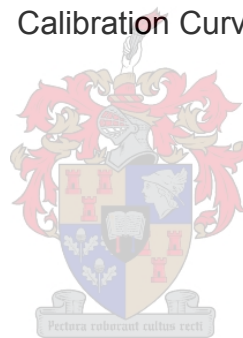
  TEMP=347.15
  IF (ICTID.EQ.6) THEN
    H=1.7466*(abs(U))**3-41.982*(abs(U))**2+598.42*abs(U)+1796.9
    S1P=(H/(0.032))*(TEMP-T)
    S2P=0
  END IF

  RETURN
  END
```



APPENDIX D

Calibration Curves



The calibration of pressure transducers is important, especially at low velocity flow, where a small pressure error can result in a large velocity error due to the relationship.

$$\Delta P = \frac{1}{2} \rho V^2 \tag{D. 1}$$

where:

P is the pressure drop

V is the velocity and,

ρ is the density of the fluid.

The higher the flow velocity the better the pressure readings become. Figure D-1 to Figure D-3 show the calibration curves obtained for the pressure transducers used.

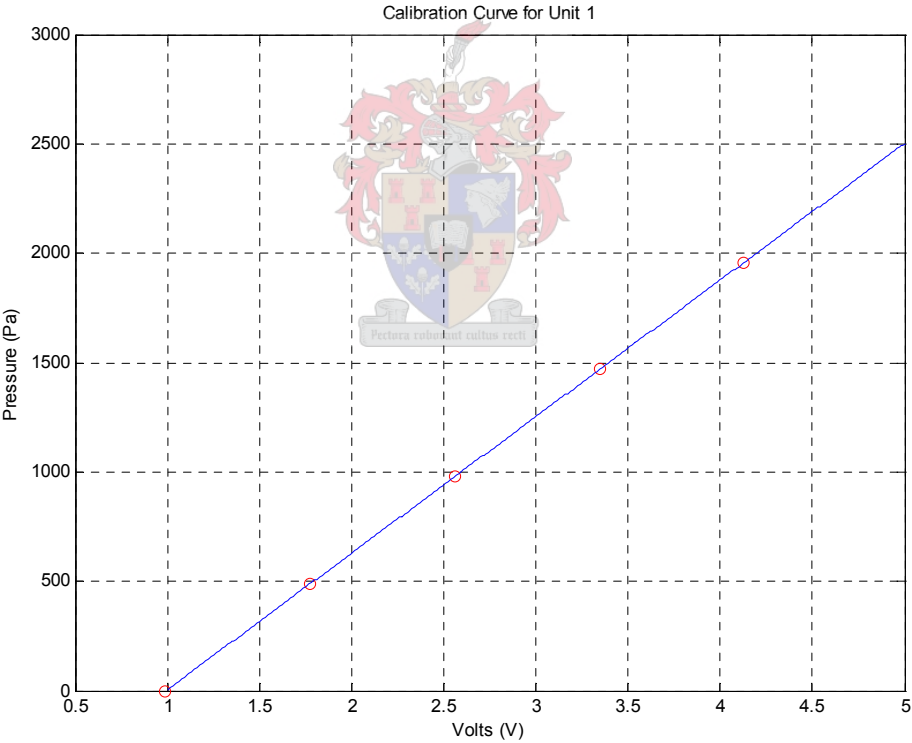


Figure D-1: Calibration curve for unit 1

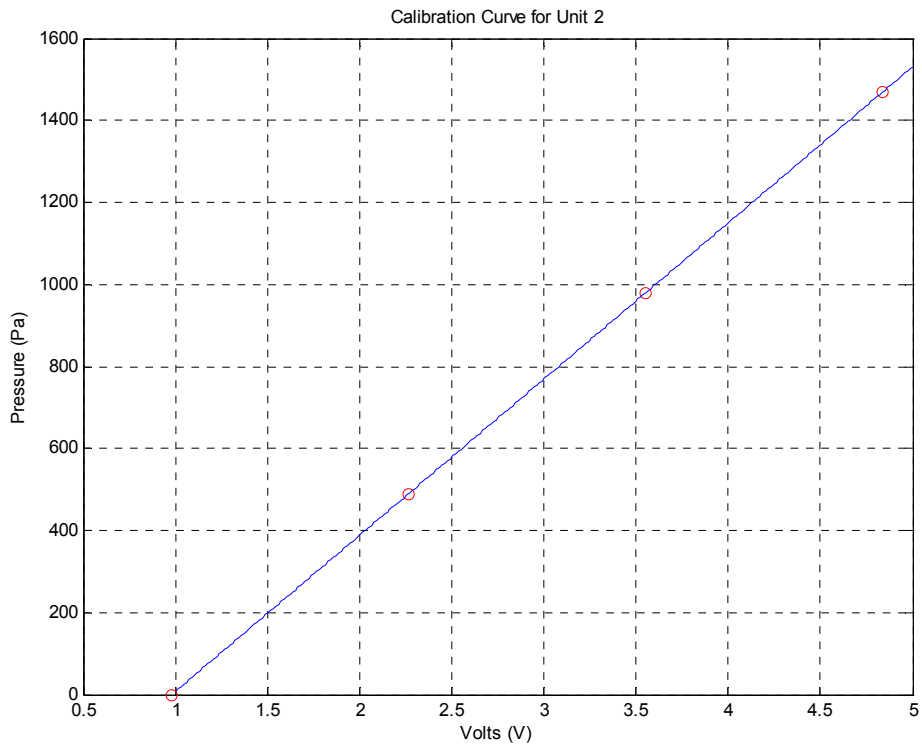


Figure D-2: Calibration curve for unit 2

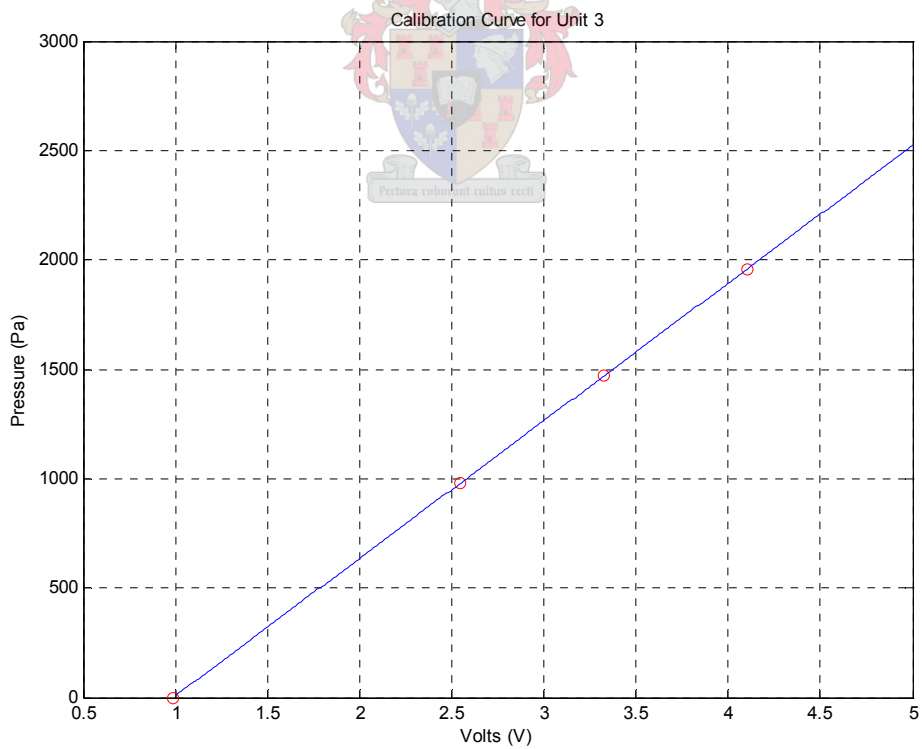
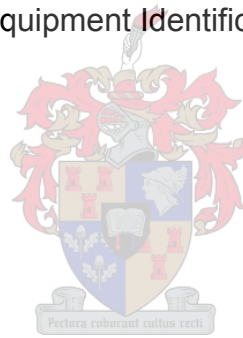


Figure D-3: Calibration curve for unit 3

APPENDIX E

Equipment Identification



The following table provides the serial numbers of the apparatus used along with the function of each.

Apparatus	Serial Number	Function
Hand held anemometer	101525	Measuring air speed
Betz manometer	12453	Calibrating Pressure Transducers
Pressure transducer unit 1	6F00142	Measure Pressure
Pressure transducer unit 2	6F00141	Measure Pressure
Pressure transducer unit 3	54Q0201	Measure Pressure
Infrared Imager	2297380101-0001	Surface temperature measurements
Data Logger	US37008090	Data Acquisition
Laptop computer	5576VMO 207	Data storage
Large Wind tunnel	47507	Varying air speed for experimental tests

